SAINT–PETERSBURG STATE UNIVERSITY

Ivanova Ekaterina Sergeevna

(U,Th)–He Dating of Pyrite to Determine the Age of Sulphide Mineralization in the Toupugol–Khanmeishor Gold District, Polar Urals

Scientific specialty 1.6.4. Mineralogy, Crystallography, Geochemistry,
geochemical methods of mineral exploration

DISSERTATION
submitted for the degree of the candidate
of geological and mineralogical sciences

Translation from Russian

Scientific supervisors:
Candidate of Geological and
Mineralogical sciences
O.V. Yakubovich
Candidate of Geological and
Mineralogical sciences
I.D. Sobolev

Saint–Petersburg
2024

CONTENTS

INTRODUCTION

Research relevance.

The age of mineralization is an important geological criterion because it allows us to relate its formation to geodynamic conditions and to discriminate the age of potential ore objects. Determining the age of ore mineralization is a difficult isotope–geochemical task due to the frequent lack of reliable mineral geochronometers.

The Re–Os method is often used for direct dating of sulfides (Stein et al., 2000; Hnatyshin et al., 2020). However, analysis of the Re–Os system often fails to provide reliable age estimates due to isotopic heterogeneity of trapped Os or perturbation of this isotopic system by superimposed processes. The complexity of estimating Os behavior during sulfide recrystallization under conditions of secondary alteration makes it difficult to distinguish the stages of ore mineralization formation. In some cases, Ar–Ar, Rb–Sr, and Sm–Nd methods have been applied for direct dating of sulfide mineralization (Smith et al., 2001; Ivanov et al., 2015; Christensen et al., 1995; Yang et al., 2002). The main limitation of these systems is the low content of parent isotopes in sulfide minerals. Also, it is not always possible to prove that mineral inclusions, which are the main concentrators of isotopes, are genetically related to sulfide mineralization. Therefore, the dating of ore paragenesis is often performed using the ^{40}Ar–^{39}Ar method on K–bearing minerals (sericite, feldspar, etc.). Recent studies have shown the promise of using one of the most common ore minerals, pyrite, as a (U,Th)–He geochronometer (Yakubovich et al., 2020, 2021). The new approach to dating ore–forming processes requires refinement of the methodology and its validation.

The Toupugol–Khanmeishor gold district (Polar Urals), which has great potential for identifying new industrial targets, was selected to evaluate the applicability of the (U,Th)–He method for determining the age of sulfide mineralization. Unlike the developed areas of the Central and Southern Urals, the inaccessible and eroded northern areas of the Ural fold system remain poorly explored, resulting in a large number of unevaluated gold deposits and individual

industrial objects. Currently, the Polar Urals are producing chromite in the Rai–Iz Massif, while in the western part of the Yamal–Nenets District more than 200 gold and gold–bearing occurrences remain unevaluated. In the Polar Urals in the Toupugol–Khanmeishor ore district, two gold deposits have been discovered: the Novogodnee-Monto gold–iron–skarn ore deposit (7 t Au) and the Petropavlovskoe gold–porphyry deposit (26 t Au), and a number of ore deposits (Kariernoe, Karachentseva, etc.) have been identified (Vikentyev et al., 2017). The region is considered promising for the discovery of new gold ore objects (Kenig and Butakov, 2013; Mansurov, 2016). Their effective search requires geodynamic and ore–magmatic reconstructions based not only on geological, but also on modern analytical data obtained using new high–precision methods and approaches. Reliable geochronological data are needed to create such reconstructions and to expand the understanding of the evolution of ore–magmatic systems in the Paleozoic Island arcs of the Urals, to which the object of study belongs.

The **objective** of this study is to develop and validate a method for (U,Th)–He dating of pyrite to determine the age of sulfide mineralization in the Toupugol–Khanmeishor district's ore occurrences and gold deposits.

To achieve this goal, the following **tasks** were set:

1. Study of pyrite grains in order to identify the shape of the location of potential sources of radiogenic helium in it to adjust the (U,Th)–He dating technique.

2. Methodological work to determine the criteria of pyrite suitability for (U,Th)–He dating, peculiarities of sample preparation, selection of optimal conditions for radiogenic helium extraction and chemical decomposition of samples, processing the results of analytical studies.

3. Assessment of reliability of application of (U,Th)–He method of pyrite dating for determination of age of sulfide mineralization on the basis of objects of known age: Novogodneye Monto, Petropavlovskoye deposits and Karyernoye ore occurrence.

4. Determination of the age of sulphide mineralization within the Toopugol–Khanmeishor gold ore district by (U,Th)–He method for pyrite dating.

The **objects** of the study are sulphide mineralization of the Toupugol–Khanmeyshor gold ore district: Au porphyry deposit Petropavlovskoe, Au–Fe–skarn deposit Novogodnee-Monto and gold ore occurrence Kariernoe.

Factual material and research methods.

The work is based on geological observations and factual material collected by the author as a member of the field team of IGEM RAS during field work in 2018, 2019 and 2021 in the northern part of the Voykar zone of the Polar Urals. Mineral determination and analysis of structural and textural features of rocks hosting ore mineralization were conducted using optical microscopy methods (SPGU) on 92 slides in transmitted light. Additionally, the chemical composition of pyrite was studied on 110 grains using a scanning electron microscope (RC 'Geomodel', SPbSU). Radiogenic helium content measurements were conducted on 50 samples using the highly sensitive mass spectrometer MSU–G–01–M at IPGG RAS. The pyrite grains' uranium and thorium contents were measured using the isotopic dilution method on a single–collector inductively coupled plasma mass spectrometer (ELEMENT XR ICP MS) at GEOCHI RAS. The Re–Os age determination was performed at the Jamstec laboratory in Japan.

The author directly participated in all stages of the work. The study involved collecting and analyzing stock and published literature, conducting field work to select actual material, and carrying out detailed petrographic characterization of volcanogenic and metasomatic formations. The rocks were typed and the mineralogical and geochemical features of pyrite from the study objects were studied. The age of ore mineralization was determined using the (U,Th)–He method, which involved measuring the concentration of radiogenic helium and preparing the sample for further determination of the contents of the (U,Th)–He mineralization.

Scientific novelty

1. The technique of selection, preparation of samples for (U,Th)–He dating of pyrite and their chemical decomposition was improved.

2. The possibility of (U,Th)–He dating of pyrite from volcanogenic and metasomatically altered rocks was substantiated.

3. New isotope–geochronological data on the age of sulfide mineralization within the limits of the Toupugol–Khanmeishor ore district were obtained.

Theoretical and practical significance

The conducted studies contribute to the development of dating methods for ore–forming processes. On the example of gold mineralization of the Toupugol–Khanmeishorsky gold ore district it is shown that (U,Th)–He method by pyrite can determine the age of sulfide mineralization. The obtained data on the age of pyrite made it possible to identify new age stages of sulfide mineralization within the study area.

Publications and approbation of the work

On the subject of the thesis 15 works have been published: 4 articles, 3 of which are indexed in WoS and Scopus databases, 1 – in the editions recommended by VAK of the Ministry of Education and Science of Russia; 11 materials of meetings and abstracts of reports. The research results were reported and discussed at international and Russian scientific conferences and meetings: 17th SGA Biennal Metting (Zurich, 2023); International conference on Thermochronology (Riva del Garda, 2023); XIII A.P. Vinogradov Symposium on Isotope Geochemistry (Moscow, GEOKhI RAS, 2023); "New in knowledge of ore formation processes" (Moscow, IGEM RAS, 2017, 2018, 2019, 2022); "Metallogeny of ancient and modern oceans, 2019. A quarter of a century of achievements in the study of submarine deposits" (Miass, IMin Ural Branch of RAS, 2019); "Actual problems of Precambrian geology, geophysics and geoecology" (Apatity, FIC KSC RAS, 2019).

Structure and scope of the work

The thesis consists of an introduction, 7 chapters and a conclusion. The volume of the work is 120 pages, including 41 figures, 7 tables and a list of literature of 148 titles. The introduction formulates the purpose and objectives of the study, substantiates the relevance, scientific novelty, theoretical and practical significance of the work, provides information about the actual material and applied research methods, presents the main provisions for defense. Chapter 1 presents brief information on the history of the discovery of the (U,Th)–He method, characterizes

its nuclear–physical basis, indicates the isotopic–geochemical limitations and the modern area of use. Chapter 2 includes information on (U,Th)–He isotope system in pyrite – stability of radiogenic helium, forms of uranium and thorium, gas–liquid inclusions in it. Chapter 3 contains a detailed description of the methodology of work at each stage of the study: peculiarities of sampling and use of analytical methods are specified. Chapter 4 describes the geological position of the Voykar zone, the history of geological development of the Polar–Ural region, peculiarities of sulphide mineralization location and geological structure of the objects of the Toupugol–Khanmeishor ore district. Chapter 5 is devoted to mineralogical and petrographic characterization of the rocks hosting the mineralization. Chapter 6 contains data on the form of uranium and thorium occurrence, the character of distribution of impurity elements and mineral inclusions in the pyrite composition, and includes substantiation of the correction of the selection and decomposition methodology for (U,Th)–He dating. Chapter 7 presents the results of isotope–geochronological studies of sulfide mineralization of the Toupugol–Khanmeyshor ore district. Using an integrated approach, the duration and stage of evolution of ore–magmatic sources, the influence of tectonic and hydrothermal–metasomatic impact on ore formation were evaluated, and the age of ore formation was correlated with geodynamic conditions. The main results of the study are formulated in the conclusion.

Acknowledgements

The author expresses gratitude to Dr. Yakubovich O.V. and Dr. Sobolev I.D. for their valuable advice, assistance, and support throughout the work. Dr. Yakubovich O.V. provided guidance on the (U,Th)–He isotope–geochronological analysis technique, while Dr. Sobolev I.D. offered constructive advice and assisted in the field study of rocks and data interpretation. The author expresses gratitude to Dr. I.V. Vikentiev for providing field experience, material, recommendations, and scientific advice. Additionally, the author thanks Dr. B.M. Gorokhovsky for technical support and Dr. E.B. Salnikova for assistance in setting up the sample decomposition technique. The author expresses gratitude to Ms. E.E. Tyukova, Candidate of Geological and Mineralogical Sciences, and Ms. Y.N. Ivanova,

Candidate of Geological and Mineralogical Sciences, for providing samples and consultations. Additionally, the author acknowledges the assistance of M.O. Anosova, N.V. Vlasenko, M.M. Podolskaya, and N.P. Konstantinova in analytical measurements.

The work was financially supported by the RNF project No. 22–77–10088. Field expeditions were conducted under the RNF project No. 14–17–00693–P and RFBR No. 18–05–70041. The research was conducted at the Laboratory of Isotope Geology of the Institute of Precambrian Geology and Geochronology (IPGG) of the Russian Academy of Sciences, using equipment from RC 'Geomodel' and RC 'X–ray Diffraction Methods of Matter Analysis' (SPbU).

Main scientific results:

1. Based on the results of a detailed study of possible sources of radiogenic helium in pyrite (Ivanova et al., 2024, p. 6-7; Yakubovich et al., 2021, p. 11-13), the methodology of sample collection and preparation was improved and the chemical decomposition protocol for (U,Th)-He dating was modified. Personal participation of the author in obtaining the results (Yakubovich et al., 2021): geological characterization, determination of the (U,Th)-He age of pyrite, interpretation of the results, compilation of graphical material.

2. On the example of gold mineralization in the Toupugol-Khanmeishor ore district, the possibilities of systematic determination of (U,Th)-He age of pyrite from different types of objects are shown (Ivanova et al., 2024, p. 11-12; Yakubovich et al., 2021, p. 10-11) under the control of certified standards (Durango apatite, Santiago River platinum (Yakubovich et al., 2023)). Personal participation of the author in obtaining these results (Yakubovich et al., 2023): mineralogical characterization, methodological part, compilation of graphical data.

3. Petrological and mineralogical study of gold-bearing rocks of the Voykar zone is presented (Ivanova et al., 2024, p. 10-11; Ivanova and Ivanova, 2021, p. 6-10). Original data on the age of pyrite from the Petropavlovskoe Au-porphyry deposit, the Novogodneye-Monto Au-Fe-scarne deposit (Yakubovich et al., 2021, pp. 10-11), and the Karyernoe gold-ore deposit (Ivanova et al., 2024, pp. 11-12)

were obtained, which allowed to distinguish new time stages of mineralization in the study area.

Protected Provisions

1. Micron inclusions of uranium (thorium)–containing minerals are one of the sources of radiogenic helium in the crystal lattice of pyrite. To ensure reliable (U,Th)–He dating of pyrite, it is necessary to decompose it completely. This can be achieved through autoclave decomposition in Teflon bouquets using a mixture of hydrofluoric, nitric, and perchloric acids (in a 10:2:1 ratio) under the following conditions: 220°C for 48 hours.

2. The (U,Th)–He dating of pyrite from the volcanics of the Kariernoe ore occurrence and metasomatites of the Novogodnee-Monto deposit agrees with the age values determined by independent methods, such as biostratigraphy and 39Ar–40Ar. This indicates the applicability of the (U,Th)–He method for determining the age of sulfide mineralization.

3. A new stage of sulfide mineralization of Permian age (293±8 Ma) was identified within the limits of the Toupugol–Khanmeyshor ore district. The sulfide stage of mineralization (424±6 Ma) is present in the Toupugol stratum's volcanics, as evidenced.

CHAPTER 1. BACKGROUND OF THE (U,Th)–He METHOD AND HISTORY OF THE DEVELOPMENT OF GEOCHRONOLOGY ON RADIOGENOUS HELIUM

1.1 History of the discovery of the (U,Th)–He method

The study of radioactivity and the structure of atoms led to the development of isotope physics, which is also applicable to geology. Progress in the study of radioactive decay processes made it possible to reconstruct the chronological sequence of rock formation and estimate the duration of geological processes based on the radioactive transformations of chemical element isotopes.

Information about helium first became available after J. Jansen and J. N. Lockyer studied the chemical composition of prominences in the Sun's atmosphere using spectral analysis in 1868 (Yakutseni, 1968). However, interest in studying helium was particularly piqued by W. Ramsay's isolation of its radiogenic isotope from the uranium–bearing mineral kleveite in the late 19th century. The first half of the 20th century was a crucial period in the development of isotope geochronology methods. During this time, E. Rutherford discovered the possibility of using decay products accumulated in the course of geological history to determine the age of natural objects (Rutherford, 1906). To achieve this goal, it was proposed to use the uranium content and the amount of accumulated helium in minerals, while the contribution of thorium was not considered. The U–He method, proposed by E. Rutherford and B. Boltwood in 1905, was the first attempt to estimate the age of rocks on Earth. They based their results on dating fergusonite (Nb–Ta oxide) (Badash, 1969; Reiners, 2017).

However, it was soon discovered that losses of radiogenic helium distorted the obtained ages, making the method extremely limited in its use (Gerling, 1939, 1961; Harley, 1956). During the first half of the 20th century, Rutherford, Holmes, and Panet, along with a group of scientists from the USSR, including Khlopin, Gerling, and Starik, attempted to eliminate the underestimated results of the (U,Th)–He method compared to other isotopic systems. The challenge was the high

diffusivity of helium, which is a characteristic of a noble gas. The physical property of helium to migrate through natural defects and dislocations in mineral structures, including those caused by metamict destruction due to radiation, has resulted in almost complete loss of helium over geological time. U–Pb dating is a more accurate and reliable method for providing consistent stratigraphic results. For a period of time, the (U,Th)–He method was considered unsuitable for determining the age of rocks.

However, in the latter half of the 20th century, research on the (U,Th)–He isotope system continued. Numerous studies were published during this period on the behavior of the system in various minerals and rocks. Among them, M. Dodson's study on the factors influencing the complete or partial loss of helium is particularly noteworthy due to the high mobility of helium even at low temperatures of the order of the first hundred degrees (Dodson, 1973). This paper provides a definition of the concept of system closure temperature and develops a mathematical solution to reconstruct the temperature–time history of rocks and minerals. The temperature at which the rate of loss of a radiogenic component equals the rate of its accumulation is elucidated. The article discusses the possibility of using helium loss data to obtain information on the duration and intensity of temperature effects on minerals during geologic processes. This information can be used to compile the thermal history of a mineral, leading to the development of thermochronology, a new direction in isotope geology. The article emphasizes the importance of understanding helium migration characteristics in this process. This information can be used to compile the thermal history of a mineral, leading to the development of thermochronology, a new direction in isotope geology.

In the 1990s, P. Zeitler and colleagues renewed interest in the (U,Th)–He research method. They studied apatite and interpreted its dating results as the time of cooling of the rock to the closure temperature, which was set at 100°C (Zeitler et al., 1987). Subsequently, scientists such as C. Farley and R. Wolf continued studying the (U,Th)–He isotope system using apatite as an example (Farley and Stockli, 2002; Wolf et al., 1996). The method's reliability was confirmed by the satisfactory results.

The study of radiogenic helium migration is ongoing and has been proposed for use in zircon research, which has positively impacted low–temperature thermochronology (Reiners, 2005). The study of helium behavior in various minerals has made it possible to date a number of uranium– and thorium–rich minerals, including accessory minerals such as uraninite, titanite, monazite, and brannerite, as well as hydrothermal minerals like hematite, magnetite, fluorite, and sphalerite (Boschman et al., 1993; Evans et al., 2005), and metamorphic minerals like garnet and rutile (Flowers et al., 2022).

Several studies have been published on the diffusion and migration patterns of helium from metals and other technical materials. These include the behavior of helium produced by nuclear irradiation and implanted by an ion beam into the structure of metals such as Pd, Ni, and Al, as well as several reactor materials (Whitmore, 1976; Benedek, 1978; Wilson et al., 1981; Puska and Nieminen, 1984; Malkin, 2018). Additionally, experiments have been conducted on the study of He conservation in the aforementioned minerals. The studies revealed a peculiarity in the cluster distribution of helium atoms within the metal structure, which leads to high–temperature conditions for its separation. This discovery makes isotope systems based on radiogenic helium in such minerals potentially useful for geochronology. To confirm this theory, researchers conducted a study on the kinetics of radiogenic helium extraction from the crystal lattice of nugget gold. The study was carried out using a highly sensitive helium mass spectrometric complex at the Institute of Geology and Geochronology of Precambrian RAS (Shukolyukov et al., 2010). The study confirmed that radiogenic helium is preserved in nugget gold as sparsely soluble helium bubble–clusters. They have low mobility (Shukoliukov et al., 2012). These clusters are positioned based on energetic benefit and migrate to metal structure defects, dislocations, or grain boundaries. The use of nugget metals is supported by their packing density, which slows down the migration rate of helium and increases its preservation in the substance (Shukolyukov et al., 2010). This makes it possible to date nugget metals, including platinum, due to the difficult thermodesorption of helium. Thermodesorption requires extremely high

temperatures for its release, up to the melting point (Shukolyukov et al., 2012). Additional research on the migration of radiogenic helium from minerals that can be attributed to semi–metals and semiconductors, based on their conductivity, has shown that sperrylite ($PtAs_2$; Yakubovich et al., 2015) and pyrite (Yakubovich et al., 2019) preserve helium at a sufficiently high rate, making them useful as He–geochronometers.

1.2 Nuclear–physical basis of the (U,Th)–He method

There are ten natural long–lived alpha–emitting radionuclides known on Earth: ^{144}Nd, ^{147}Sm, ^{148}Sm, ^{152}Gd, ^{174}Hf, ^{186}Os, ^{190}Pt, ^{232}Th, ^{235}U, and ^{238}U. Radiogenic helium (^{4}He) is one of the stable products of their radioactive decay. The (U,Th)–He method is based on the alpha decay of uranium isotopes ^{235}U, ^{238}U, and thorium ^{232}Th. These isotopes undergo a series of consecutive alpha and beta decays, forming radioactive series. If the age of the mineral is over 1 million years, intermediate decay products can be ignored in further calculations, and simplified formulas for nuclear reactions (1) can be used.

$$^{232}_{90}\mathrm{Th} \rightarrow {}^{208}_{82}\mathrm{Pb} + 6\,{}^{4}_{2}\mathrm{He}$$

$$^{235}_{92}\mathrm{U} \rightarrow {}^{207}_{82}\mathrm{Pb} + 7{}^{4}_{2}\mathrm{He} \qquad (1)$$

$$^{238}_{92}\mathrm{Th} \rightarrow {}^{206}_{82}\mathrm{Pb} + 8{}^{4}_{2}\mathrm{He}$$

In the decay series of Uranium and Thorium, 6 to 8 helium atoms are emitted. The equation for the accumulation of radiogenic helium from uranium and thorium is as follows (Farley and Stockli, 2002):

$$He^4 = 8 \cdot \frac{137.88}{(137.88+1)} C_U \cdot \left(e^{\lambda_{238} t} - 1\right) + 7 \cdot \frac{1}{(137.88+1)} C_U \cdot \left(e^{\lambda_{235} t} - 1\right) + 6 \cdot C_{Th} \cdot \left(e^{\lambda_{232} t} - 1\right) \qquad (2)$$

The concentrations of helium, uranium, and thorium (in atoms) are represented by He^4, C_U, and C_{Th}, respectively. The decay constants for the isotopes are represented by λ_{238} (1.55125×10^{-10} g^{-1}), λ_{235} (9.8485×10^{-10} g^{-1}), and λ_{232} (4.94775×10^{-10} g^{-1}).

The coefficients 8, 7, and 6 correspond to the number of helium atoms produced by the decay of the respective atom. The value 137.88 represents the modern isotopic ratio of ^{238}U to ^{235}U.

Equation (2) does not have an analytical solution for the parameter t, so its value must be obtained numerically with a given accuracy. Based on the uranium and thorium content in the sample being studied, as well as its helium concentration, it is possible to determine the age of the mineral.

A peculiarity of isotope systems based on radiogenic helium is the presence of the alpha–recoil effect (nucleus–recoil), which requires correction. Radioactive decay releases kinetic energy (4–8 MeV), causing the alpha particle to travel a relatively long distance (10–18 μm in apatite; Farley et al., 1996) before coming to a complete stop in the mineral. If the parent isotope is located more than the length of the α–braking path away from the grain boundary, the particle will be trapped inside the crystal regardless of its trajectory (Figure 1.1). On the other hand, if the radioactive isotope is situated at the grain boundary, there is only a 50% chance that the alpha particle will remain within the grain boundary. The reverse process can also occur based on a similar principle, resulting in helium implantation from the outside. It is important to consider the uneven distribution of parental isotopes in the mineral and host rocks. Underestimating this phenomenon in grains less than 200 μm can significantly underestimate the helium age of the mineral. For larger grains, the contribution of this surface effect can be considered negligible (Farley et al., 1996).

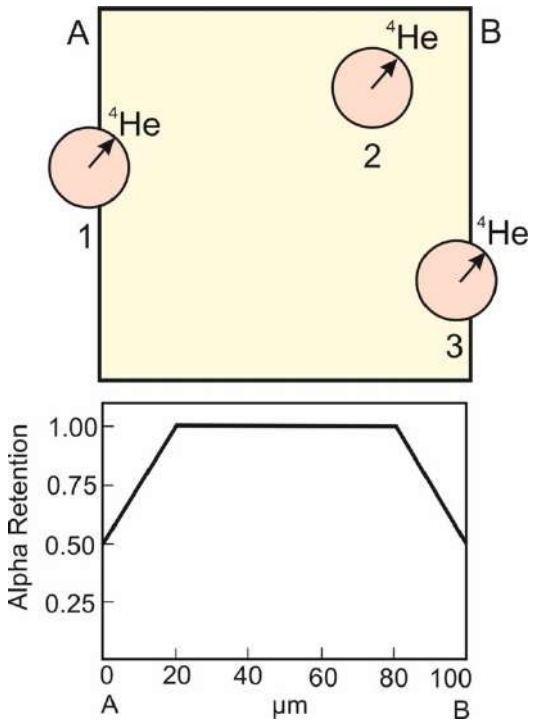

Figure 1.1. – α–recoil effect in the boundaries of a schematic crystal. 1) implantation of α–particle; 2) retention of α–particle; 3) possible ejection of α–particle. The center of the circle is the position of the parent isotope, the boundaries are the area for possible α–particle arrest, and the arrow is one of the possible trajectories of the α–particle during radioactive decay (Farley et al., 2002).

There are various methods to calculate the 'average' age of a set of (U,Th)–He analyses. The traditional approach of determining the arithmetic mean is less accurate than alternative methods, such as the 'pooled' age, isochronal age, and central age (Vermeesch, 2008).

The pooled age is determined by analogy with the division track method. The age calculation is based on a single 'synthetic' measurement that is reconstructed mathematically by adding the respective U, Th, and He contents of several grains together. Pooling multiple grains increases signal strength and may improve averaging of the alpha particle emission correction error for inhomogeneous mineral structures (Vermeesch et al., 2007). One disadvantage of this approach is the potential for bias in the combined age towards samples with high U, Th, and He contents. Additionally, there may be an exaggeration of the α emission contribution, particularly in the presence of radiation damage and implanted helium in the studied grains.

The isochron age is calculated by determining the slope of the linear approximation of the diagram depicting the relationship between the helium content in the sample and the modern rate of its formation. The presence of U– and Th–rich inclusions may affect the helium age, as reflected in the isochrone plot. The plot will not pass through the origin of He–P coordinates, where P is the modern helium formation rate:

$$P = \left(8 \cdot \frac{137.88}{(137.88+1)} \lambda_{238} + 7 \cdot \frac{1}{(137.88+1)} \lambda_{235}\right)[U] + 6 \cdot \lambda_{232}[Th] \qquad (3)$$

To avoid age bias toward coarse grains, the helium amount is recalculated in concentration units.

To calculate the age of a sample using the parameter P for (U,Th)–He dating, use the following approximate equation, which has high accuracy for samples younger than 1 billion years (Mesters and Dunai, 2005)

$$t = \frac{1}{\lambda_{wm}}\, ln\left(1 + \frac{\lambda_{wm}}{P}[\mathrm{He}]\right) \qquad (4)$$

t represents the age of the sample in million years, λwm is the weighted decay constant, P is the modern helium formation rate in at./million years, and [He] is the helium content of the sample in at.

The formula for calculating the weighted decay constant is

$$\lambda\lambda_{wm} = \frac{\left(8\frac{137.88}{138.88}\lambda_{238}^2 + \frac{7}{138.8}\lambda_{235}^2\right)[\mathrm{U}] + 6\lambda_{232}^2[\mathrm{Th}]}{P} \qquad (5)$$

where λn are the decay constants of U and Th isotopes with mass number, [U] and [Th] are the uranium and thorium contents in the sample (at.).

The central age is recognized as the most accurate method from a mathematical point of view (Vermeesch, 2008). In the calculations, the geometric mean of U, Th, and He contents for individual grains is used. This method is applicable for computing the mean value of grains with varying Th/U ratios using the (U,Th)–He ternary system.

1.3 Noble gas migration models and their limitations

The migration process determines the conditions for the loss of helium from the crystal lattice of a mineral during geologic history. Even a slight increase in temperature up to 100–200°C can cause partial or complete loss of helium, resulting

in an underestimation of the obtained age value (Farley and Stockli, 2002). Migration parameters are estimated empirically or through mathematical modeling (Yakubovich et al., 2010; Flowers et al., 2022).

The method of stepwise annealing is a common empirical approach for determining migration parameters. This involves determining the amount of released helium at a given temperature during gradual heating. The resulting spectra of radiogenic helium release kinetics can be used to calculate kinetic parameters for the mineral.

Currently, two main theoretical approaches are emphasized to describe the migration of helium and other noble gases from the crystal lattice of a mineral.

1.3.1 First order monomolecular chemical reaction model

The single–jump model, also known as the first–order monomolecular chemical reaction model, was initially proposed by E.K. Gerling in 1939. This model gained popularity among Russian researchers and is now commonly used in isotope–geochemical models of Earth's evolution and in the study of helium migration from reactor materials. The model assumes that the crystal lattice of minerals is defective in the region of alpha particle formation. In this model, it is worth noting that the binding energy of atoms in the crystal lattice is around 2–4 eV. On the other hand, the decay of the uranium atom nucleus through alpha particles is characterized by the release of energy, which is approximately equal to 10^8 MeV, and its subsequent dissipation in the mineral structure. As a result, a defect is formed in the crystal lattice where helium atoms can accumulate due to the large amount of energy released during radioactive decay. The energy required for migration is determined by the time it takes for the atom to detach from the accumulation center, which is its escape from the defective position. This explains why a radiogenic atom behaves similarly during migration and simple chemical reactions (Gerling, 1961). The one–jump model is based on the hypothesis that the primary complexity for an atom is the first jump, which is the atom's exit from the energy trap after radioactive decay. Further diffusion from the mineral grain along the disturbed structure requires less energy costs.

1.3.2 Classical Fick diffusion

The alternative model of helium migration is based on Fick's diffusion laws, which describe the change in the concentration of radiogenic gas atoms in minerals due to temperature (Yakubovich, 2013). The size of helium atoms, which is much smaller than the distance between interatomic bonds in minerals, is the key factor in this model. Unlike the single–jump model, this model assumes that the diffusion process incurs the highest energy cost. In the former case, the exit of an atom from the mineral lattice is limited by the time required for its separation from the accumulation center. On the other hand, the diffusion model suggests that the main contribution is made by the time taken for the atom to wander in the grain. The diffusion model assumes that mineral grains are of equal size, spherical or of another specified shape, and have a homogeneous concentration of radioactive and radiogenic isotopes when describing helium migration from minerals. The concentration of remaining gas is determined by a function of the diffusion coefficient, temperature, and size (spherical grain radius) (Fechtig and Kalbitzer, 1966). The fraction of gas lost can be calculated from the laws of classical diffusion (6).

$$F = 1 - \frac{6}{\pi}\sum_{n=1}^{\infty}\frac{1}{n^2}e^{-n^2Bt} \qquad (6)$$

$B = \pi^2\frac{D}{R^2}$, *D – the diffusion coefficient, t – time, R – the grain radius, and n – a natural number.*

1.3.3 Advantages and limitations of the models

The single–jump model offers the advantage of proving multidirectional migration of radiogenic atoms in real mineral structures. It also confirms the existence of defect zones with varying degrees of disorder in the crystal lattice, including primary traps for mobile atoms. The variation of uranium and thorium forms in mineral grains and different energy states of atoms help to clarify the complex kinetics of the migration process. The empirical evidence also establishes the nonhomogeneous distribution of radiogenic helium in the crystal lattice, which is not supported by uranium (Figure 1.2). The mathematical apparatus used to estimate migration parameters from experimental data is characterized by its

simplicity of use. However, the method's resolving power is limited, making it difficult to distinguish between migration processes with different kinetic parameters (Shukolyukov et al., 2009).

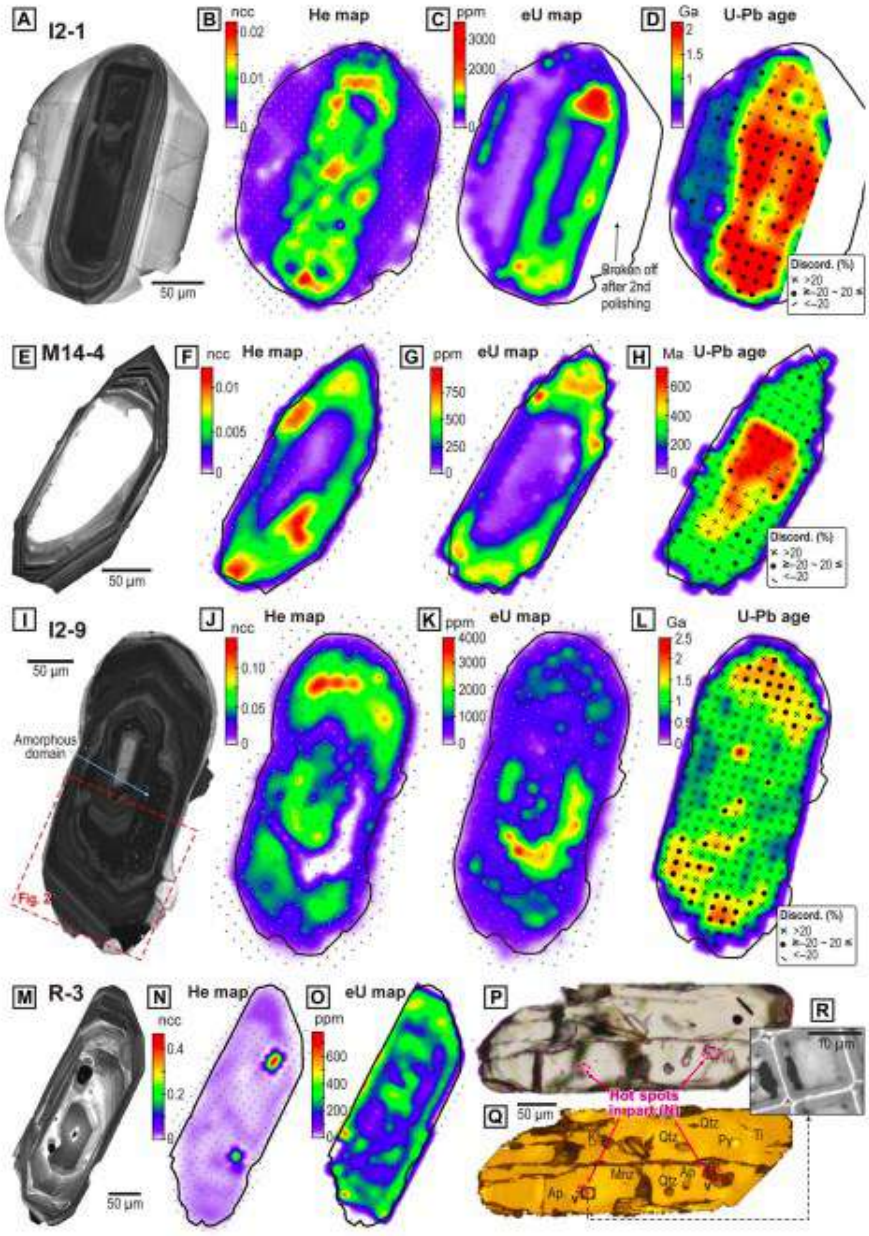

Figure 1.2. – CL images of zircon grains (A,E,I,M) and distributions of helium (B,F,J,N) and uranium(C,G,K,O) contents in them (Danisik et al., 2017)

The model based on the diffusion process is subject to certain limitations. Therefore, grains are approximated by a regular shape, such as a sphere, cylinder, or cube, with a homogeneous distribution of radioactive parent isotopes and radiogenic noble gas isotopes to prevent any disturbance of the diffusion profile. However, interpreting experimental data can be challenging due to the discrepancy between

practical migration conditions and idealized assumptions about the distribution of uranium and thorium in the crystal structure. This distribution is not always homogeneous (Tugarinov and Bibikova, 1980; Shukolyukov, 1970; Krasnobaev, 1986), and the energy position of all atoms of the migrating gas in the structure is also a factor (Shukolyukov et al., 2009). Accordingly, the nonhomogeneous distribution of uranium and thorium can affect the emission of alpha particles, influencing the diffusion behavior and gradient of the helium concentration distribution (Farley, 2002). To address these issues, modeling approaches are used, and in some cases, minerals are irradiated to generate homogeneously distributed 3He isotopes (Flowers et al., 2022).

Migration of radiogenic helium can occur through both mechanisms (Figure 1.3). Limited helium solubility in some minerals can cause saturation of the solid solution with helium, which is then relieved by diffusion towards defects that subsequently serve as a cell of helium accumulation in the crystal lattice (Yakubovich, 2013). Initially, helium diffuses towards energetically favorable positions such as grain boundaries or radiation defects, where it accumulates in the form of atomic clusters. Detaching a helium atom from such a center requires a large amount of energy, which is enough to destroy the bulk defects enclosing the formed clusters.

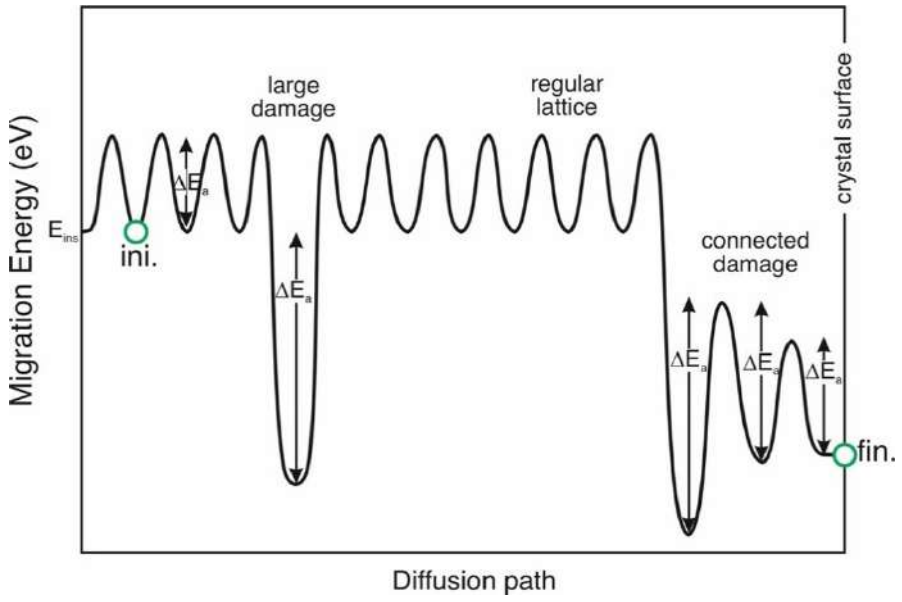

Figure 1.3. – Schematic of the diffusion path (Gautheron et al., 2022). Ea – activation energy, green circle – radiogenic helium atom.

In summary, it is important to note that in practice, using real minerals as examples, each of the above models leads to the calculation of similar values of the migration activation energy (Yakubovich et al., 2010; Reiners, 2005). Therefore, differences in the results will be determined by the interpretation of the data, specifically, whether grain sizes need to be taken into account for subsequent operations. Accordingly, both models are appropriate for their respective fields. However, in the field of low–temperature thermochronology in silicate minerals, the diffusion model (Rosso, 2005) is more commonly used. In describing helium migration from metals, a single–skip model is employed (Shukolyukov et al., 2012ab).

In recent years, there has been an increase in works focused on mathematical modeling of helium migration processes from the crystal lattice of various minerals. These works include those by Balout et al. (2017), Djimbi et al. (2015), Gerin et al. (2017), Gautheron et al. (2020), and Bassal et al. (2022), which have all benefited from the development of modern computing power. The simulations model ideal crystals, which have significantly different helium migration from natural samples. However, they help establish factors important for understanding migration processes, such as the influence of impurity elements and the presence of defects on helium conservation in minerals.

1.4 Challenges of using the (U,Th)–He system and their solutions

1.4.1 Nuclear recoil effect

The (U,Th)–He system presents a challenge in interpreting results due to the presence of the alpha–recoil effect. When the parent isotope undergoes radioactive decay, it releases energy of approximately 5–6 MeV, with binding energy values of 2–4 eV (Yakubovich, 2013). As a result, the radiogenic helium nucleus has a relatively high energy and requires a distance of tens of micrometers (11–34 μm) to be completely trapped in the mineral (Zeigler et al., 2010). The selection of suitable grains for analysis is limited by the presence of the alpha–recoil effect. Grains that are less than 30 μm are not suitable for analysis because they do not allow for helium

accumulation, as there is a high probability of radiogenic isotope escape from the grain into the environment.

In addition to the potential loss of helium, there is also the risk of alpha particle implantation (alpha–ejection) from neighboring minerals near the dated sample (Farley, 2000). This can result in overestimated age measurements.

For grain sizes larger than 200 μm, the contribution of the ejected and implanted component can usually be disregarded. For smaller grains, the issue is resolved by abrading the edge by 15–20 μm (Farley et al., 2000; 2002), or by applying a mathematical correction based on grain size and shape to account for the fraction (FT) of α U and Th decay particles that are not retained in the crystal (Figure 1.4; Farley et al., 1996).

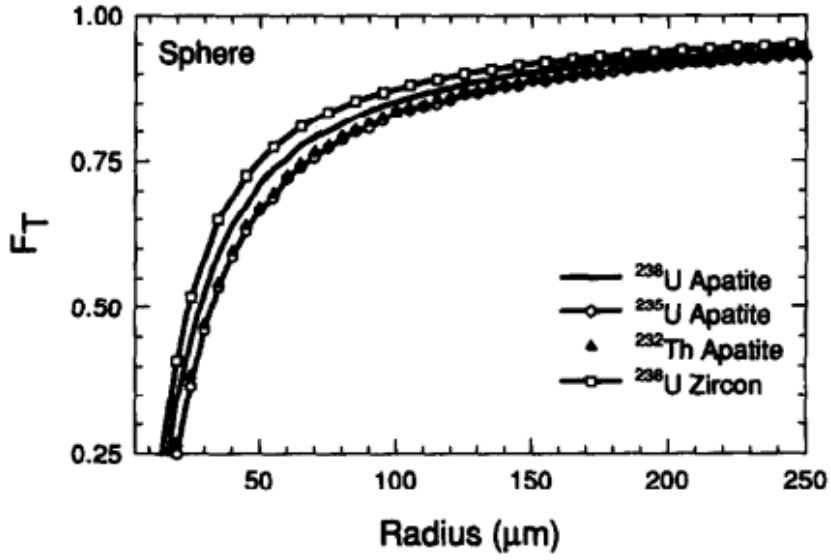

Figure 1.4. – Fraction of retained helium in spheres of different radius for ^{238}U, ^{235}U, and ^{232}Th decay chains in apatite and zircon (Farley et al., 1996). The distribution of the parent isotopes is homogeneous.

1.4.2 Gas–liquid inclusions

Mineral cavities frequently preserve mineral–forming solutions that were trapped during their growth, reflecting the environmental conditions of formation. These cavities also fill secondary fractures that indicate changing physicochemical conditions. Inclusions in these cavities may contain trapped helium, which can cause an increase in (U,Th)–He age. Magmatic fluid typically has a low ^4He content (10^{-8}–10^{-10} cm^3/g) compared to the average radiogenic helium concentrations in

minerals, which exceed 10^{-6} cm^3/g (Yakubovich et al., 2019). However, in certain geological settings, such as when a mineral crystallizes in the presence of groundwater, the concentration of trapped He can be significant (Cabral et al., 2022). If a significant fraction of trapped helium is present, the derived age values may be overestimated and not reproducible. This behavior can be identified by the lack of correlation between U and He contents.

1.4.3 The problem of radiation damage

A series of radioactive decays of uranium and thorium cause radiation damage through alpha–particle recoil, resulting in alpha damage. These defects act as isolated traps for diffusing helium atoms, which can affect the helium diffusion characteristics by slowing down the normal diffusion jumps, leading to the retention of radiogenic helium. This phenomenon has been studied by Zeitler (2014) and Gautheron et al. (2022). Therefore, the migration rate of helium in a mineral is not constant, and its closure temperature is dependent on the time elapsed since its formation. If the rock cools rapidly or has low U and Th contents, the impact of alpha damage on helium age is insignificant.

1.5 Current applications of the (U,Th)–He isotope system

The (U,Th)–He method is a thermal or geochronometer used to determine the age of geologic events and decipher the thermal history of a mineral. It covers a wide range of temperatures and time periods, applicable for ages ranging from 4.5 billion years to 2 thousand years (Min et al., 2003; Marsden et al., 2021) and temperatures ranging from 20 to 300°C.

The (U,Th)–He method is commonly used to reconstruct the evolution of orogenic regions, estimate cooling rates of magmatic bodies, and determine the thermal history of sedimentation basins (Farley, 2002; Reiners, 2005; Aciego et al., 2003; Dunai, 2005; Wolf et al., 1998). Iron oxide dating results provide a record of weathering processes (Farley et al., 2018; Flowers et al., 2022). The method enables the inference of eruption time for young volcanoes and the formation of young rupture faults, as well as the age of archaeological finds (references in Yakubovich, 2013). The data obtained can be used to model the evolution of sedimentary systems

and determine the genesis of mineral deposits. Analysis of extraterrestrial material can be conducted to assess the history of impact (Kelly et al., 2018; Tremblay and Cassata, 2020). The method has various applications, including determining paleofire distribution fields and paleolandscape reconstruction (Reiners, 2005). Additionally, computer modeling can be used in conjunction with track and/or other geochronological research methods to generate different scenarios of rock cooling and exhumation (Dunai, 2005; Wolf et al., 1998).

CHAPTER 2. (U,Th)–He isotope system in pyrite

2.1 Mineralogy of pyrite

Pyrite has a crystal structure based on a cubic face–centered lattice, which is characteristic of the NaCl structural type (Betekhtin, 2008) (Figure 2.1). The anionic group $[S_2]^{2-}$ is formed by close pairs of sulfur ions. The crystal habitus is mainly cubic, pentagondodecahedral, and octahedral, with combinations of their forms, pseudomorphs on minerals, and organic residues also occurring. Pyrite is a semiconductor based on its electrical properties. The chemical formula FeS_2 is considered ideal, with characteristic impurities including Co, Ni, As, and Sb, and less frequently Cu, Au, and Ag. These impurities are scattered throughout the composition as small mineral inclusions or fine impurities.

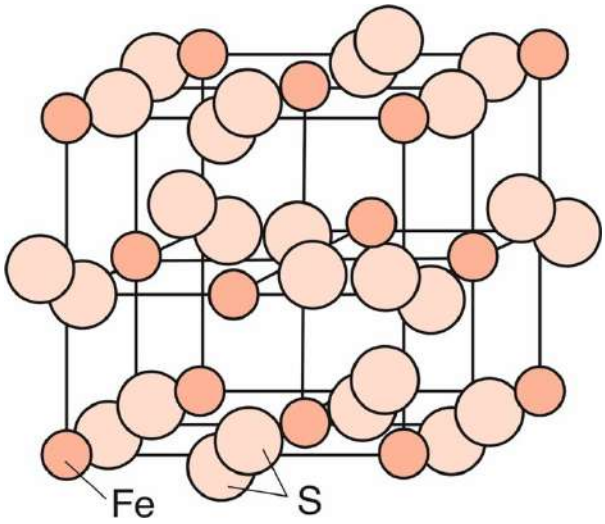

Figure 2.1. – Scheme of crystal structure of pyrite (Betekhtin, 2008)

Pyrite is a frequently occurring ore mineral that forms in various geological settings (Betekhtin, 2007; Pshenichkin et al., 1976; Reich et al., 2013) due to the redistribution and concentration of matter during diagenesis or crystallization from hydrothermal solutions. In the oxidation zone, pyrite is unstable and transforms into iron (II) sulfate, which then oxidizes to iron (III) sulfate in the presence of excess free oxygen. Under hydrolysis conditions, the resulting product transforms into limonite and releases sulfuric acid, forming pseudomorphoses on pyrite. The stability of pyrite in oxygen–free conditions is limited by its thermal decomposition temperature into pyrrhotite and sulfur (approximately 500–600°C).

2.2 Stability of radiogenic helium in pyrite

Pyrite exhibits high thermal stability of radiogenic helium (Yakubovich et al., 2019). The stability of radiogenic helium in minerals is determined by their high bulk density and electrical conductivity (Yakubovich et al., 2015), which prevent helium dissolution. As a result, helium atoms occupy energetically favorable positions in various defects (Shukolyukov et al., 2012). This location of helium limits its diffusion, ensuring high conservation in the mineral structure. This effect is most pronounced for nugget metals (Shukolyukov et al., 2012ab).

The increase in the conductivity of semiconductor compounds is directly dependent on the temperature increase, which allows for the thermal preservation of helium in semiconductor compounds. The stability of helium in a natural conductive nonmetallic compound, sperrylite (PtAs2), was experimentally demonstrated, taking into account the peculiarities of the conductivity of compounds (Yakubovich et al., 2015). This information enables the consideration of other minerals with similar crystallographic structures as geochronometer minerals, including pyrite. Pyrite has been identified as the most promising sulfide mineral for (U,Th)–He geochronometry based on migration characteristics and helium release kinetics (Yakubovich et al., 2019). The high preservation of helium in pyrite is supported by its cubic lattice, high packing density of atoms, and electrical conductivity. These three conditions are necessary for complete preservation of helium in the mineral. The example of pyrrhotite and chalcopyrite proves the opposite. These minerals have a high packing density of atoms and specific conductivity, but possess low activation energy due to the monoclinic singony (Yakubovich et al., 2019). Helium is retained in pyrite up to the temperatures of thermal transition to pyrrhotite with sulfur release. Abrupt explosive release of helium occurs at temperatures around 450°C. High frequency factor values confirm that pyrite crystal lattice alteration activates helium migration from the mineral.

2.3 Forms of uranium and thorium in pyrite

Pyrite can contain uranium in the form of inclusions of primary uranium or uranium isomorphous minerals, or in sorbed form as a relatively homogeneous impurity (Baranov and Vertepov, 1966). The most common inclusions are uraninite, monazite, xenotime, rutile, zircon, and apatite. The concentration of radioactive isotopes depends on the ore type and can vary from μg/t to g/t (Baranov and Vertepov, 1966; Large et al., 2014). On average, pyrite contains 0.2 to 11 μg/g of uranium (Melekestseva et al., 2014; Yakubovich et al., 2020). Uranium accumulation in mineral inclusions smaller than 10 μm does not occur due to the peculiarities of the α–recoil effect. Radiogenic helium is implanted into the crystal structure of the mineral, and the (U,Th)–He age reflects the timing of helium accumulation in pyrite.

2.4 Gas–liquid inclusions in pyrite

The grains may contain gas–liquid inclusions, in addition to mineral inclusions, that trap excess helium with the fluid. The helium isotopic composition of these inclusions has been used to reconstruct fluid sources (Stuart et al., 1995; Kendrick et al., 2001; Burnard and Polya, 2004). Typically, the concentration of helium in magmatic fluid does not exceed 10^{-8}–10–10^{-10}cm3/g (Bortnikov et al., 2000; Luders and Niedermann, 2010; Yakubovich et al., 2019). Pyrite grains with radiogenic helium concentrations greater than 10^{-8} cm^3/g are suitable for (U,Th)–He age determination. Figure 2.2 illustrates the relationship between the concentration of radiogenic helium in pyrite, its age, and uranium content. For the average range of uranium concentrations in pyrite, the mineral suitable for dating should be at least 10 million years old to avoid overestimation and ensure reproducibility.

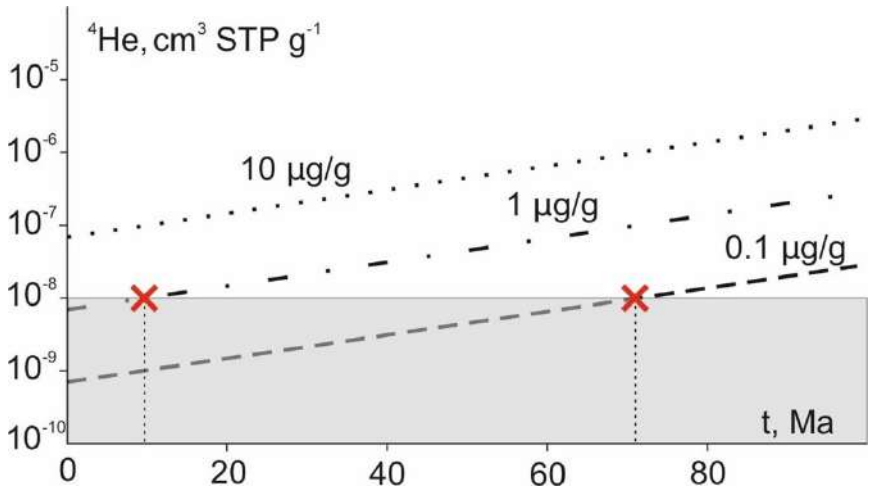

Figure 2.2. – Dependence of 4He concentration on age and uranium content in pyrite, where gray indicates the range of helium concentrations characteristic of fluid inclusions; red – threshold values of age suitable for dating based on uranium content.

CHAPTER 3. LABORATORY RESEARCH METHODS

3.1 Methods of field work and selection of material for research

The author conducted geological observations and collected factual material as a member of the field team of IGEM RAS during field work in 2018–2019 and 2021 in the northern part of the Voykar zone on the eastern slope of the Polar Urals in the Toupugol–Khanmeishor ore district. The area includes the Au–Fe–skarne deposit Novogodnee-Monto, the gold porphyry deposit Petropavlovskoe, and the gold ore occurrence Kariernoe.

During the pre–field season preparation, the author reviewed literature and stock data related to the object of study. Additionally, the author familiarized themselves with the collection of samples and previous works. The field work involved documenting natural outcrops and collecting petrographic and geochemical samples through reconnaissance routes that were approximately 10 km in length. Field studies were conducted with consideration of the actual outcrop of the territory. Special attention was given to the signs of hydrothermal alteration of volcanogenic–sedimentary rocks and the distribution of sulphide mineralization near tectonic zones and intrusive contacts. During the traverses, macroscopic diagnostics were performed, and structural and textural features were noted. The size and occurrence parameters of the host rocks were also determined. During macroscopic diagnostics of samples, we determined their mineral composition, textures, and macrostructures. We paid increased attention to the degree and nature of superimposed alteration. We collected characteristic representative samples at each observation point with appropriate GPS georeferencing.

3.2 Methodology of petrographic studies

The mineral composition of the host rocks was determined using optical microscopy methods. The microscopic analysis consisted of diagnosing the rock, identifying the mineral composition, studying mineral relationships (determining structure and texture), determining forms of separation and sizes of minerals, and quantitatively counting minerals. The study analyzed 92 polished stone splits

selected during field work and from the collection of I.V. Vikentyev (IGEM RAS). Transmitted light was used with a polarizing microscope (Leica DM750P) at the Department of Mineralogy, Crystallography, and Petrography (MCP) at St. Petersburg Mining University. X–ray diffraction methods of matter research were conducted on a Leica microscope at the resource center of St. Petersburg State University.

To achieve the most precise results in the petrographic study, a detailed characterization of the rock types was performed using the 'group description' method (Naumov et al., 2017). Following this methodology, each schist was described individually to compile a comprehensive characterization of the rock group. In determining the minerals comprising the rocks, only the necessary properties for identification were considered. These properties include mineral coloration, refractive index, relief, shagreen surface, cleavage, birefringence value, extinguishing character, elongation sign, optical axis, and optical axis angle value. Conclusions about the shape and size of the outcrops were drawn by comparing different cross sections of a particular mineral. The identification of rock structures and textures was based on several features, including the degree of crystallinity, absolute size of mineral grains, and the shape, relationships, and orientation of grains in space. Mineral content in the slides was quantitatively calculated through visual estimation using low magnification lenses (10x, 20x). The estimation presents the average measurements of quantitative relations among minerals in various fields of view. The results are presented as a percentage relative to the total area of the slip, which is considered 100%. Photographs of the sections were taken using a Leica DM4P microscope equipped with a camera for graphical imaging. The recorded features of the structure and composition of a particular rock type are the most representative and characteristic.

3.3 Scanning Electron Microscopy

Monofractions of pyrite were isolated from rocks using heavy liquid separation (CH_3Br) at IGEM RAS (Moscow) for (U,Th)–He dating. To determine

the form of uranium and thorium occurrence in pyrite, 110 grains ranging from 100–500 μm in size were selected and mounted in epoxy resin washers. The washers were then polished using 6 and 3 μm sandpaper and diamond slurry. A scanning electron microscope equipped with an energy dispersive X–ray spectral analysis detector AzTec Energy 350 in the resource center 'Geomodel', St. Petersburg State University (St. Petersburg, analyst N.V. Vlasenko) was used for microanalysis.

The study of pyrite grains focused on the composition and size of uranium–bearing mineral inclusions, which directly affect the results of (U,Th)–He dating. The pyrite's generation was diagnosed by considering the paragenesis of ore minerals and the distribution of chemical elements. Silicate inclusions were noted to prevent distortion of the dating results and to enable reconstruction of the ore formation's geologic history.

3.4 (U,Th)–He Dating Technique

3.4.1 Sample Preparation

For (U,Th)–He dating, pyrite crystals larger than 250 μm without visible inclusions were selected using a stereomicroscope with a magnification of up to 5 times (IPGG RAS). Each sample consisted of a suspension of 1.5–2.5 mg of substance, on average containing 4–5 pyrite grains. To determine the He, U, and Th contents in each sample sequentially, we placed the sample in a quartz ampoule and sealed it under forevacuum conditions (10^{-3} torr) using a LIGA oxygen–hydrogen torch (Figure 3.1a). The crystallochemical properties of quartz allow helium released during heating to freely diffuse through the walls of the ampoule, while thermal decomposition products of pyrite (pyrrhotite, sulfur) containing uranium and thorium impurities remain inside the ampoule (Figure 3.1b).

Figure. 3.1. – Pyrite sample in a quartz ampoule. a – pyrite before annealing; b – decomposition products (pyrrhotite and sulfur) after the experiment.

3.4.2 Determination of radiogenic helium concentration

The microquantities of radiogenic helium concentration were measured using a highly sensitive mass spectrometer MSU–G–01–M at IPGG RAS, as shown in Figure 3.2. A cuvette containing the prepared sample is placed inside a rhenium cylinder using a special device made of refractory material. The language used is clear, concise, and objective, with a formal register and precise word choice. The sample is gradually heated in static mode under high vacuum conditions (2×10^{-7} torr). High vacuum is achieved through a three–stage pumping process. First, a mechanical oil pump provides forvacuum. Second, a diffusion oil pump maintains high vacuum. Finally, getter pumps (SAES NP 10) in the extractor and analyzer sorb the active gases (H_2, N_2, O_2, etc.) released during the experiment. Helium atoms are ionized through electron impact. The charged particles enter the analyzer and are separated based on their mass–to–charge ratio under the influence of a magnetic field. The focused ion beams entering the receiver were registered by the secondary electron multiplier.

Figure. 3.2. – Magnetic–sector mass–spectrometric complex MSU–G–01–M (IPGG RAS)

To remove the low–temperature atmospheric helium remaining in the ampoule after pumping, the samples are heated to 200ºC for 30 minutes. The samples are then gradually heated in steps of 200–250ºC for 10 minutes each to 1100°C, allowing complete helium release from the pyrite. The quantity of helium released was recorded after each heating step to estimate the amount of helium released in the relatively low temperature range (<500ºC). The measurements were conducted using the following analyzer settings: emission current of 0.05 mA, acceleration voltage of 2.5 kV, and counting time of 300 msec.

To determine the representative blank of the procedure, empty quartz ampoules were utilized. The blank signal was -10^{-10} cm^3, with an instrument sensitivity of 10^{-13} cm^3 ^4He per pulse (counting time 300 msec). The reliability of analytical 4He measurements was checked using a certified standard, Santiago River platinum (39.6 ± 0.7 Ma; Yakubovich et al., 2023).

3.4.3 Determination of Uranium and Thorium Isotope Content

The isotope dilution method was used to determine the uranium and thorium content. The degassed quartz ampoule was completely decomposed with the thermal decomposition products of pyrite containing uranium and thorium impurities in a mixture of acids (0.4 ml tsar vodka, 0.5 ml conc. HF, 0.05 ml HClO4) with the addition of 1 drop of mixed tracer 230Th–235U in closed Teflon vials at a

temperature of 180°C for 24 hours. The samples were dried on a hot plate at 200 C and the resulting dry residue was transferred to a 2 mL solution of 5% HNO3 for further U and Th measurements. The isotope ratios of 235U/238U and 230Th/232Th were measured using an ELEMENT XR ICP MS magnetic sector mass spectrometer at GEOCHI RAS in Moscow by analysts M.M. Podolskaya and M.O. Anosova (Figure 3.3). Simultaneous experiments were conducted with Durango apatite, which is recognized as the international standard for the (U,Th)–He method (31±1 Ma; McDowel et al., 2005), to evaluate the accuracy of the analytical procedure. The complete chemical blank of the procedure, including background U and Th concentrations, was determined from blank quartz ampoules dissolved by a similar technique. The blank values were -1×10^{10} for U and 6×10^{10} for Th.

Figure. 3.3. – ELEMENT XR magnetic–sector inductively coupled plasma mass spectrometer (GEOHI RAS)

CHAPTER 4. GEOLOGICAL SKETCH

4.1 Geological Situation of the Toupuogol–Khanmeyshor Ore District

The studies were conducted in the Toupuogol–Khanmeyshor ore district, which is situated in the northern part of the Voykar zone of the East Ural megazone of the Polar Urals (Figure 4.1). This region is one of the less explored segments of the Urals. The Voykar zone is located south of the Sob transversal uplift and north of the Khulga River. It has a submeridional (S–SW) strike and its structure includes Paleozoic paleoceanic and paleostrovoductal formations thrusting along the Main Ural Fault (sutura) over the Late Precambrian–Paleozoic formations of the West Ural Megazone, which represents the deformed edge of the East European platform. This information is based on the works of State (2007, 2014), Kuznetsov and Romanuk (2014), and other references cited in this paper. The northwestern part is composed of Early Paleozoic oceanic formations of ophiolite association, which are represented by metamorphosed hyperbasites and gabbroids. These formations have been extensively studied by Perevozchikov (1974), Savelyev (1974), Savelyev and Savelyeva (1977), Savelyeva (1987), Dobretsov et al. (1977), Yazeva and Bochkarev (1984), Remizov (2004), and others (Figure 4.1). The southeastern part of the zone is dominated by Late Ordovician–Middle Devonian island–arc rocks of the Malouralsky volcanic–plutonic belt. The island arc intrusives and associated volcanogenic formations extend more than 250 km N–NE in the form of a narrow band 10–40 km wide. These formations are the northern continuation of the Tagil Zone structures of the Middle and Northern Urals (Kuznetsov and Romanuk, 2014).

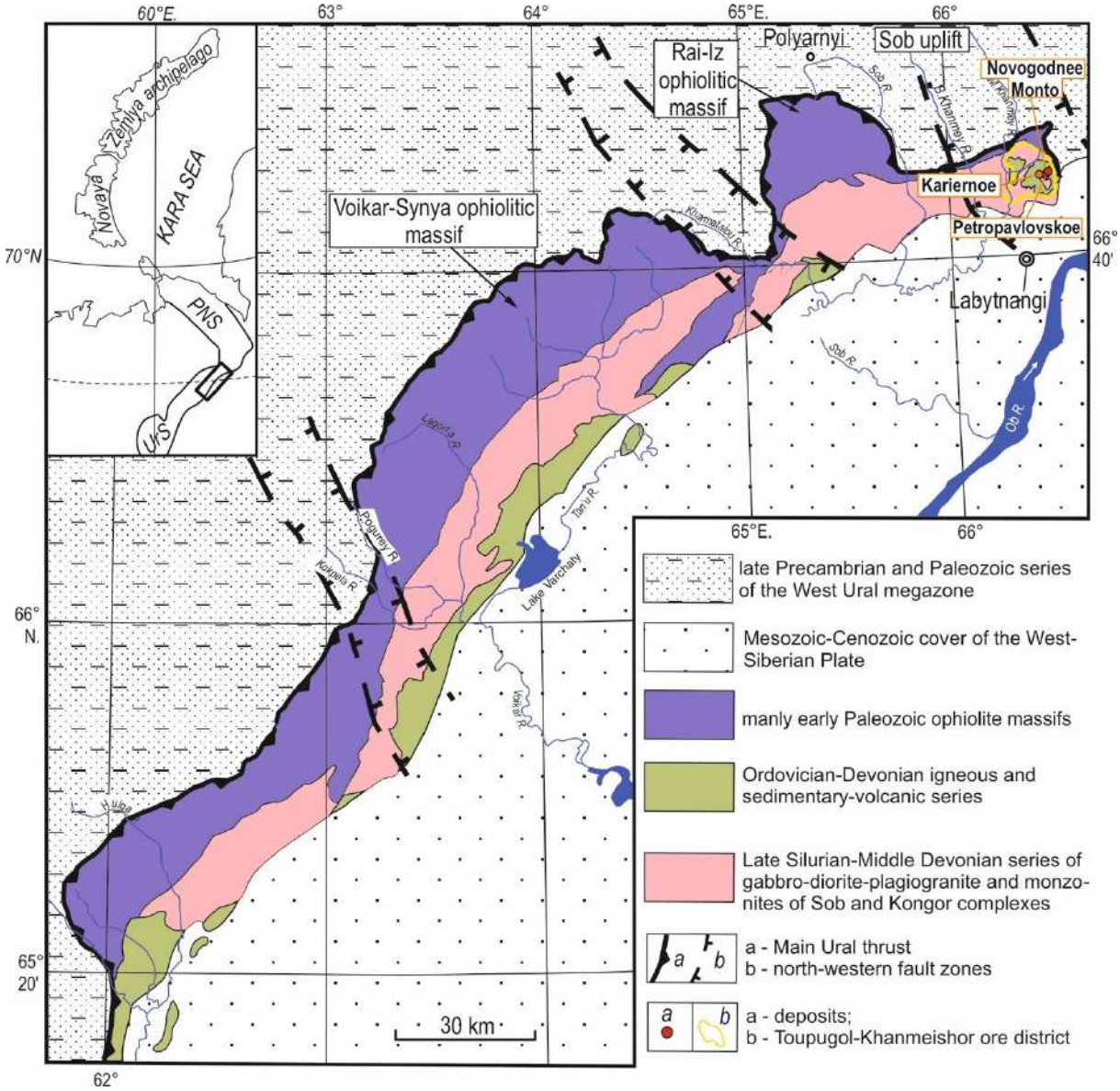

Figure 4.1. – Geological position of the Toupugol–Khanmeyshorskoye gold ore district in the structures of the eastern slope of the Polar Urals, compiled using data (State...2007; 2014; Sobolev et al., 2017 and references in these papers).

The Toupugol–Khanmeishor gold ore district is located at the northeastern end of the Voykar zone, among the Paleozoic Island arc formations. Within this district, the Novogodnenskoe ore field (Figures 4.1; 4. 2) contains two identified gold deposits in the Polar Urals: Petropavlovskoe gold–porphyry (26 t Au) and the Novogodnee-Monto gold–iron–skarn (7 t Au), as well as several ore deposits (Karachentseva, Kariernoe et al) (Vikentyev et al., 2017).

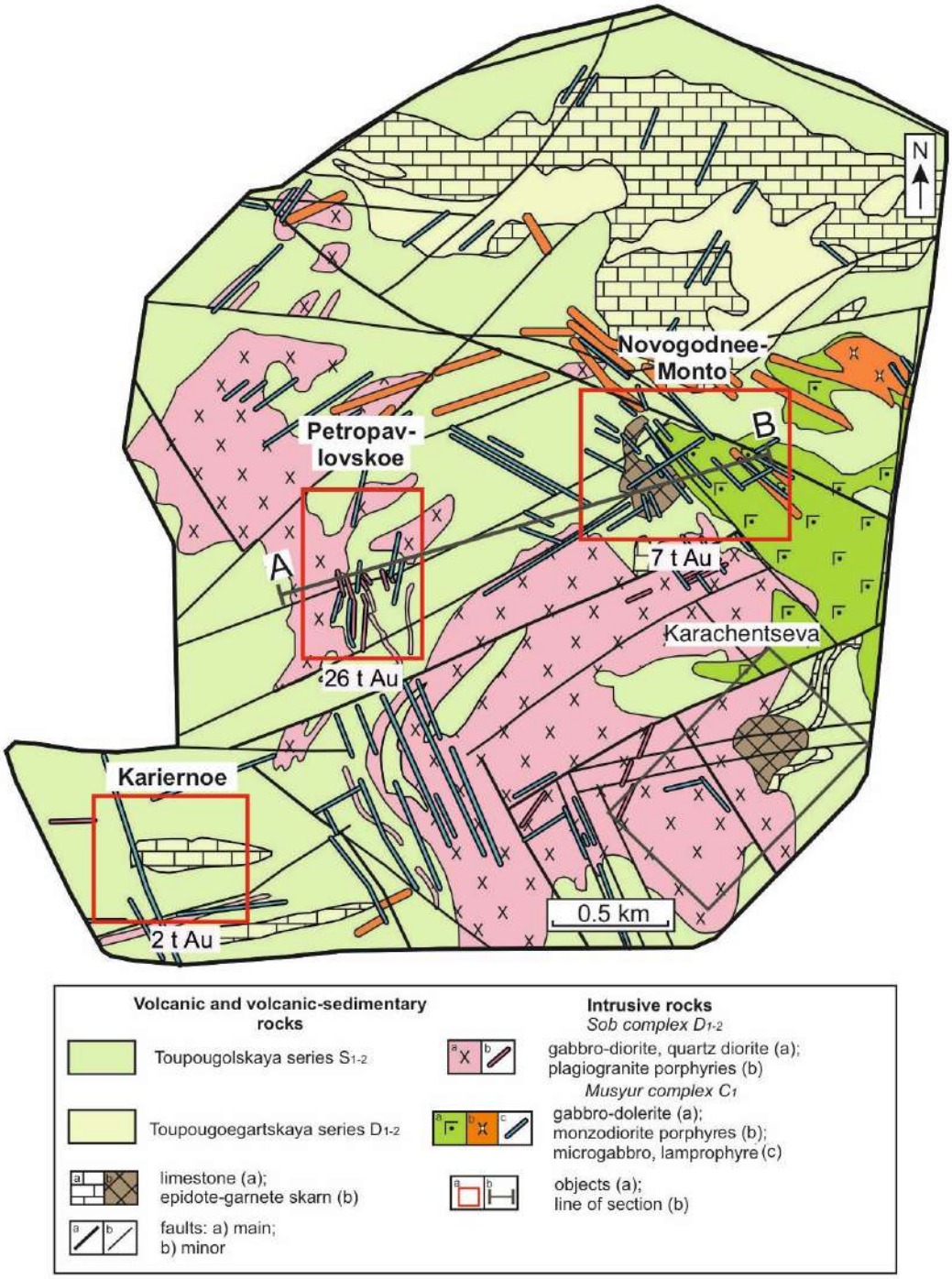

Figure 4.2. – Geological map of the Novogodnenskoe ore field according to (Volchkov et al., 2008) with modifications.The ore field's structure comprises the following strata, listed from bottom to top: Sokolinskaya ($O_{2–3}$ sk), Khanmeishorskaya ($O_3–S_1$ hn), Toupugolskaya ($S_{1–2}$ tp), and Toupugol'egartskaya ($D_{1–2}$ tg) (Figure 4.3) (Prymanosov et al., 2004; Zyleva et al., 2014).

The rocks in this area that contain ore are Silurian–Middle Devonian island–arc volcanogenic and sediment–volcanogenic rocks, which consist of tuffs, tuffites, and lavas of basalt–andesite composition, as well as limestones from the Toupugolskaya and Toupugol'yegartskaya strata. Additionally, Early–Middle

Devonian plagiogranitoids from the Sobs Batholith penetrate these rocks. The rocks of volcanogenic and volcanogenic–sedimentary origin form a monocline that is complicated by a series of flexural bends with a southeastward dip (Figure 4.4).

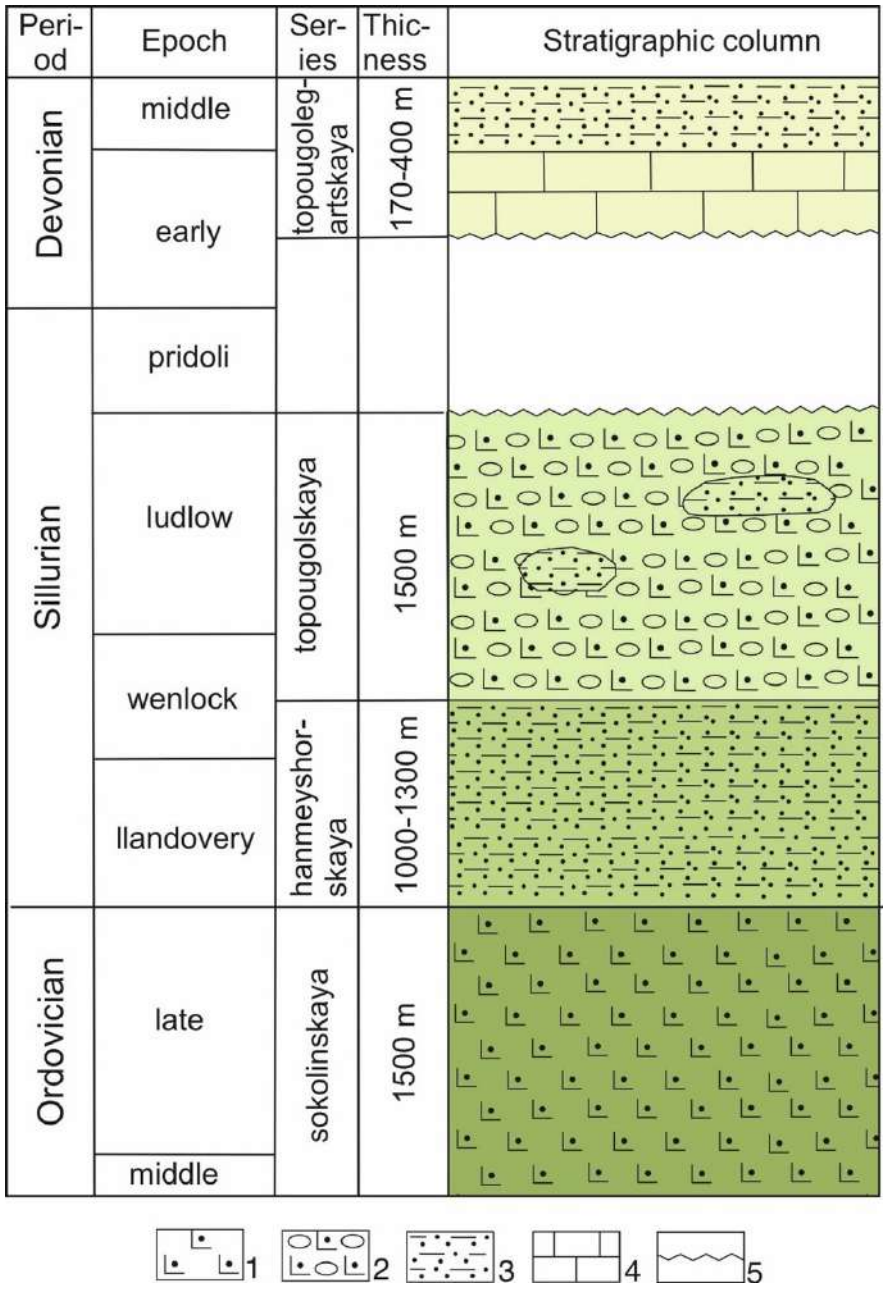

Figure 4.3. – Stratigraphic column for the Toupugol–Khanmeishor ore district of the Voykar zone of the Polar Urals (after (State..., 2007, 2014; Sobolev, 2019) with modifications: 1 – lavas of basic composition; 2 – interbedded basalts and basalts, andesites and their tuffs; 3 – interbedded sandstones and siltstones; 4 – limestone; 5 – break in sedimentation, angular unconformity.

The **Toupugol Formation** ($S_{2–3}$ tp) is exposed in the section along the Sokoliny and Khanmeishor creeks. It consists of lavas and clastolavas of aphyric, pyroxenophyric basalts, pyroxene–plagiophyric andesibasalts, less frequently

andesites, and their tuffs. Lateral replacement of volcanics by volcanomictic and polymictic variegated gravels, often with fragments of reefogenic limestones of Venlockian–Ludlovian age, sandstones, siltstones, and limestones express intraformational erosions (Zyleva et al., 2014). Stratiform sulfide mineralization, predominantly pyrite in composition, is hosted by layers of thinly clastic carbonate rocks (Zyleva et al., 2014). The rocks of the Toupugol formation are dissected by veins with hydrothermal-metasomatic mineralization: chlorite-sericite-quartz, quartz-sericite-chlorite, carbonate-quartz-sericite, chlorite-epidote. Additionally, the contact zones between the rocks and intrusions exhibit brecciation and orogenization. The age of the Topougol strata rocks was determined based on the findings of fauna, including foraminifera, corals, brachiopods, crinoids, and conodonts, in limestones, sandstones, siltstones, and flints (Zyleva et al., 2014). The sedimentary packs are rhythmically layered and cumulatively reach 500 m, with a total formation thickness of 1500 m.

The **Toupugoljegarta Formation** ($D_{1–2}$ tg) is exposed by mine workings and boreholes in the area of Mt. Toupugol, as well as in local quarries of building stone (Zyleva et al., 2014). The formation comprises of carbonate and terrigenous flyschoid rocks that overlie the volcanics of the Toupugol Formation, despite stratigraphic disagreement. The lower section consists of white and pinkish organogenic limestones, ranging from 50–170 meters in thickness, with occasional inclusions of limestone breccias and conglobreccias. These limestones are overlain by ribbon–layered cherry clayey–siliceous and calcareous–clayey siltstones and silt–sandstones. The section consists of layered gray sandstones with occasional packs of alternating gray and variegated polymictic sandstones, siltstones, conglomerates, and gravelites containing fragments of rifted limestones, andesites, basalts, and their tuffs. Locally, weathering crusts up to 0.2 m thick are observed at the contact between the Toupugol and Toupugoljegart strata (Zyleva et al., 2014); metasomatic processes are not present. The Toupugoljegarta Formation rocks' age is Ems–Eifelian, determined by foramenifera, stromatoporoids, tabulate corals, rugose corals, brachiopods, crinoids, algae, radiolarians, and conodonts finds

(Pryamonosov et al., 2009; Dushin et al., 2014; Plotitsyn et al., 2022). The strata's total thickness ranges from 80 to 295 m.

In the studied ore district, the Soba batholith is the primary ore–magmatic source. It is composed of Early Devonian gabbroids and plagiogranitoids, as shown in Figure 3.4. According to the latest legend of the Polar Urals series of Gosgeolkarta–200 sheets (State..., 2007, 2014), the Soba complex is divided into three intrusive phases. The intrusion is composed of three phases. The first phase is represented by porphyritic hornblende gabbro, which most often occurs as xenoliths in rocks of the second phase. The second (main) phase is composed of diorites, quartz diorites, and tonalites, and it makes up the overwhelming part of the intrusions. The third intrusive phase is represented by numerous low–thickness dikes of hornblende quartz diorite–porphyrites, tonalite–porphyries, plagiogranite–porphyries, and aplitic leucoplagiogranites. The Paleozoic formations in the area are interrupted by a sill of gabrodolerites and dikes of dolerites, montsodiorite porphyries, and lamprophyres. The sources cited for this information are Mansurov et al. (2017) and Sobolev et al. (2020). These formations are commonly attributed to the Early Carboniferous Musyur (Malokhanmean) complex, which is associated with the accretion of the Polar–Ural island arc and the formation of the Early Ural orogen.

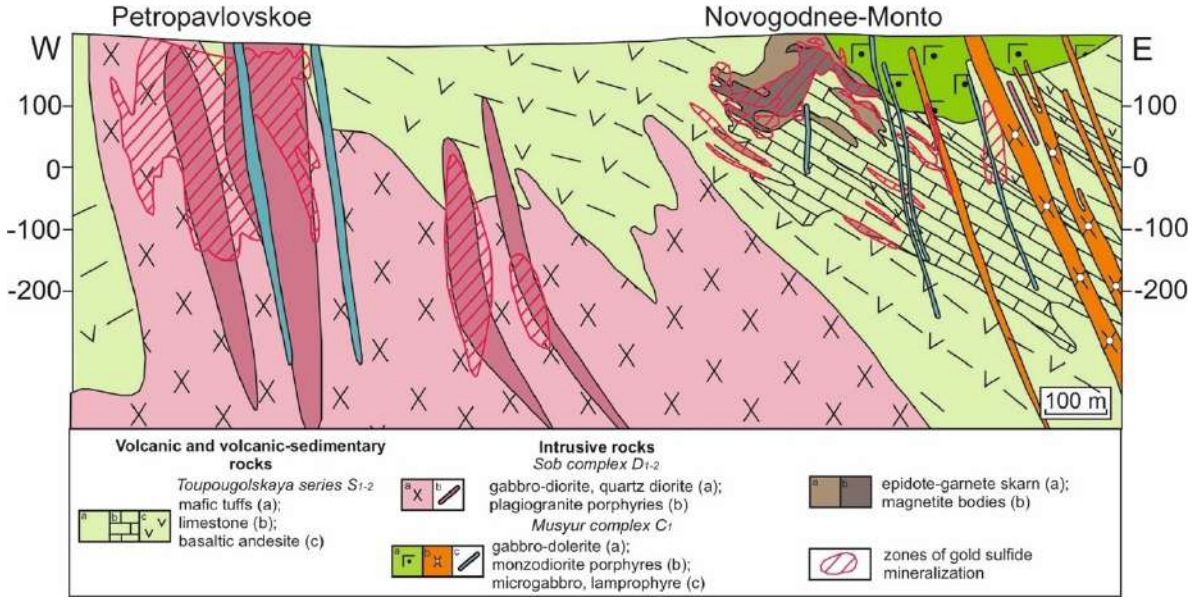

Figure 4.4. – Geologic section of the Novogodnenskoe ore field along the A–B line (Figure 4.2) (according to (Volchkov et al., 2008) with modifications).

The area under study is situated in a long–standing tectonic zone and is characterized by a mosaic–block structure resulting from a combination of disjunctive faults with different orientations, including east–northeast and northwest (submeridional) strikes. The first type of tectonic disturbances is represented by steeply dipping faults and shears (Volchkov et al., 2008). The main ore–bearing structures are the north–west strike–slip faults, which coincide with the orientation of basite dikes of the Musyur complex and zones of vein–vein and vein–embedded mineralization.

4.2 Geodynamic model of Voykar structural–formation zone formation

Previous works proposed various ideas about Paleozoic geodynamics of the Polar–Ural region (Yazeva and Bochkarev, 1984; Didenko et al., 2001; Remizov, 2004; Samygin and Burtman, 2009; Kuznetsov and Romanuk, 2014). N.B. Kuznetsov and T.V. Romanuk's work (2014) outlines a modern concept of geodynamic evolution of the region, summarizing geological and modern analytical data. The Late Cambrian marks the beginning of Ural's history with continental rifting at the Ural margin of the Arct–Europe. During the Early Ordovician period, the process of rifting was replaced by oceanic spreading. This resulted in the detachment of a fragment of continental lithosphere from the Ural margin of Arct–Europa, which led to the opening of the Voykar basin with oceanic–type crust. At the beginning of the Silurian period, the Caledonian orogeny caused Arct–Europe to become part of Arct–Laurussia. During the Silurian period, the oceanic lithosphere of the Ural paleoocean began to subduct under a detached fragment of the continental lithosphere. This process led to the formation of the Polar–Ural island–arc system and the back–arc basin. The Sob–Maloural volcanic–plutonic belt complexes were formed in the subduction zone until the beginning of the Carboniferous. During the latter half of the Carboniferous period, the island arc accreted and the Voykar basin closed. The Sob–Maloural volcanic structure was thrust over the Voykar ophiolites and then pushed onto the Uralic margin of Arct–Laurussia. The end of the Carboniferous period marked the beginning of the main

Ural collision, which lasted until the Early Permian. This was the collision of the Ural margin of Arct–Laurussia with the Siberian–Kazakh–Kyrgyz continent. The Ural orogeny was accompanied by the introduction of collisionial granitoids.

Recent studies have corrected this model. Sobolev et al. (2017) and Shadrin and Sobolev (2017) showed that subduction processes in the Polar–Ural region began significantly earlier than the Caledonian orogeny, in the middle–late Ordovician. It was demonstrated that the final occurrences of island–arc magmatism in the Voykar zone ceased at the boundary of the Middle and Late Devonian, rather than in the Early Carboniferous (Sobolev et al., 2018). Additionally, the accretion of the island arc to Arct–Laurussia took place earlier, in the Early Carboniferous (Sobolev et al., 2020).

4.3 Geological structure of ore objects

The discovery of gold ore objects in the Toupugol–Khanmeishor ore district dates back to the end of the 20th century. In 1993, during geological exploration, high gold content were found in the area of the future Novogodnee-Monto deposit (7 t Au), which was previously classified as an iron ore contact–metasomatic object. In 2004, appraisal work was facilitated by the prospectivity of the deposit, leading to the identification of the Petropavlovskoe deposit (26 t Au) as an independent large–volume object due to its western mineralized zone. The gold deposits garnered attention from various organizations, including CNIGRI, OJSC Yamalzoloto, OJSC Yamalskaya GK, OJSC PUGGP, LLC Yamalgeo, LLC NPO Geosphere, IMGRE, GIN RAS, IG Komi NTs Ural RAS, IGEM RAS, UGGU, RUDN, and others (Vikentyev et al., 2017). Several occurrences of ore were identified in the ore district, including the Kariernoe prospect (5 t Au by P_2 category), which is located 2 km southwest of the Novogodnego–Monto deposit and is considered promising.

4.3.1 Kariernoe ore deposit

The Kariernoe ore deposit is situated on the southwest flank of the Novogodnee ore field (Figure 3.2). The host rocks are Upper Venlock–Ludlovian (Pryamonosov et al., 1994; Dushin et al., 2014) volcanogenic–sedimentary rocks

(flyschoids, polymict breccias with fragments of volcanogenic, intrusive and carbonate rocks) and Toupugol Formation volcanogenic rocks of basalt–andesite formation (Figure 3.5). The stratified formations are located in the roof of the Sob batholith, a multiphase gabbro–diorite–plagiogranite formation from the Early–Middle Devonian period. All Middle Paleozoic island–arc formations in this area are interrupted by dikes of dolerites, lamprophyres, and montsodiorite porphyries from the Musyur complex (Volchkov et al., 2008), which have been dated to the Early Carboniferous period (Sobolev et al., 2020). The ore occurrence site is situated in a zone of intense stratification, cataclasis, and brecciation, which is bounded by the Toupugol and Yevyegan faults (Figure 4.2). The layers of thinly clastic volcanogenic–sedimentary, terrigenous, and terrigenous–carbonate rocks host stratiform sinter and significant pyrite mineralization.

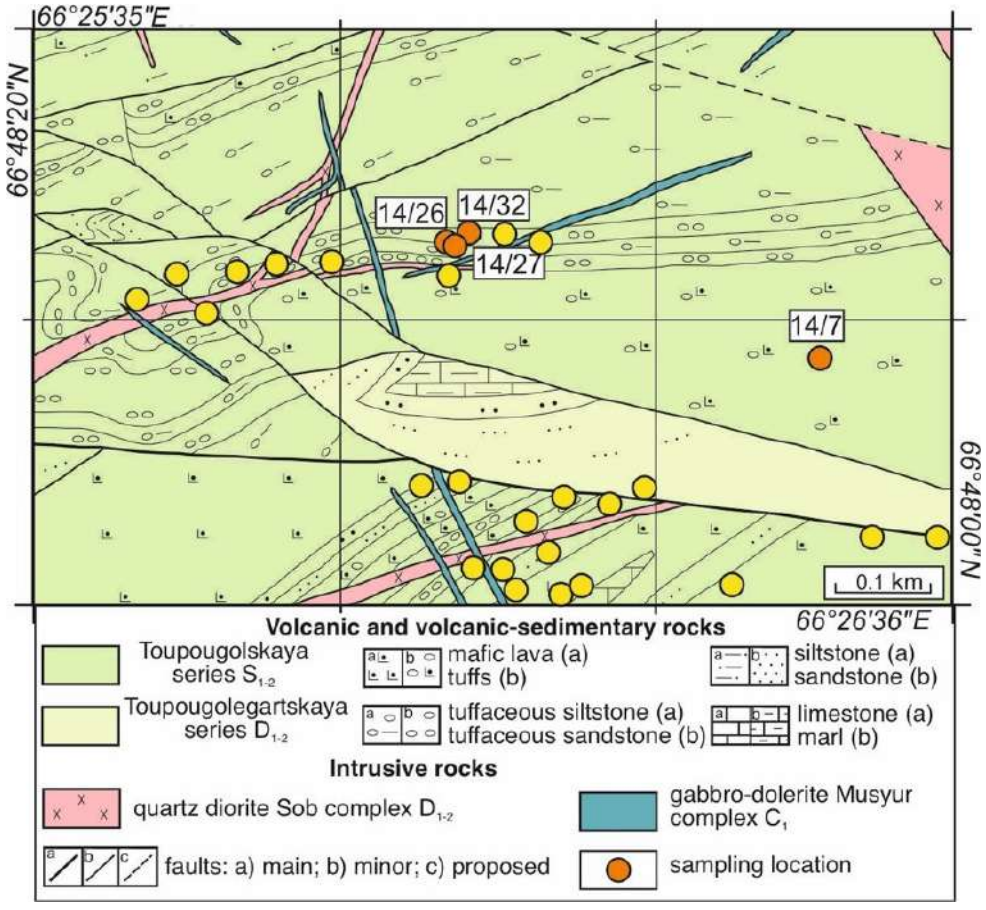

Figure 4.5. – Scheme of the geologic structure of the Kariernoe ore occurrence with sampling points (according to (Pryvnanosov et al., 2004) with modifications).

Linear zones of gold mineralization are identified in weakly altered berezite rocks, which are limited to stratified areas composed of sulfide–quartz and quartz–

carbonate veins. The thickness of mineralized zones ranges from one to tens of meters, with gold content reaching up to 10 g/t (Volchkov et al., 2008). Several mineral associations are present within the ore deposit, with pyrite being the predominant mineral and occasionally accompanied by magnetite, chalcopyrite, and sphalerite. Based on its mineralogical and geochemical features, the gold ore mineralization at the Kariernoe ore deposit is classified as the gold–sulfide–quartz type. This type is found in the zones of hydrothermal–metasomatic changes at the Novogodnee-Monto deposit.

4.3.2 Novogodnee-Monto deposit

The Novogodnee-Monto Au–Fe–skarn deposit is situated in the central and eastern parts of the Novogodnenskoe ore field (Fig. 4.2). The deposit is located in the exocontact zone of a large diorite stock of the Sobo complex among Silurian volcanics of basic and medium composition, sedimentary volcanogenic rocks with lenses and packs of marbleized limestones belonging to the Toupugol Formation (Andreev, 2006). Volcanogenic and intrusive rocks form a single volcanic–plutonic association. The Sobo complex intrusive formations consist of diorites, quartz diorites, and tonalites from the second (main) intrusive phase, as well as dikes of quartz diorite–porphyrites, tonalite–porphyries, plagiogranite–porphyries, and leucoplagiogranites from the third phase (Figure 4.6) (Mansurov, 2009). The Paleozoic rocks of the deposit are all intruded by Early Carboniferous basite intrusives of the Musyur complex (Mansurov, 2009; Sobolev et al., 2020).

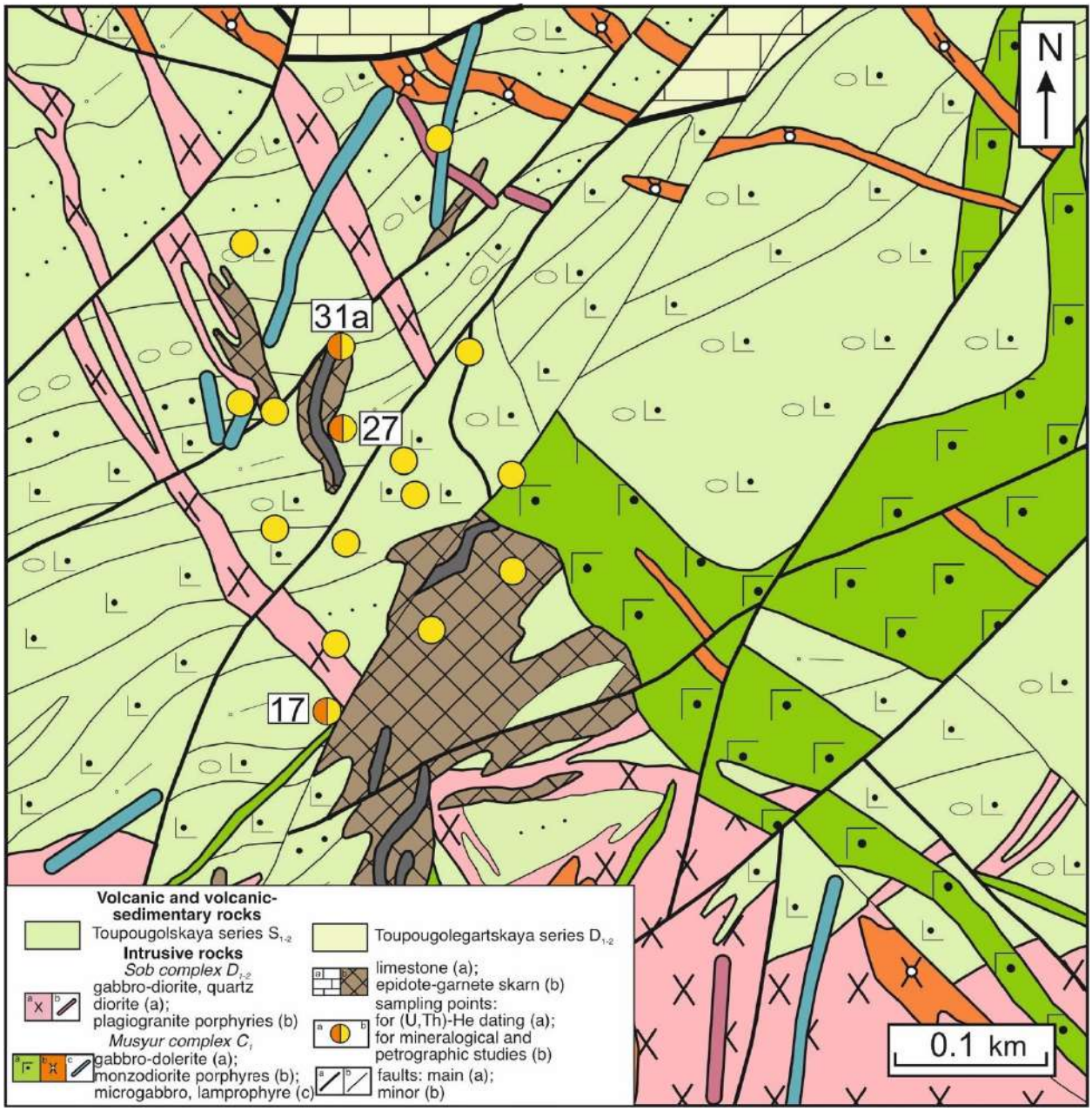

Figure 4.6. – Scheme of the geologic structure of the Novogodnee-Monto deposit with sampling points (according to (Pryvnanosov et al., 2004) with modifications).

Autometasomatic alteration of volcanogenic rocks is widespread near the intrusions of the Sob complex. Among the metasomatic processes, propylitization, skarnization and berezitization are prominent (Trofimov et al., 2005). It is believed that the formation of the ore district occurred in several stages: 1) volcanogenic–sedimentary (S_2–D_1); 2) skarn–porphyritic ($D_{1–2}$); 3) berezit (D_3) (Vikentyev et al., 2017).

Calcareous skarns form at the contact of volcanics with limestones and carbonate–bearing volcanogenic–sedimentary rocks due to tectonic disturbances.

The skarns are located in the intrusive part of diorites of the Soba complex. Morphologically, the skarn bodies have a lenticular–ribbon shape in cross–section. The composition of skarns corresponds to the pyroxene–granate–epidote facies (Figure 4.7a). Skarn formation is completed through magnetite mineralization, resulting in the creation of magnetite bodies with pyrite phenocrysts and ore minerals. These are associated with areas of gold–magnetite–sulfide mineralization. The alteration thickness is typically tens of meters.

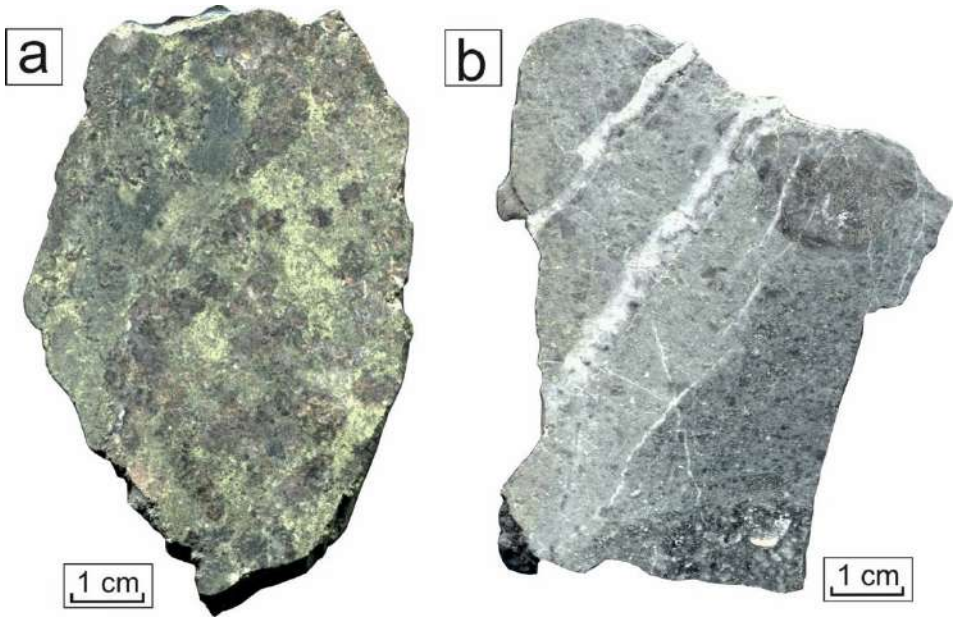

Figure 4.7. – Scan of samples of the Novogodnee-Monto deposit: a – pyroxene–garnete–epidote skarns (NM–27); b – pyrite–sericite–quartz metasomatites (NM–17).

The process of propylitization is represented by epidote–chlorite, carbonate–chlorite, and actinolite–epidote facies. It is confined to the outer zones of development of the halo skarns. It should be noted that representatives of epidote–chlorite alteration form halos with a larger distribution area, including endocontact parts of the diorite massif. In contrast, actinolite–epidote rocks are limited to discontinuous structures of submeridional and northeastern direction. The propylitization zone extends for hundreds of meters and has a thickness of up to tens of meters.

The final stage is characterized by the berezitization process, which is represented by pyrite–sericite–carbonate–quartz alteration (Soloviev et al., 2013). These quartz–sericite–sericite metasomatites (Figure 4.7b) contain disseminated

gold–sulfide–quartz mineralization in low–thickness quartz and quartz–carbonate veins, including linear veinlets. It is likely that these metasomatites are related to the die–off and cooling of the magmatic sources of the Sob batholith during the final stage of island–arc magmatism (Vikentyev et al., 2017, 2019; Sobolev, 2019). The distribution of metasomatic alteration is controlled by northwest–trending strike–slip fault systems. The quartz–sericite metasomatite zone is typically tens of meters thick and extends for hundreds of meters.

The deposit contains several different types of ores, which are superimposed on each other and occur in a relatively small area of 2.5 km^2. Two main industrial types of ores are distinguished based on the structural and morphological characteristics of the deposit: 1) gold–sulfide–magnetite, which is confined to skarn–magnetite bodies; and 2) vein–embedded gold–sulfide–quartz, which is associated with zones of propylitization (epidote–chlorite–albite association ± calcite) of host rocks and pyrite–sericite–quartz metasomatic alteration (Ivanova, Ivanova, 2021).

The gold–sulfide–magnetite mineralization is linked to skarn and skarn–magnetite subplast lenses located above the diorite massif in the contact zones of carbonate and tuffogenic–sedimentary rocks. The sulfide–magnetite ore bodies that contain gold consist of lenses, nests, and bedded deposits that can be several tens of meters thick. The ore structures are massive, banded–stained, and spotted–embedded. This mineralization type is directly linked to the intrusion of diorites from the Soba intrusive complex. The ore minerals present are magnetite, pyrite, chalcopyrite, cobaltite, pyrrhotite, arsenopyrite, and marcasite. Nugget gold is rare, and generally corresponds to low assay values (757–893). However, its assay increases when associated with cobalt–bearing cobaltite, pyrite, and chalcopyrite (Vikentyev et al., 2021).

The gold–sulfide–quartz mineralization is primarily linked to hydrothermal metasomatic formations of pyrite–sericite–quartz composition. The low thickness steeply dipping quartz and carbonate–quartz veins are limited to weakened zones of buckling and faulting. These ores represent subvertical low thickness (ranging from

1 to 10 m) vein–embedded zones of mineralization with an average gold content of up to 3.7 g/t (Volchkov et al., 2008). The mineral association comprises mainly of pyrite, with smaller amounts of galena, sphalerite, chalcopyrite, and hematite. Nugget gold is found in association with pyrite and galena. Inclusions in quartz and chlorite are rare and typically small (up to 20 microns) (Andreev, 2006).

4.3.3 Petropavlovskoe deposit

The Petropavlovskoe gold porphyry deposit is located in the western part of the Novogodnenskoe ore field and corresponds to the central part of the western mineralized zone of the Novogodnee-Monto deposit, which is a steeply dipping east–striking linear stockwork (Koenig and Butakov, 2013) (Figure 4.2). The Petropavlovskoe deposit consists of Wenlock–Ludlow metasomatized sedimentary volcanogenic (siltstone – psephitic) rocks of the basalt–andesibasalt series, with rare lenses of carbonates of the Toupugol Formation intruded by subangular subvolcanic bodies of abundant porphyritic andesibasalts (Koenig and Butakov, 2013). Plutonic formations are widespread in the field and are represented by linearly elongated, submeridional dyke–shaped bodies in varying degrees of metasomatized Early–Middle Devonian (Vikentyev et al, 2017; Sobolev et al., 2018a, b; Sobolev, 2019) porphyritic gabbro–diorites, diorites, quartz diorites, tonalites, and plagiogranites of the Sob Complex, and later – Early Carboniferous dikes of montsodiorite porphyries, lamprophyres, and dolerites of the Musyur Complex (Sobolev et al., 2020) (Fig. 4.8).

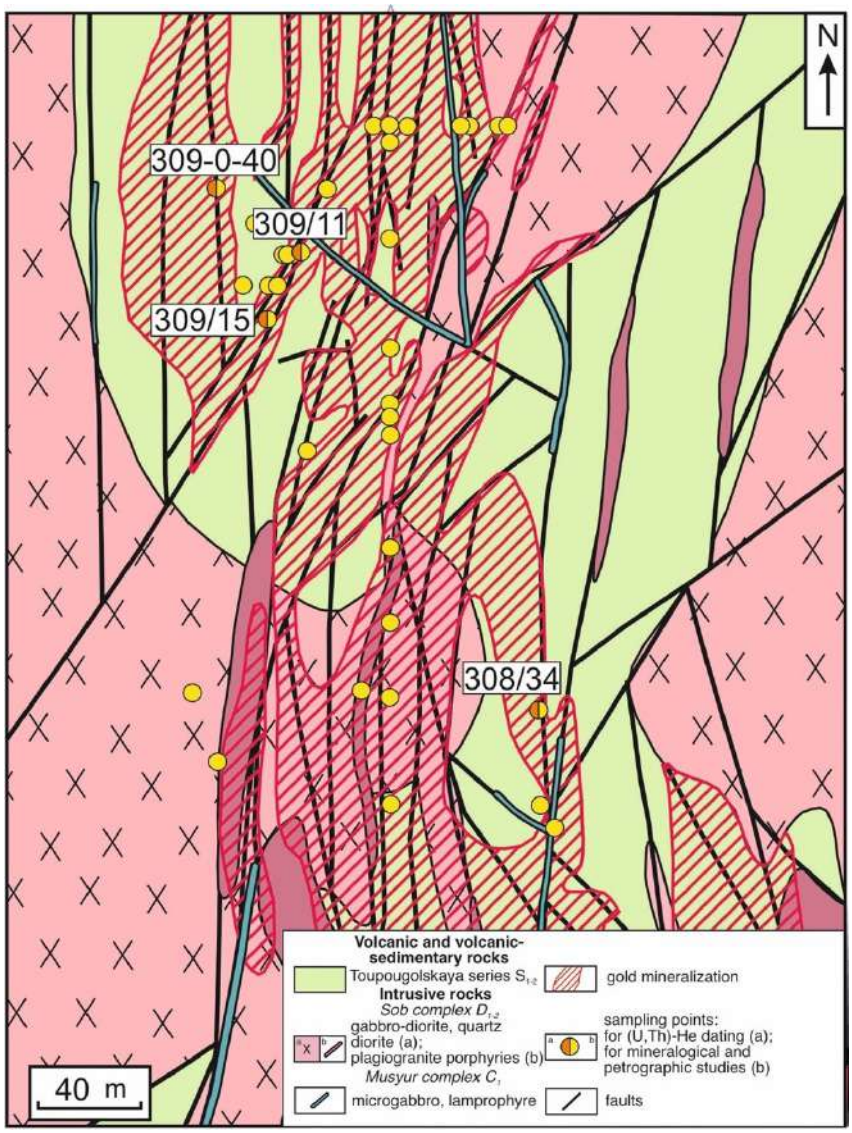

Figure 4.8. – Scheme of the geological structure of the Petropavlovskoe deposit with sampling points for (U,Th)–He dating (according to (Vikentyev et al., 2017) with modifications).

The hydrothermal–metasomatic alteration (Figure 4.9) of the rocks resulted from the processes of berezitization, oquartzization, albitization, propylitization and skarnization. The deposit shows the following metasomatic zonation: (epidote)–carbonate–chlorite rocks (propylites) – pyrite–chlorite–albite and pyrite–albite rocks – pyrite–sericite–quartz formations (Mansurov, 2009; Mansurov et al., 2017). Skarns and skarnoids are distributed in minor amounts and are locally manifested in the southern part of the deposit.

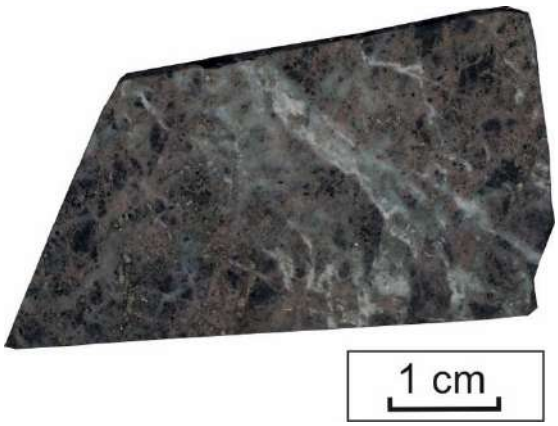

Figure 4.9. – Hydrothermally altered volcanogenic rocks of the Petropavlovskoe deposit (309/15)

Low and intermediate temperature epidote–carbonate–chlorite hydrothermal–metasomatic formations are widespread throughout the deposit. In morphology, the alteration halos are represented by submeridionally extending lenticular and oval zones with widths from the first meters to the first tens of meters, with lengths from tens to hundreds of meters, traced (according to exploration data) to a depth of more than 300 m (Mansurov, 2009). The distribution halo of hydrothermal–metasomatic transformations is limited by the diorite–porphyrite bodies of the Soba Complex and the system of steeply dipping faults to the east and west. All volcanogenic rocks of the deposit, as well as gabbroids and granitoids of the Soba Complex, have undergone propylitization, with chlorite–carbonate metasomatites developing on volcanics and epidote–chlorite metasomatites on intrusives. The propylites are characterized by low pyrite (<1%) and gold (up to 0.1 g/t) contents (Vikentyev et al., 2017).

Calcareous skarns have a limited distribution and are extremely rare. The skarns are spatially associated with northwest trending faults that control the mineralized zones of the deposit. Thin lenticular bodies (up to 50 m) are localized in the central part of the deposit (Mansurov, 2009). The skarnization process affected dikes of diorite porphyrites and volcanogenic–sedimentary rocks of the Toupugol Formation. In terms of mineral composition, the formations correspond to garnet–magnetite mineralization, which is the final stage of formation of the productive skarns of the Novogodnee-Monto deposit.

Metasomatic formations of pyrite–(chlorite–)–albite composition are represented by bodies of complex morphology confined to the contacts of porphyritic dikes (Mansurov, 2009). Secondary alteration is manifested in sedimentary volcanogenic rocks of the Toupugol Formation. Metasomatites of mainly albite composition are distinguished in a separate group in connection with increased concentrations of gold – more than 1 g/t (Mansurov, 2009). Pyrite–(chlorite)–albite metasomatic alterations determine the gold content of the deposit ores and are associated with the main productive gold–sulfide stage of ore formation (Vikentyev et al., 2017).

Pyrite–sericite–quartz formations are characterized by superimposed vein–vein gold–quartz–carbonate–sulfide mineralization, forming a mineralized zone that determines the industrial value of the Petropavlovskoe deposit. The width of this type of alteration halo is estimated at 350–400 m, the length at the surface is not less than 700–800 m, and the depth is up to 300 and more meters (Vikentyev et al., 2017). Pyrite–sericite–quartz metasomatites were formed on previously propylitized gabbroids, granitoids and volcanogenic rocks, and their distribution halo coincides with the propylitization area. Late–production pyrite–sericite–quartz rocks are characterized by the highest gold grades (up to 1.5 g/t) due to the superposition of all previous types of metasomatic alteration (Mansurov, 2009).

Several types of precious metal mineralization are distinguished at the deposit: 1) vein–vein disseminated gold–sulfide ores in pyrite–albite metasomatites; 2) vein–vein disseminated gold–malosulfide–quartz ores in pyrite–sericite–quartz metasomatites (Vikentyev et al., 2017). At the same time, it should be noted that the first type of mineralization significantly exceeds the second type in terms of distribution area.

Gold–sulphide mineralization is represented mainly by vein–embedded pyrite, the content of which reaches 15–20 vol%, less frequently by chalcopyrite and pyrrhotite, magnetite is extremely rare in deep horizons. Native gold is present as microinclusions in fractures and other defects of pyrite cemented by chalcopyrite,

sometimes together with galena. The average gold content in such ores is 25–30 g/t (Vikentyev et al., 2017). This type of ore contains on average 1.5–2 g/t gold.

The gold–malosulfide–quartz ore type is controlled by host pyrite–sericite–quartz metasomatites in the inner part of the bodies. Mineralization formed in two sub–stages: pyrite–carbonate–quartz and gold–telluride with galena (Koenig et al., 2013). The ores morphologically represent secant steeply dipping quartz veins and thin veins within large volume lenticular zones of metasomatic alteration. The main ore mineral is pyrite, less common are galena, chalcopyrite, pyrrhotite, and micron–sized isolations of antimonite, hessite, nugget gold, tellurium bismuthite, altaiite, and petzite, the total of which does not exceed 1.5 vol%. The vein mineralization is superimposed on the previously productive gold–sulphide ores and as a result is defined by higher gold grades averaging up to 5–10 g/t.

The sulfur isotopic composition of pyrite in the Toupugol–Khanmeyshor area varies widely, ranging from –17 to +3‰ (Figure 4.10). Pyrite from stratiform ore deposits of the Kariernoe ore deposit has the lightest sulfur isotopic composition ($\delta^{34}S$ from –17 to –16‰), according to unpublished data from Tyukova and Vikentyev. The sulfur isotopic composition of pyrite in skarn ores of the Novogodnee-Monto deposit corresponds to $\delta^{34}S$ from 0 to +3‰. The sulfur isotopic composition of the chlorite–albite metasomatites closest to skarns at the Petropavlovskoe deposit is characterized by values of $\delta^{34}S$ ranging from –0.5 to +1.7‰. The gold–sulfide–quartz type of mineralization within the Novogodnee-Monto deposit is characterized by a sulfur isotopic composition ranging from –2 to 0‰. The pyrite–sericite–quartz metasomatites of the Petropavlovskoe deposit exhibits variations in sulfur isotopic composition, with $\delta^{34}S$ values ranging from –12 to +0.5‰ (Vikentyev et al., 2017). The deposit's central portion has a uniform sulfur isotopic composition with deviations of approximately ±0.5 from the meteoric standard. In contrast, pyrite with notably lower $\delta^{34}S$ values (< –5‰) is present in the deposit's northwestern region.

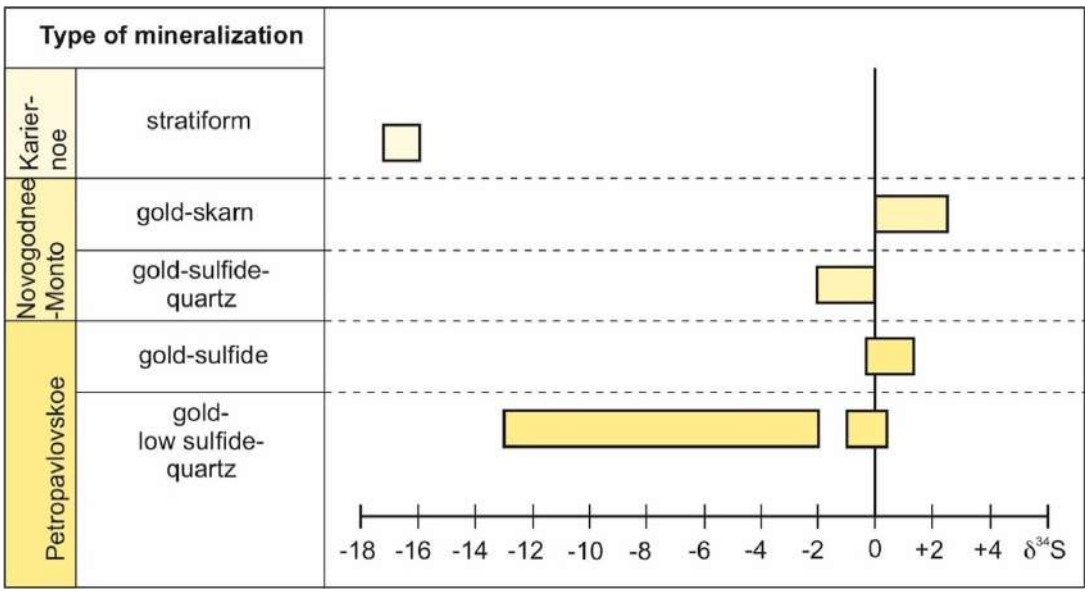

Figure 4.10. – Sulfur isotopic composition of δ34S pyrite of the Toupugol–Khanmeshora ore district (Vikentyev et al., 2017; unpublished data Tyukova, Vikentyev)

CHAPTER 5. MINERALOGICAL AND PETROGRAPHIC CHARACTERIZATION OF ORE OBJECTS

5.1 Volcanogenic rocks

The Novogodnenskoe ore field's stratigraphic section comprises volcanogenic and sedimentary rocks from the Toupugol ($S_{1–2}$) and Toupugolyegart (D1–2) strata. The Kariernoe ore occurrence contains volcanogenic rocks that lack obvious signs of hydrothermal alteration. These rocks consist of medium–small clastic crystalline andesite and tuffite tuffs with abundant disseminated and layer–by–layer phenocrysts of pyrite (Figure 5.1) (Ivanova et al., 2024). The alternating layers of tuff are determined by the wavy, layered texture of the rocks (Figure 5.1a).

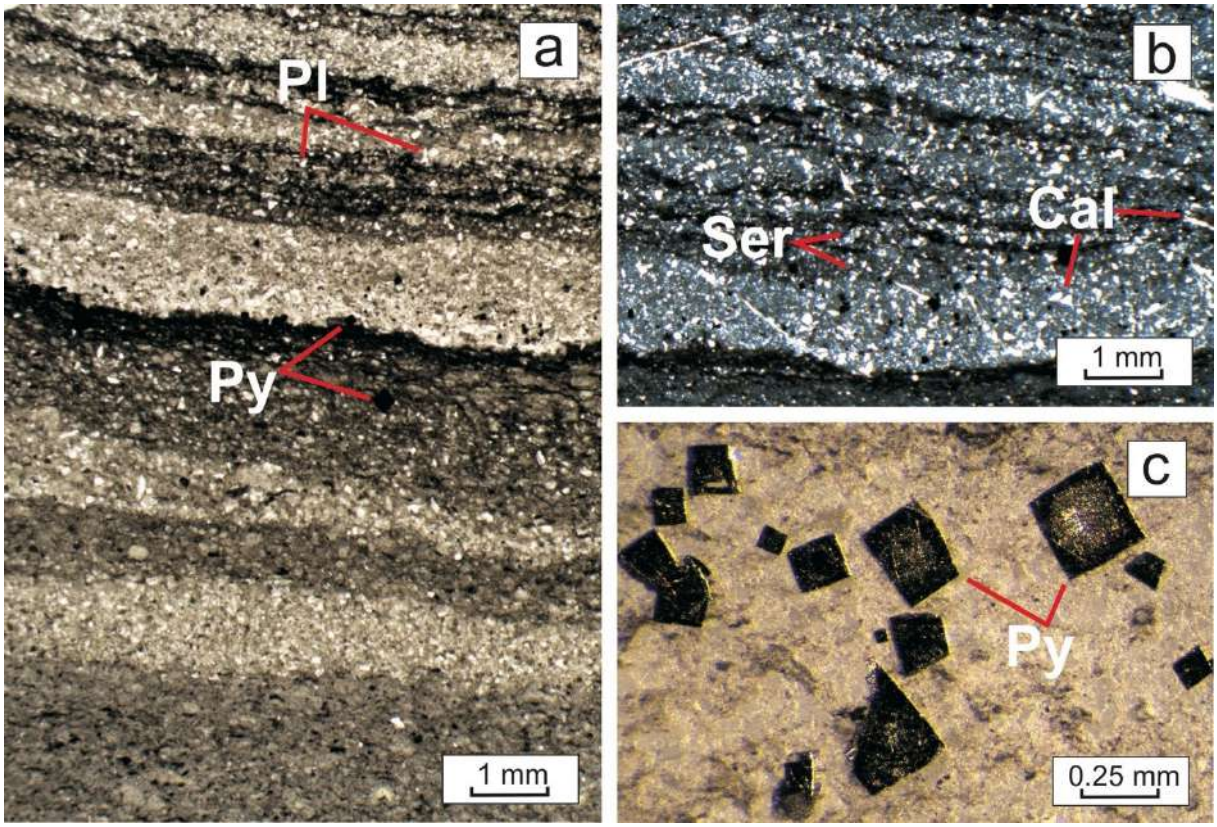

Figure 5.1. – Petrographic peculiarities of tuffites of the Kariernoe ore deposit (14/32): a, b – wavy–layered texture of tuffites. (a – without analyzer; b – with analyzer); c – idiomorphic cubic crystals of pyrite. Cal – calcite; Pl – plagioclase; Py – pyrite; Ser – sericite.

The interbeds of tuff are classified into gradational series, with a gradual decrease in the size of pyroclastic material up the section (Figure 5.2). The thickness of gradational lithocycles reaches the first tens of centimeters. The variably oriented

unsorted angular clasts are composed of plagioclase, quartz, and ore minerals (Figure 5.1a). The plagioclase composition corresponds to andesine in terms of the angle of extinguishment of polysynthetic twins. The clasts range in size from silt to sand (0.05–0.25 mm). The rock base consists mainly of finely clastic volcanogenic material. The tuffites contain fragments of carbonate composition (Figure 5.1b). Additionally, carbonate (calcite) and sericite are present as secondary minerals replacing feldspars, as evidenced by the jagged outlines of calcite among quartz–feldspar clastic material.

Figure 5.2. –Tuffogenic rocks of the Kariernoe ore deposit, crumpled in the rift fold (ob. 14/26)

The ore mineralization is found in stratiform deposits with subplast and lenticular morphology at different levels of lithological series. It is mainly in the form of scattered or layer–by–layer pyrite phenocrysts. In schliffs, it is represented by small sections of cubic grains and their aggregates, with larger crystals occurring less frequently (up to 0.4x0.4 mm) (Figure 5.1c). Pyrite forms ellipse–shaped outcrops, reaching a size of 0.04x0.4 mm, and clusters up to 0.12x0.2 mm. The rocks are dissected by veins of quartz–carbonate and carbonate compositions (0.5–2 mm thick).

5.2 Altered rocks

The metasomatic formations in the Novogodnenskoe ore field have a similar mineral composition and structure, but each deposit has its own peculiarities. The

rocks are categorized by the type of alteration and will be discussed in the order they were formed.

5.2.1 Propylitized igneous rocks

5.2.1.1 Volcanic rocks

The basalt–andesite series volcanics at the Novogodnee-Monto deposit are the least altered.

The andesibasalts are porphyritic, hyalopylitic, massive, and slightly to moderately propylitized. In isolated cases, the pilotaxite structure of the main mass is noted due to subparallel arrangement of plagioclase microlites oriented in the form of flows. Additionally, newly formed minerals such as chlorite (5–10% by volume), epidote (5% by volume), and carbonate (10% by volume) are present. Ore minerals are evenly dispersed throughout the sample and constitute about 10% by volume. The main minerals in the sample are plagioclase (45–60% by volume), clinopyroxene (10% by volume), and quartz (5–10% by volume). The phenocrysts consist of sericitized and sossuritized plagioclase tabulars measuring 3–5 mm in size (20% by volume), as well as rare grains of clinopyroxene. Isolated occurrences of zonal plagioclase have been observed, with pure albite composing the rims (Figure 5.3c). The main mass consists of microlites of weakly sericitized and albitized plagioclase, as well as chloritized volcanic glass.

Greenish epidote is a component of the sossurite mass, which fills the spaces between plagioclase microlites (Figure 5.3b). It forms thin veins (ranging from 0.1 to 0.25 mm) and lenses (ranging from 0.05 x 0.2 to 0.4 x 2.25 mm), and develops on plagioclase phenocrysts together with chlorite, while also replacing rare olivine grains. Quartz and calcite form thin veins (0.05 – 0.25 mm).

Volcanogenic rocks are more exposed to hydrothermal alteration in the area of the Petropavlovskoe deposit. The rock contains plagioclase (45–50 vol. %), quartz (10–15 vol. %), and carbonate (15 vol. %) as its main minerals. Ore minerals constitute 15 vol. %, while titanite (1–2 vol. %) is present in single samples. Chlorite (5–10 vol. %), carbonate (5 vol. %), and sericite (5 vol. %) are newly formed minerals. The rocks maintain their original primary structure, which is porphyritic.

Breccia structure with fine–grained cement is rarely formed. The main mass structure remains primary, exhibiting hyalopilitic, intersertal, and pilotaxitic textures (Figure 5.3a and b). The textures vary from massive to spotted, with less common veined and nested textures.

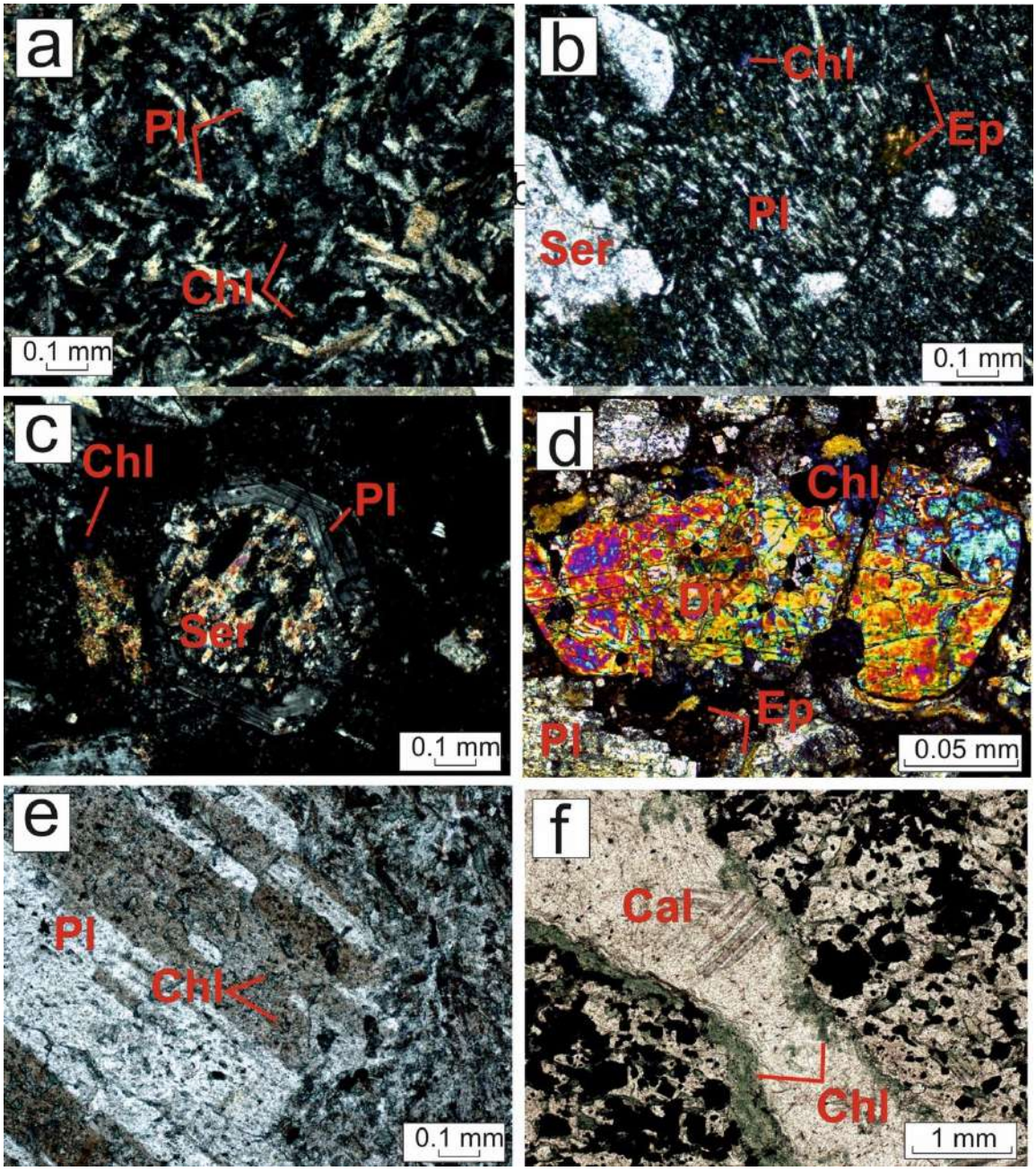

Figure 5.3. – Petrographic features of propylitized igneous rocks of the Novogodnenskoe ore field, with analyzer (a–d), without analyzer (e, f) a – hyalopylitic structure of the main mass (cl. 308/2), b – pilotaxitic structure of the rock base (cl. NM–9), c – sericitized plagioclase with direct zonality (cl. NM–11), d – idiomorphic diopside grain of elongated–prismatic habitus (cluster NM–8); e – chlorite–1 develops along cracks in plagioclase phenocrystal (cluster 308/4), f – chlorite–2 in carbonate vein zalbands (cluster 309–60–31). Cal – calcite; Chl – chlorite; Di – diopside; Ep – epidote; Pl – plagioclase; Ser – sericite.

Plagioclase phenocrysts are tabular crystals that are single, fractured, and less frequently fused. They measure up to 0.4 x 0.8 mm. Grains that have undergone secondary alteration have a turbid grayish–brown tint. Small sericite flakes with color interference staining are visible when the analyzer is inserted. The main mass consists of randomly oriented strongly sericitized microlites of plagioclase with an elongated–prismatic habitus (up to 0.01 x 0.05 mm), immersed in a fine–grained aggregate of sossyurite, probably replacing phenocrysts of dark–colored minerals and volcanic glass. Rare grains of clinopyroxene occur less frequently together with chaotically arranged microlites of plagioclase, forming an intersertal structure.

Milky–white quartz–1 is represented by rare large crystals of elongated habitus with wavy extinguishment, possibly acquired as stresses increase as a result of tectonic impacts (Marin, 2015).

5.2.1.2 Intrusive rocks

The rock type known as diorites has a porphyritic and massive texture. It is composed of plagioclase, clinopyroxene, and titanomagnetite, with small amounts of quartz in some varieties. Plagioclase phenocrysts are represented by elongated–prismatic crystals (0.5 to 1.5 mm), with rare simple twins. Colorless clinopyroxene occurs as phenocrysts (Figure 4.3g), less frequently in the bulk, exclusively near the Novogodnee-Monto deposit. The grains have a prismatic habitus (up to 1.15 | 3.1 mm). The clinopyroxene phenocrysts were weakly affected by secondary alteration.

During the propylitization process, secondary changes such as albitization, quartzization, chloritization, carbonatization, and epidotization occurred.

Chlorite is present in two generations. The first generation is pale green chlorite–1, which is part of a fine–grained epidote–carbonate–chlorite aggregate that fills the interstices between plagioclase leucites in the base of the andesibasaltic rock. Large thinly scaly aggregates of chlorite–1, up to 1.1 x 1.75 mm, likely pseudomorphically replacing rare grains of dark–colored minerals. Chlorite–1 develops on the surface of plagioclase phenocrysts, together with sericite and carbonate (Figure 5.3d), and fringes carbonate veins (Figure 5.3e). Chlorite–2 has a

brighter, light green color and forms irregular, small, lenticular, and vein–like clusters, ranging from 0.05 to 0.2 mm.

Calcite often develops alongside chlorite and epidote, potentially replacing dark–colored minerals and volcanic glass in the rock's main mass. It can also be found in large grains of plagioclase. Calcite forms small carbonate veins (up to 0.2 mm), less frequently carbonate–quartz veins (up to 3 mm), or small nests.

Near deformed quartz–1 grains, newly formed small granular clusters of quartz–2 are observed, likely due to recrystallization. The rock sample contains small quartz veins measuring 0.01 to 0.05 mm, quartz–carbonate veins measuring 0.2 to 1 mm, and quartz–epidote veins measuring 0.1 to 0.3 mm. Additionally, there are rare nests and lenses measuring 0.05 to 0.1 mm filled with finely granular quartz measuring 0.2 x 0.25 to 0.3 x 0.4 mm, which create vein and nest textures.

Sericite is present as a secondary mineral, forming finely disseminated phenocrysts in plagioclase phenocrysts measuring up to 0.03 mm.

The secondary transformations of the volcanogenic and intrusive rocks in the Soba complex of the Petropavlovskoe deposit are characterized by the presence of leucoxene. Leucoxene is represented by small, irregularly shaped grains, less often rhomboidal crystals, with a size range of 0.02 to 0.1 mm. It is closely associated with chlorite and ore minerals such as pyrite and magnetite. Leucoxene is likely a product of the replacement of magmatic titanomagnetite.

5.2.2 Skarns

Near–ore skarns dominate the Novogodnee-Monto deposit. The pyroxene–granate–epidote skarns are characterized by irregularly grained granoblast and nematogranoblast structure, often with brecciated elements. The texture is massive, rarely veined, and in isolated cases nested. The Novogodnee-Monto deposit skarns are primarily composed of diopside (30–45% by volume), andradite garnet (10–30% by volume), epidote (10–20% by volume), calcite (10% by volume), chlorite (5% by volume), quartz (1–2% by volume), and titanite (up to 2% by volume). Diopside crystals can reach sizes of 2.75 x 4.75 mm and are colorless and prismatic in shape (Figure 5.4a).

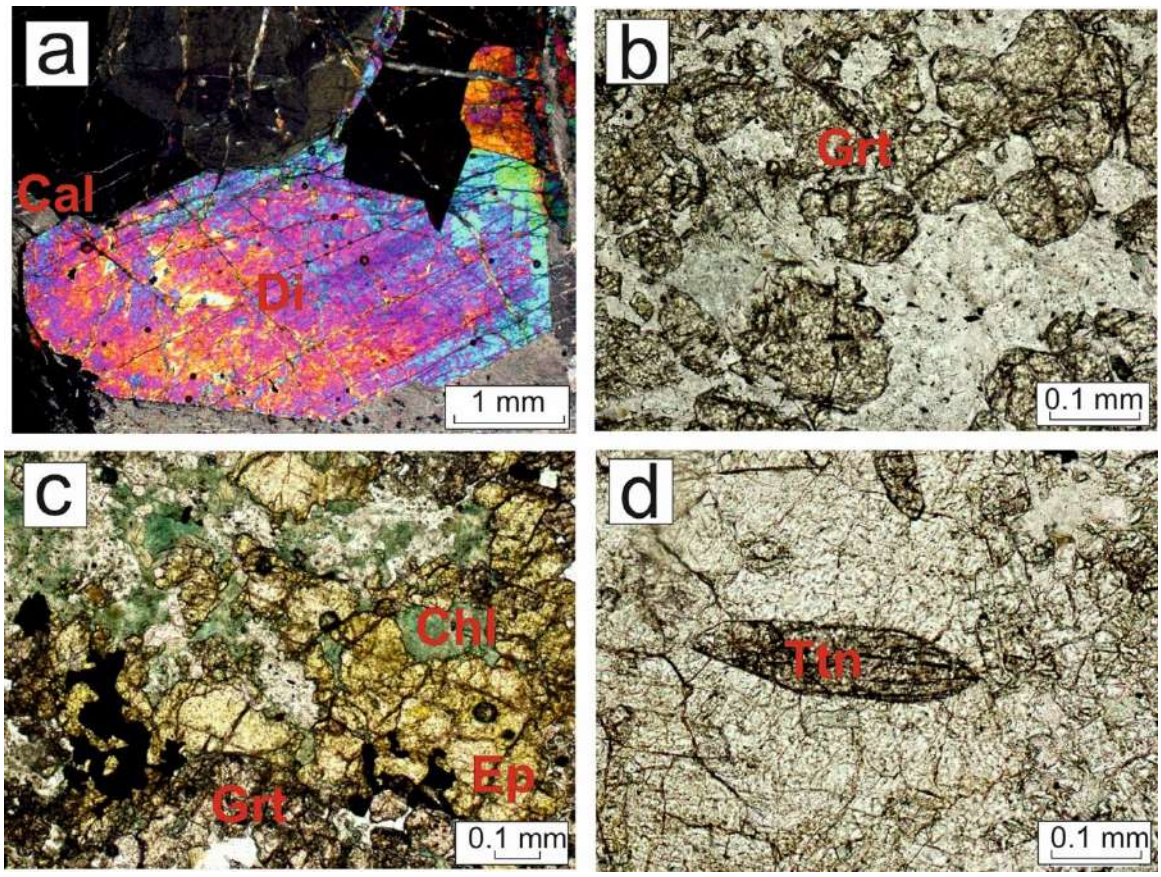

Figure 5.4. – Petrographic features of skarns of the Novogodnee-Monto deposit, with analyzer (a), without analyzer (b–d) a – a large hypidiomorphic diopside grain (cl. NM–3c); b – irregularly shaped garnet grains (cl. NM–3b); c – irregularly shaped epidote outcrops (cl. NM–26); d – idiomorphic rhombic titanite crystal (cl. NM–31a). Cal – calcite; Chl – chlorite; Di – diopside; Ep – epidote; Grt – garnet; Pl – plagioclase; Ttn – titanite.

Garnet is represented by small yellowish grains, often irregularly shaped (from 0.04 ×0.05 to 0.15 ×0.13 mm) (Figure 5.4b).

The minerals belonging to the epidote group are represented by tabular clinozoisite individuals (measuring from 0.1 ×0.2 to 0.5 ×0.55 mm), clusters of colorless or yellowish grains of epidote with irregular shapes (Figure 5.4c), and less frequently by small scatterings of elongated–prismatic crystals.

Calcite is present in the form of colorless isometric grains, which are often fractured. Sometimes, there are signs of its plastic deformation. The rock contains thin carbonate veins and less frequently, carbonate–quartz outcrops that have an elongated or irregular shape.

Milky–white colored quartz with wavy extinguishing is occasionally found in carbonate–quartz veins, and in some cases, it forms nested outcrops.

Titanite is present in irregularly shaped grains, and rhomboidal crystals reaching 0.25 ×0.65 mm are less frequently observed (Figure 5.4g). These formations are typically associated with ore accumulations.

Chlorite is represented by a light green thinly scaly aggregate, with rare chlorite aggregates averaging 0.07 ×0.12 mm.

5.2.3 Pyrite–(chlorite)–albite metasomatites

The Petropavlovskoe and Novogodnee-Monto deposits exhibit extensive low–temperature alteration, including albitization and quartzization, of volcanogenic rocks near the contacts of porphyritic dyke dykes (Mansurov, 2017). The medium crystalline rocks are composed mainly of albite (60–70 vol.%), chlorite (15–20 vol.%), and pyrite (15–20 vol.%). Albite is present in the form of xenomorphic grains (ranging from 0.02 ×0.04 to 0.08 ×0.12) with wavy twins (Figure 5.5d). The Petropavlovskoe deposit features rare large veins composed of short prismatic albite grains (0.2–0.3 mm), along with thin albite veins (up to 0.2 mm) in some samples.

Chlorite is widespread at the deposit, with two generations present. The first generation of pale green chlorite forms uniformly disseminated thinly scaly clusters (ink–violet interference coloring) up to 0.25 mm. Thick veins of carbonate and quartz–carbonate composition are often surrounded by brighter light–green chlorite–2, which frequently forms a network of branching micro veins (Figure 5.5c). Ore minerals are often found as inclusions in these veins. Chlorite–2 is also commonly associated with clusters and independent veins of ore minerals. In some cases, large thinly scaly aggregates (up to 0.3 mm) that replace dark–colored minerals can be observed. The concentration of chlorite in the rocks of the deposit decreases as depth increases. At deeper horizons, it is mainly present in thin, flaky aggregates and occasionally in the form of veins with indistinct edges. Light–green chlorite is uncommon at the Novogodnee-Monto deposit and only occurs in the form of worm–like branching veins.

5.2.4 Pyrite–sericite–quartz metasomatites

The formation of pyrite–sericite–quartz metasomatites forming vein–vein zones is attributed to the intrusion of later massifs of acidic composition (Vikentyev et al., 2017). The rocks consist of fine– to medium–grained quartz with vein clusters of chlorite and fine– to medium–grained sericite. The prevailing texture is fine- and medium-grained granoblast structure, with less frequent occurrences of massive, vein, and nested textures. The Novogodnee-Monto deposit rocks are composed mainly of quartz (55 vol. %), carbonate (20 vol. %), and sericite (10 vol. %). Chlorite (5 vol. %) and titanite (less than 1 vol. %) are less common. At the Petropavlovskoe deposit, the chlorite content increases (up to 15 vol.%) and albite (25–40 vol.%) is the predominant mineral.

The quartz at the Petropavlovskoe deposit corresponds to the first generation of large–crystalline quartz with an elongated habitus and wavy extinguishing. Near these sites, small granular quartz outcrops corresponding to the second generation are occasionally observed. At the Novogodnee-Monto deposit, quartz–1 forms scattered grains and clusters that constitute the rock's total mass. The second generation of milky–white quartz forms relatively thick quartz–carbonate veins, up to 0.4 mm in size (Figure 5.5a), as well as nests of quartz composition up to 0.5 mm in size, creating vein and nest textures.

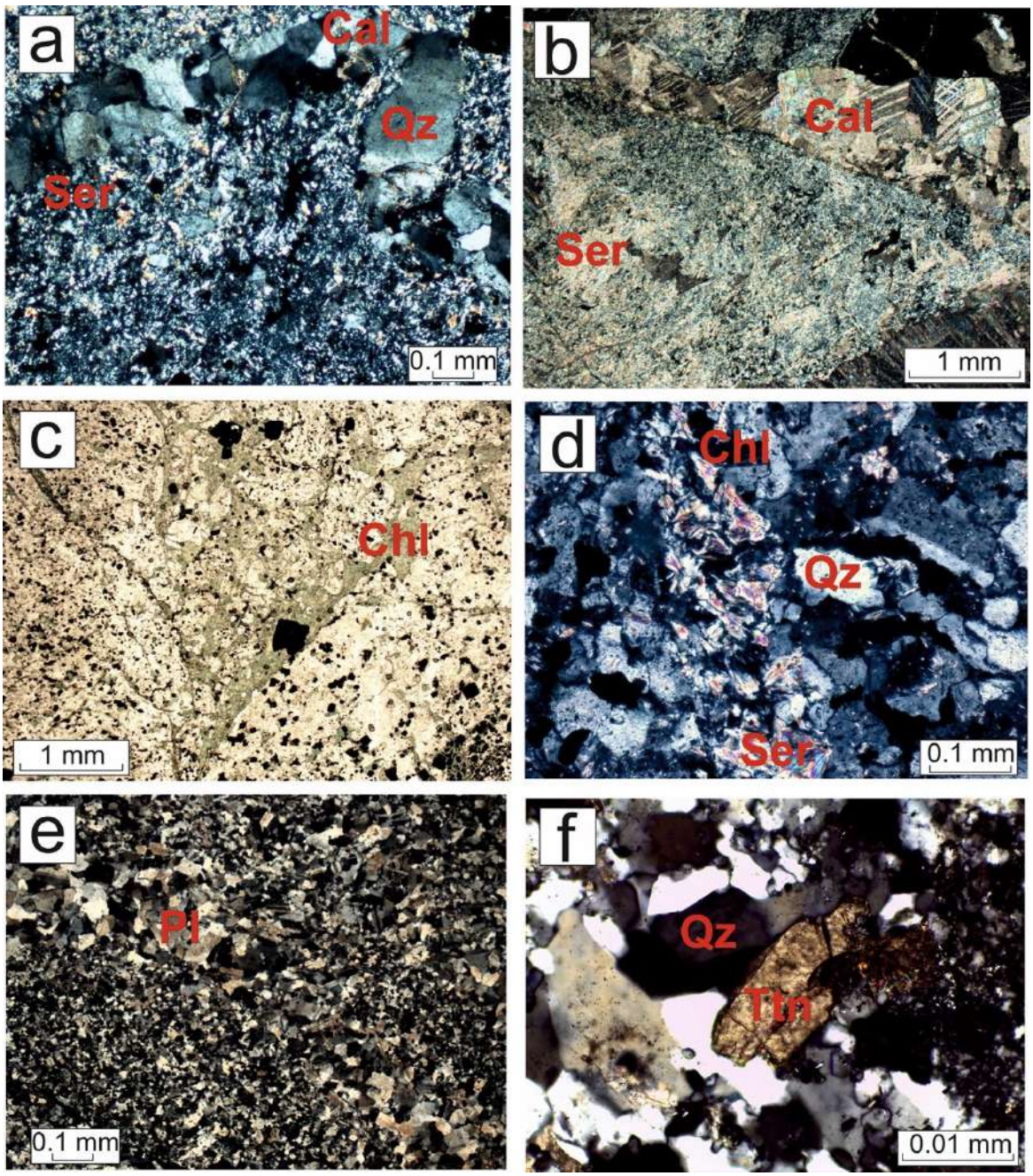

Figure 5.5. – Petrographic features of pyrite–sericite–quartz rocks (berezites): with analyzer: a – quartz–carbonate vein (cl. NM–25a); b – thick vein of carbonate composition (cl. NM–21); d – sericite–chlorite vein (cl. 309–20–70); e – albite vein (cl. 309/8); f – titanite of elongated habitus (cl. NM); without analyzer: c – branching chlorite vein (cl. 309/7). Cal – calcite; Chl – chlorite; Pl – plagioclase; Py – pyrite; Qz – quartz; Ser – sericite; Ttn – titanite.

Colorless calcite with brownish-gray interference coloration represents carbonate. It is distributed in the form of veinlets (0.05 to 0.1 mm) and composes numerous variably oriented carbonate (Figure 5.5b) and quartz-carbonate veins 0.01–0.2 mm thick. These veins intersect quartz, quartz-carbonate, and chlorite

veins, often with a shift. Point–like carbonate outcrops are observed in association with quartz in the case of complete replacement of plagioclase by sericite.

Sericite replaces plagioclase grains with small flake aggregates and also occurs in clusters. Sericite–chlorite veins (0.05–0.1 mm) (Figure 5.5g) are present, as well as low–thickness monomineral veins at the Novogodnee-Monto deposit. Sericite development in chlorite grains (up to 0.05 mm) is observed along with carbonate.

At the Novogodnee-Monto deposit, titanite forms clusters of small, irregularly shaped grains. Single individuals of elongated habitus (up to 0.12 ×0.28 mm) are also present (Figure 5.5e).

5.3 Interpretation

Volcanic rocks of the Topogol strata, which show no signs of hydrothermal alteration, are frequently found on the flanks of the Novogodnee ore field. The gradational rhythmic layering of tuffogenic interlayers, with a gradual decrease in the grain size of pyroclastic material towards the upper parts of the rhythms, and increased concentration of ore minerals at the boundary of the layers, indicate that the rocks were deposited in a submarine environment, either on the ocean floor or near it. The layered texture's waviness indicates the mobility of the water column. The clasts' angular, unrolled shape, their volcanomictic composition, and the stratigraphic stability of the interbeds testify to the pyroclastic nature of the ore–bearing rocks of the Toupugol Formation.

Hydrothermal–metasomatic alteration is strongly developed in the studied region, with propylites being the most widespread. The process of propylitization is significant for the metallogeny of the area because it indicates the powerful influence of upward syn– and postmagmatic solutions (Korzhinsky, 1953). Propylites form due to the impact of near–neutral and weakly acidic low–temperature solutions on shallow–depth rocks of medium and basic composition (Marin, 2015). In this case, they form in the volcanics of the andesibasalt formation. This alteration type represents the earliest stage and forms the outer near–ore halo of the mineralized zone in the deposit (Vikentyev et al., 2017). It was formed with the involvement of

a neutral near–alkaline solution, which has a weaker effect on the rocks resulting in only minor alteration. The rocks have a relict porphyritic structure, and the original structures of the main mass of volcanics, namely intersertal, pilotaxite, and hyalopylite, are also preserved. The texture is massive.

The analysis of propylitized rocks from the Petropavlovskoe deposit, sampled at various depths in well cores, indicates a decrease in the amount of chlorite with increasing depth. Chlorite is scarce at deeper horizons, occurring mainly in the form of thin, flaky aggregates of pale green color. This may be associated with an increase in temperature and changes in other parameters of postmagmatic fluids closer to the magmatic source. Based on the X–ray microanalysis results (Ivanova, 2016), the secondary minerals of rocks in the Petropavlovsk deposit contain chlorite with a magnesian–iron composition (f=0.56–0.7). The chemical composition of the chlorite corresponds to repidolite and pycnochlorite, as per the classification diagram of M. Hey (Hey, 1954). The rock mass contains pale–green thinly lenticular chlorite–1, which is mostly interstitial and pseudomorphosed by dark–colored minerals. It occasionally develops in plagioclase crystals and corresponds to the composition of the ferruginous group (Fig. 5.6). The hydrothermal stage of the intrusion is directly related to the development of numerous veins of saturated light–green chlorite–2, which belongs to the magnesian–iron group. At the upper horizons, the more magnesian variety of chlorite was prevalent, while at deeper horizons, the ferruginous variety was more common. This change in chemical composition may be due to the intensive development of the propylitization process, which is characterized by a decrease in iron content in the final stage upwards along the metasomatic column. Thus, the development of hydrothermal processes is characterized by the chemical zonation of chlorite, caused by the diffusion–infiltration spreading of a solution from its source at depth.

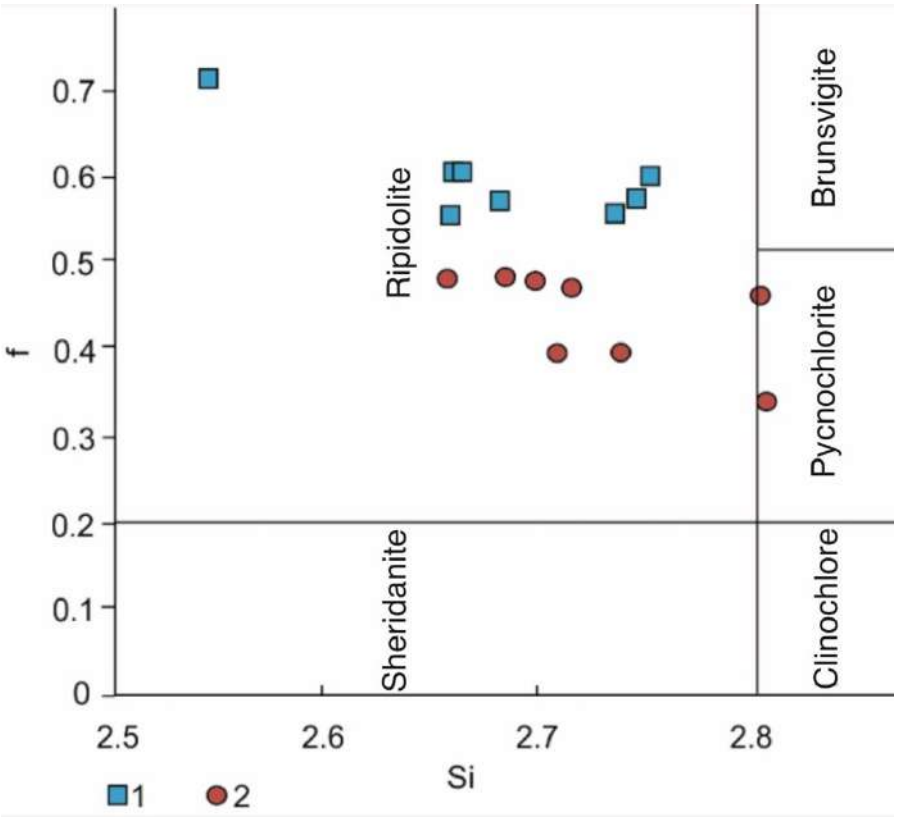

Figure 5.6. – Positions of chlorite composition points on the classification diagram of M. Hey (Hey, 1954): 1 – xenomorphic chlorite–1; 2 – veins of chlorite–2; f – ferricity. (Ivanova, 2016).

Regarding mineral composition, the metasomatites of the deposits differ in the content and morphology of chlorite and epidote. At the Petropavlovskoe deposit, a common occurrence is the flake aggregate of chlorite, while at the Novogodnee-Monto deposit, the development of idiomorphic epidote grains prevails, indicating a higher–temperature regime. The difference in mineral composition may be related to the geological position of the Novogodnee-Monto deposit. Specifically, the distribution of lenses and interlayers of carbonate composition in the protolith thickness resulted in a wider formation of synskarnous epidote. The aposkarnic nature of gold–sulfide–magnetite mineralization determines the ore prospectivity of skarn development zones and is overlain by lower–temperature metasomatites. Skarns are sparsely distributed at the Petropavlovskoe deposit and are only locally present due to the lack of carbonate bodies in the geological structure of the site (which has not been exposed on the surface).

Pyrite–sericite–quartz hydrothermal–metasomatic formations are the most recently formed and host the superimposed vein–vein association of gold–quartz–

carbonate–sulfide mineralization. This mineralized zone determines the industrial value of the Petropavlovskoe deposit (Mansurov, 2009).

The Novogodnee-Monto and Petropavlovskoe deposits are characterized by fully manifested low–temperature alteration of moderately acidic composition. The distribution of sericite in propylitized volcanogenic rocks at the Petropavlovskoe deposit indicates a transition zone to berezites. It is important to note that chlorite is the predominant mineral in the Petropavlovskoe deposit, where rare albite veins were also discovered, indicating the outer zone of the berezitization halo (Zharikov, 1998). At the Novogodnee-Monto deposit, dark–colored minerals and feldspars underwent decomposition in rocks of basalt–andesibasalt composition, resulting in the removal of Mg, Fe, Ca, Na, and K. As a result, quartz metasomatites, which are practically monomineral, are the most altered. This suggests that the metasomatic zonation of berezites is most fully manifested in the Novogodnee-Monto deposit.

Based on detailed mineralogical and petrographic studies of volcanogenic rocks, it can be concluded that the ore–bearing rocks of the Toupugol formation in the Kariernoe ore field were formed through pyroclastic processes.

The propylitization process was developed in the area of the studied ore deposits. At the Petropavlovskoe and Novogodnee-Monto deposits, propylitized volcanics form the outer peripheral halo of the mineralized zone. The intensity of propylitic alteration is shown by the chemical zonation of chlorite, which is characterized by a decrease in iron content at the final stage up the metasomatic column. The variability of iron content in chlorite is caused by the diffusion–infiltration spreading of the solution with the removal of the source located at depth.

The near–ore hydrothermal–metasomatic alteration shows a zonality of epidote–carbonate–chlorite, pyrite–chlorite–albite, and pyrite–sericite–quartz rocks. The rear zone of the metasomatic column at the Novogodnee-Monto deposit approaches a monomineral quartz composition. The difference is attributed to the probable export of magnesium, iron, calcium, sodium, and potassium during the dissolution of relict dark–colored minerals and feldspars.

CHAPTER 6. CHEMICAL COMPOSITION OF PYRITE

The mineral's chemical composition varies depending on its formation conditions, which are determined by physicochemical parameters of the environment. These parameters also affect the composition and content of impurity elements, structural features, and physical properties of the mineral. Changes in the paragenesis of mineral inclusions can indicate the evolution of hydrothermal systems. Reconstructing the history of mineral formation provides insight into the geological setting and associated processes.

Pyrite, a common companion in both endogenous and exogenous formations, is particularly informative in reconstructing formation stages. The shapes and sizes of uranium–bearing mineral inclusions in pyrite can be used to estimate their influence on the (U,Th)–He isotope system.

6.1 Kariernoe ore occurrence

Pyrite is represented by idiomorphic crystals of cubic, pentagon–dodecahedral habitus and their intergrowths, and less frequently by irregularly shaped grains (cl. 14/40) (Fig. 6.1). The grain size varies from 250 to 500 μm. Chemical heterogeneity due to arsenic admixture (up to 3 wt.%) was detected in 9 of the 25 studied pyrite grains (Fig. 6.1b). The arsenic distribution mainly emphasizes correct ('concentric') zoning, with spotty distribution observed less frequently. The arsenic pyrite grains contain relatively high levels of other minerals, primarily sulfides such as galena, chalcopyrite, and occasionally pyrrhotite, sphalerite, and arsenopyrite (Ivanova et al, 2024). Small outcrops (less than 10 microns) of other minerals, including potentially uranium–bearing minerals like titanite, rutile, and rarely apatite, are also present (Figure 6.1a). Pyrite is occasionally fractured, and its brecciated grains contain chalcopyrite and calcite outcrops. Iron oxides/hydroxides develop along fractures (Figure 6.1c).

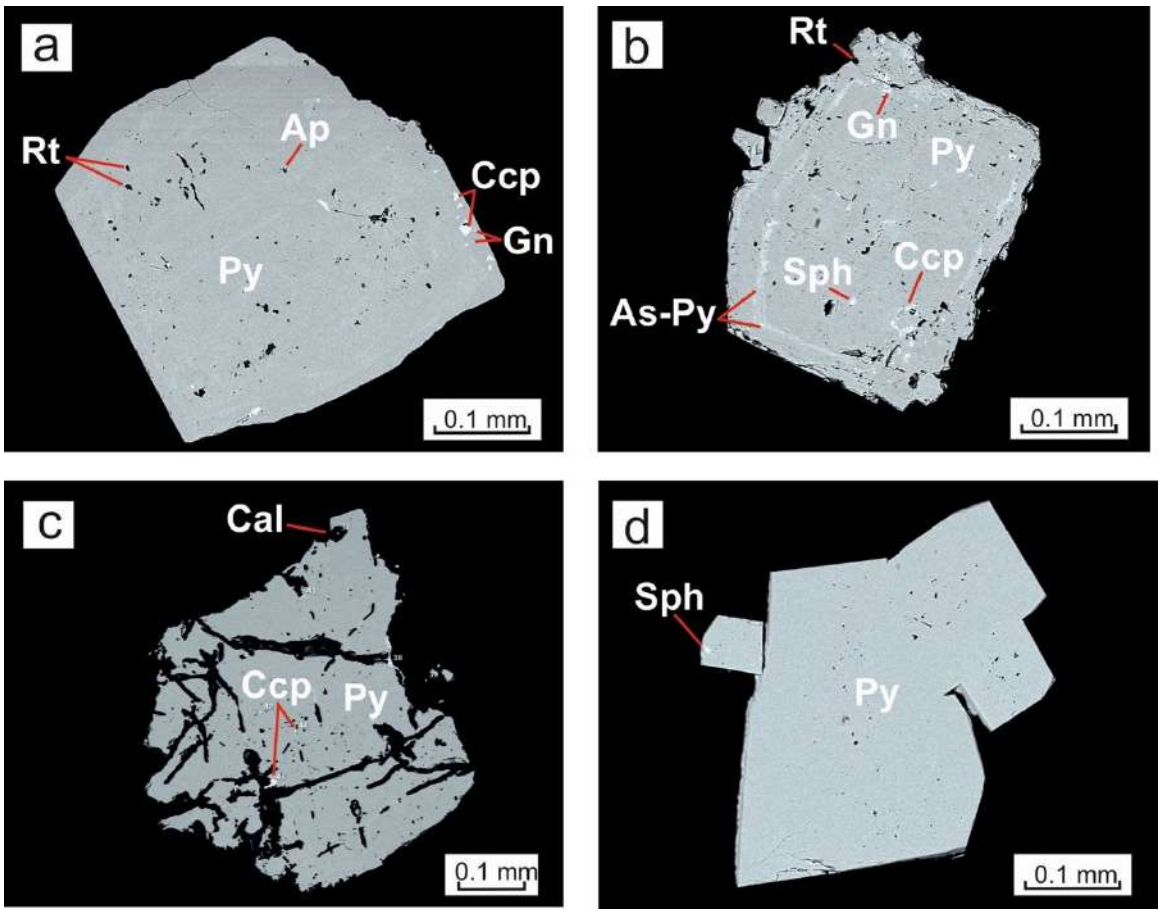

Figure 6.1. – BSE–images of pyrite of the Kariernoe ore occurrence: a – mineral inclusions in pyrite crystal (cluster 14/7); b – zonal distribution of arsenic in pyrite (cluster 14/32); c – brecciated pyrite (cluster 14–40); d – intergrowth of idiomorphic pyrite grains (cluster 14/26). Ap – apatite; As–Py – arsenic pyrite; Cal – calcite; Ccp – chalcopyrite; Gn – galena; Py – pyrite; Rt – rutile; Sph – sphalerite.

6.2 Novogodnee-Monto deposit

Pyrite crystals have a pentagonal–dodecahedral or cubic shape, with less frequent combined shapes (Figure 6.2). The regular growth zonation indicates elevated arsenic contents. Fine arsenopyrite outcrops can accompany arsenic–enriched zones (Figure 6.2b). Galena is present as fine disseminated phenocrysts and thin veins. Galenite, hessite, and nugget gold are confined to grain boundaries. In rare instances, gold and silver tellurides (such as petzite and hessite) develop along microcracks of cataclazed pyrite (Figure 6.2c). Silicate minerals, such as clinopyroxene and quartz, occasionally aggregate with pyrite in the form of small pinpoints (Figure 6.2a). Pyrite from the skarn–magnetite association is closely associated with chalcopyrite, which occurs in intergrowths and films on pyrite.

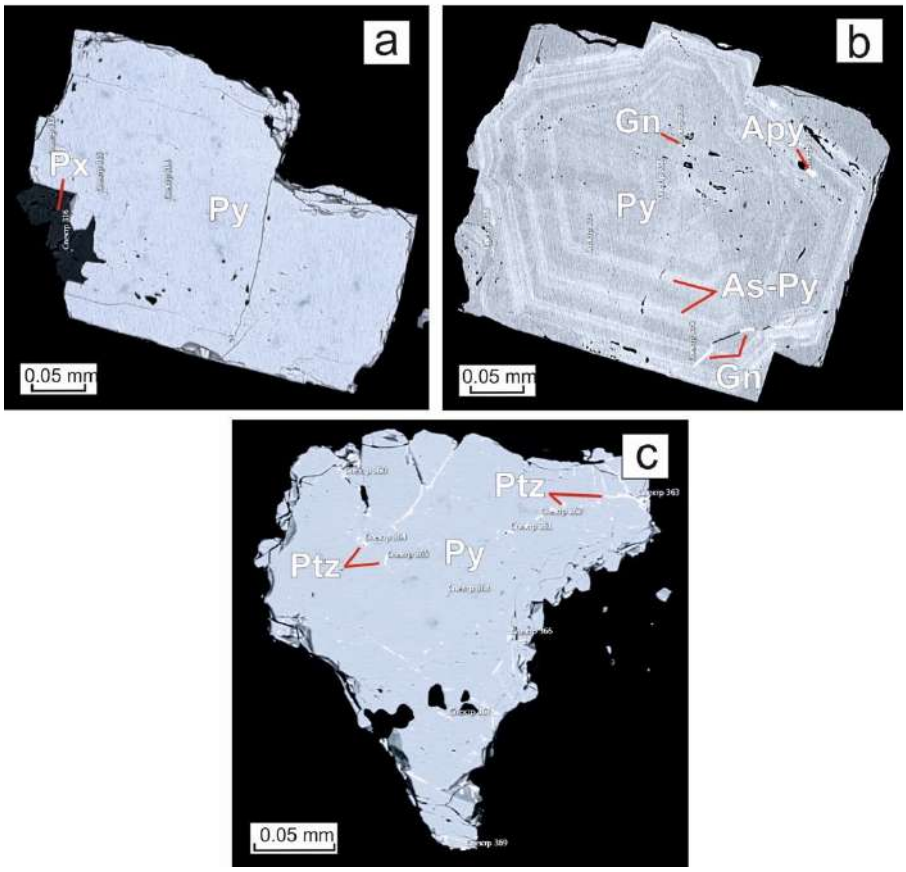

Figure 6.2. – BSE–images of pyrite of Novogodnee-Monto deposit (outcrop NM–32). a – intergrowth of idiomorphic pyrite with pyroxene; b – growth zoning, with increased arsenic content; c – thin veins of petzite in pyrite Mineral designations: Apy – arsenopyrite; As–Py – arsenic pyrite; Gn – galena; Ptz – petzite; Px – pyroxene; Py – pyrite.

6.3 Petropavlovskoe deposit

The sample contains predominantly irregularly shaped pyrite, sometimes with partial crystalline faceting. Pentagonal–dodecahedral habitus idiomorphic individuals are observed less frequently (Figure 6.3). The crystal structure contains numerous inclusions of nonmetallic minerals, characterized by greater saturation of inclusions in irregularly shaped grains (Figure 6.3c). The most common inclusions are large calcite, quartz, and plagioclase, and less frequently pyroxene. Irregularly shaped inclusions of galena and chalcopyrite are present among the ore minerals. Independent disseminated point xenomorphic microinclusions of gold and silver tellurides (hessite, petzite) and nugget gold (Au, Ag) are often found in pyrite interstices, sometimes in association with galena, and as thin veins along cracks in

cataclazed pyrite (Fig. 6.3c,d). In one instance, tellurium bismuthite was observed near inclusions of silicate composition. The grains contain numerous small, scattered inclusions of minerals that are presumed to contain uranium, such as zircon, xenotime, monazite, rutile, apatite, and titanite (Figure 6.3g).

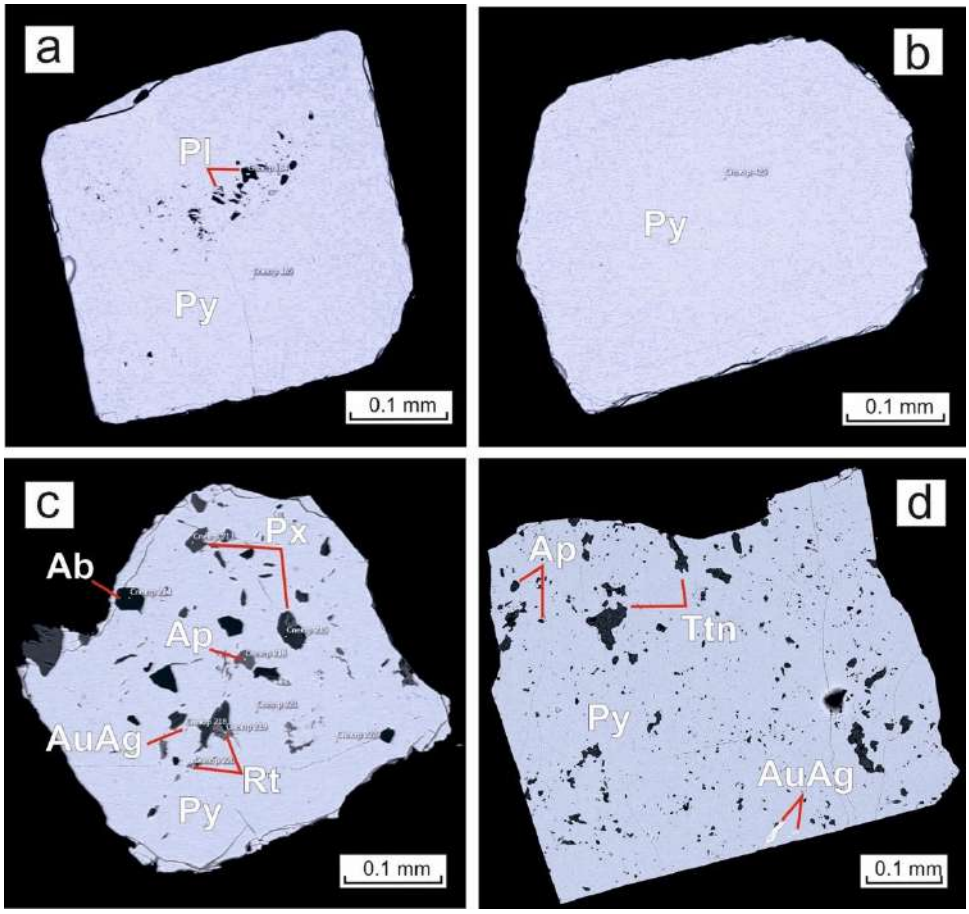

Figure 6.3. – BSE–images of pyrite of the Petropavlovskoe deposit from berezites: a – fine dissemination of plagioclase inclusions in pyrite (sample 309/15); c – scattered dissemination of non–metallic minerals in pyrite of irregular shape (sample 309–0–40). 309–0–40); from propylites: b – idiomorphic grain of pyrite (outcrop 309/11); from dolerites: d – pyrite grain saturated with titanite and apatite (outcrop S85/15). Ab – albite; Ap – apatite; AuAg – Au–Ag mineral phase; Pl – plagioclase; Px – pyroxene; Py – pyrite; Rt – rutile; Ttn – titanite.

6.4 Interpretation

The scanning electron microscopy results revealed significant differences in the chemical composition, distribution of mineral inclusions, and crystal appearance of pyrite.

Composition of pyrite

Pyrite's crystal structure contains numerous trace elements, with arsenic being the most significant. Arsenic contributes to the substitution of impurity elements in the mineral lattice, as noted by Kesler et al. (2010). The scanning electron microscopy results indicate that the pyrite of the Novogodnee-Monto deposit and some of the grains of the Kariernoe ore deposit have a zonal structure of arsenic distribution. This suggests the involvement of multiple generations of pyrite in the ore formation process. Arsenic is the most significant minor trace element due to its association with gold in most hydrothermal ore deposits. According to Reich et al. (2005), Au–Ag epithermal, Au mesothermal, Cu–porphyry, Cu–Zn volcanogenic massive sulfide ores, and other gold deposits are present. The incorporation of Au into the inter–nodes of the pyrite lattice, along with sulfur position substitution, may be facilitated by the presence of As, as noted by Vikentyev et al. (2016). Therefore, sections of arsenic–enriched pyrite may indicate favorable conditions for gold deposition.

Pyrite rich in arsenic is an indicator of the impact of hydrothermal processes (Kesler et al., 2010). The zonal distribution of arsenic provides insight into the nature of hydrothermal flows, such as changes in temperature or composition of the influencing fluid. It is probable that the hydrothermal solutions were saturated with gold, which precipitated on arsenic pyrite. Using arsenopyrite from a low–temperature Carlin–type deposit as an example, Deditius et al. (2009) and Reich et al. (2006) demonstrated that gold nanoparticles (<2 nm) dissolve and migrate at increasing temperatures (>350°C), accumulating as larger particles up to 8 nm at further stages. The zonal distribution may indicate the evolution of geochemical specialization of solutions through time. The presence of arsenic–distributed pyrite grains in the granitoid Soba batholith suggests that magmatic fluids had a pulsational impact on the ore formation. It is possible that the formation of arsenic–distributed pyrite rims resulted from the later superimposed impact of magmatic fluids on earlier pyrite from volcanogenic rocks.

Mineral inclusions

The composition and paragenesis of mineral inclusions can indicate the nature of the superimposed processes and their temperature. The low degree of saturation of the crystal lattice of pyrite in the Kariernoe ore occurrence with mineral inclusions, particularly the absence of visible gold and its minerals, presumably indicates that pyrite belongs to the first pre–metallic stage of ore formation. A portion of pyrite from the Kariernoe ore occurrence has a varied arsenic composition and is distinguished by a higher mineral saturation, including sulfides, likely due to overlapping processes. The presence of fluid components such as tellurium, fluorine, and chlorine in hydrogen sulfide solutions increases the migration capabilities of noble metals (Marakushev, 1979). Novogodnee-Monto pyrite contains rare inclusions of nugget gold and gold and silver tellurides, which may have resulted from precipitation in arsenic zones. The pyrite from the Petropavlovskoe deposit is the most mineral–saturated. Inclusions of quartz and calcite indicate a close connection between pyrite and host rocks during formation (Sedayeva et al., 2013). The variability of inclusions, predominance of low–temperature paragenesis, and sharp development of telluride complexes of noble metals may be due to changes in the hydrothermal regime. The poikilite structure of pyrite grains at the Petropavlovskoe deposit suggests the capture of grains of relict nonmetallic minerals from the replaced host rocks, indicating the hydrothermal–metasomatic origin of pyrite.

Crystal shape

Morphological transformations can indicate differences in the genetic nature of the mineral and suggest possible recrystallization. The shape of pyrite crystals in several objects, including Kariernoe–Novogodnee-Monto–Petropavlovskoe, undergoes gradual changes. The Kariernoe ore occurrence contains isometric grains with cubic and pentagon–dodecahedral habitus. In the Novogodnee-Monto deposit, these grains are complicated by a combination of forms, which may be a result of syn–ore metasomatosis of ore material. At the Petropavlovskoe deposit, pyrite loses its faceting and irregularly shaped grains predominate. The morpho–genetic

differences of pyrite at the Petropavlovskoe deposit are widely manifested, indicating the full manifestation of the ontogenic cycle of hydrothermal transformation of pyrite.

Conclusions

The Kariernoe ore deposit's volcanogenic pyrite is believed to serve as a primer during the crystallization of arsenic pyrite from residual solutions of the Sobo complex. The active process of oreogenesis involves accumulated sedimentary ore masses that transform during subsequent tectonic–metasomatic processing. The gold content of pyrite increases as it evolves from primary volcanogenic to hydrothermal–metasomatic. It is likely that gold was deposited on thin arsenic–enriched pyrite rims. When exposed to a saturated hydrothermal solution and as the temperature decreases, gold is released in the form of mineral phases. The variation in pyrite crystal forms within one site indicates the participation of several types of mineral–forming processes. The traceable successive mineralogical rearrangement of pyrite appearance suggests possible recrystallization of ore substance under the influence of superimposed hydrothermal processes.

The ore material in the Toupugol–Khanmeishor ore district, which is of volcanogenic–sedimentary origin, underwent metasomatic transformations due to superimposed processes. The data obtained allowed for a partial reconstruction of the hydrothermal workings, new formation, and/or re–deposition of sulfides during the geological process. Importantly for the interpretation of subsequent results of (U,Th)–He dating, it is indicated that there are several generations of pyrite present in the objects of study. Pyrite has a similar manifestation in gold deposits, characterized by one to several generations corresponding to certain stages and steps of mineral deposition (Pshenichkin et al., 1976). The data obtained suggests that the earliest generations of pyrite are associated with the Kariernoe ore occurrence, where the little–altered volcanics of the Toupugol Formation are preserved.

6.5 Adjustments to sample preparation and decomposition techniques

The method of grain selection for age determination needs improvement when dealing with the presence of multiple generations of pyrite within a single sample.

It is proposed to locally select pyrite of a specific generation, identified through mineralogical studies, from rock samples using a diamond 'miniborer' (Figure 6.4).

Figure 6.4. – Local sampling of pyrite from an ashlip with a diamond miniborer

The analysis of pyrite grains for uranium– and thorium–bearing inclusions revealed a high prevalence of micron–sized hard–to–soluble minerals, such as zircon, monazite, xenotime, and rutile, which are a source of 4He. During uranium and thorium decay, an alpha particle travels a distance of 11–34 μm in such inclusions (which do not exceed the first tens of μm), and it is implanted into the structure of the host mineral without accumulating in the relict mineral (Zeigler et al., 2010). A precise calculation of the (U,Th)–He age necessitates complete data on the uranium and thorium contents that served as the source of the accumulated helium. Therefore, the chemical and thermobaric conditions of its decomposition for (U,Th)–He dating were revised.

Pyrite decomposition work was carried out in autoclaves at a temperature of 220°C, providing additional pressure. An experiment was conducted to decompose an artificial mixture of pyrite (1 grain, 3–4 mg), zircon (6 grains, <50 μm), and quartz ampoule (60–70 mg) (Figure 6.5). Chemical preparation of the samples was modified during the experiment by eliminating the use of HCl and adding HF, HNO_3, and 0.05 mL of $HClO_4$ to the sample. Teflon bouquets containing solutions were sealed and immersed in coverslips. The coverslips were then placed in

autoclaves (Figure 6.5) with 2 ml of HF added to the bottom of the container. The autoclaves were kept in a thermostat at 220ºC for 48 hours.

Figure 6.4. – Experiment on the decomposition of a pyrite sample (pyrite, quartz ampoule, zircon mixture), including difficult to dissolve uranium–bearing minerals, under pressure in autoclaves.

The experimental results demonstrate that the chosen conditions guarantee complete decomposition of the artificial mixture, as shown in Figure 6.5. This technology minimizes losses of uranium and thorium due to incomplete decomposition of insoluble inclusions, ensuring the reliability of (U,Th)–He dating results.

CHAPTER 7. RESULTS OF PYRITE DATING

7.1 Results of (U,Th)–He dating

To identify the age stages of ore formation in the Voykar zone and the spatial and temporal relationships of sulfide mineralization with magmatic and/or hydrothermal processes, pyrite was dated. A total of 45 suspensions from 15 samples were analyzed, including metasomatites from the Novogodnee-Monto deposit (9 samples), the Petropavlovskoe deposit (25 samples), and tuffites of the Toupugol formation of the Kariernoe ore occurrence (11 samples) (Table 7.1).

Table 7.1 – Description of samples selected for (U,Th)–He dating, according to geological and petrographic data.

Sample number	Description
Kariernoe	
14–7	tuffites with scattered and layered pyrite
14–26	
14–27	
14–32	
14–40	quartz–carbonate vein with sulphide mineralization
Novogodnee-Monto	
HM–17	quartz–sericite metasomatites with vein–embedded pyrite mineralization
HM–27	pyroxene–epidote–garnet skarns
HM 31a	pyroxene–epidote–magnetite skarns with pyrite–chalcopyrite phenocrysts
Petropavlovskoe	
308/4	propylites
308/34	carbonate vein with rare disseminated pyrite mineralization

309–0–40	quartz–sericite metasomatites
309/11	propylites
309/15	quartz–sericite metasomatites with vein–embedded pyrite mineralization
S85/15	diorites of the Sob complex
Amphibolitovoe	
*S205b/21	dolerite dyke of the Musyur complex

**The Amphibolitovoe ore occurrence (66°48′ N, 65 ° 49′ E) is located 27 km east of the Petropavlovskoe deposit*

Pyrite ages ranging from 268 to 426 Ma (Tables 7.2, 7.3, 7.4) were obtained from (U,Th)–He dating of pyrite from the Toupugol–Khanmeishor ore district. The variation in (U,Th)–He ages could be due to several factors, including loss or excess of ^{4}He, loss or introduction of U and Th, and multistage formation of pyrite with different ages.

Excess and lost He

Excess ^{4}He in minerals can result from several factors, including trapping of hydrothermal ^{4}He, accumulation of ejected components from inclusions, or implantation of radiogenic ^{4}He.

The specific volume of extracted 4He from pyrite (10^{-6} –10^{-5} cm^3/g) significantly exceeds the known values for helium content in hydrothermal fluids (10^{-8} –10^{-10} cm^3/g; Bortnikov et al., 2000; Luders and Niedermann, 2010; Yakubovich et al., 2019) at all sites. Concentrations of trapped hydrothermal 4He can rarely reach 10–6 cm^3/g (Burnard and Polya, 2004). Even under such conditions, the specific volume of trapped hydrothermal ^{4}He could only increase the (U,Th)–He age by 10%. Therefore, the scatter of (U,Th)–He ages in the studied samples cannot be explained by the contribution of trapped helium.

The mass fractions of U and Th in pyrite are relatively small (0.1–6.0 μg/g), and in most cases, their contents are dominated by the host rocks. In this regard, it is important to consider the presence of implanted ^{4}He. Assuming mass fractions of U and Th equal to 1 and 3 μg/g, respectively, in the surrounding host rocks (average

values for island arc andesites, volcanogenic–sedimentary deposits, and carbonates; SRIM database) and a density of 2.65 g/cm^3, the amount of implanted and ejected ^{4}He would be nearly equal. Furthermore, the absence of correlation between the U, Th, and He contents and the age distribution (as shown in Figures 7.1, 7.4, and 7.6) decreases the likelihood of the implanted and ejected component's contribution. This is because its impact is most significant for low uranium grains.

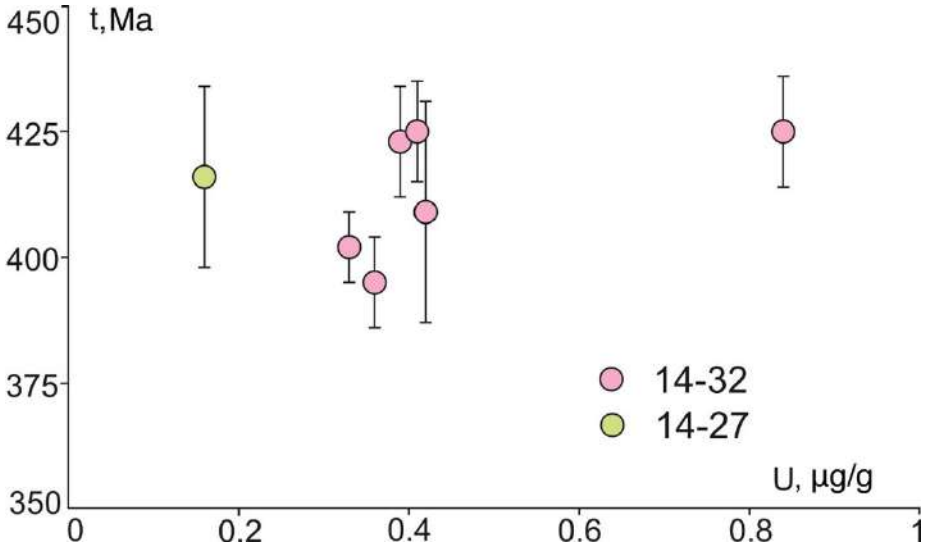

Figure 7.1 – Dependence of (U,Th)–He age on uranium content in pyrite of the Kariernoe ore deposit

4He losses

Radiogenic ^{4}He was released from the studied samples at temperatures close to the pyrite decomposition temperature (>450 °C). The fraction of low–temperature helium did not exceed 12% (Table 7.2; 7.3; 7.4; 7.5), indicating high retention of radiogenic helium in the studied pyrite grains. The pyrite crystal lattice has a high thermal retention of radiogenic helium (Yakubovich et al., 2019), which excludes the possibility of its diffusive losses. The closure temperature concept, when hypothetically applied to the behavior of the (U,Th)–He isotope system in pyrite, cannot explain the scatter of age values in grains of similar size within a small area.

Calculation of (U,Th)–He ages requires corrections for nuclear recoil (Farley et al., 1996). Considering the size of the studied pyrite grains (200–500 μm) and the average α–stopping pathway of 14 μm (calculated using SRIM; Ziegler et al., 2010), it can be estimated that less than 4% of He may have been lost due to the effect of nuclear recoil (Farley et al., 1996).

Losses and introductions of U and Th

Experiments conducted on pyrite from the Uzelga deposit have shown that interaction with weak acids can result in the loss of U (Yakubovich et al., 2020). Iron oxides and hydroxides that may develop on pyrite in the oxidation zone of sulfide ores can concentrate uranium (Moses et al., 1987; Scott et al., 2007). The presence of such phases could rejuvenate (U,Th)–He ages. The pyrite grains used for (U,Th)–He dating did not show any signs of oxidation or alteration that would be expected from prolonged contact with slightly acidic groundwater or atmosphere, except for samples 14–40, 308/34 which were excluded. Additionally, the samples were collected from fresh quarry walls, and no secondary alteration was observed in the slurries or in pyrite microanalysis. Therefore, it is unlikely that weathering processes disturbed the (U,Th)–He system of pyrite.

Pyrite can undergo recrystallization during dynamic and thermal metamorphism (Vikentyev et al., 2017; Barrie et al., 2011; Craig and Vokes, 1993). Currently, there is no precise data on the behavior of the (U,Th)–He system during pyrite recrystallization. However, evidence suggests a low degree of metamorphism of the Novogodnee-Monto deposit up to the zeolite facies (Puchkov, 2010). Based on the stability of the (U,Th)–He system during low–temperature metamorphism up to the prehnite–pumpellite facies at the Uzelginskoye deposit (Yakubovich et al., 2020), it can be assumed that the (U,Th)–He isotope system behaves in a closed manner even under low–grade conditions of the zeolite facies in the Toupugol–Khanmeishor area.

Methodological difficulties

The main methodological difficulties that can lead to scattering of (U,Th)–He ages are incomplete release of 4He from pyrite grains and incomplete decomposition of pyrite. According to Yakubovich et al. (2019), ^{4}He is released from pyrite grains at ~1100°C, which is a sufficient temperature to release all ^{4}He from pyrite.

Electron microscopy of pyrite revealed inclusions of uranium–bearing minerals such as zircon and rutile in some grains. The chemical decomposition technique used for these samples does not allow for complete dissolution, which

may result in overestimated age values. Because inclusions are distributed heterogeneously, their contribution can lead to irreproducible age values, as seen in the case of samples 14–7 and 14–26, which were excluded from subsequent calculations. To eliminate the influence of this factor in the future, changes to the method of pyrite decomposition are necessary (Figure 6.5). In cases where hard–soluble inclusions in pyrite's composition are rare, a mixture of HF, $HClO_4$, and tsar vodka should suffice to decompose U and Th from other inclusions.

Pyrite, the most common sulfide mineral in gold deposits, is characterized by one or several generations corresponding to certain stages and steps of mineral deposition (Pshenichkin et al., 1976). The high SCWO observed in some samples may be attributed to later processes of ore matter formation. The pyrite ages obtained from the samples (268–444 Ma) suggest that the mineral may have undergone multistage formation or partial/complete recrystallization during geological history. It is important to note that this interpretation is based solely on the obtained data and does not involve any subjective evaluations. In the following subchapters, clusters of ages will be identified based on mineralogical characteristics such as chemical composition and morphology of grains, as well as isotopic data.

7.1.1 Kariernoe ore occurrence

A total of eleven samples of pyrite extracted from five samples of volcanogenic rocks of the Kariernoe ore field were analyzed. Pyrite in samples 14–26 and 14–7 contained rutile and zircon inclusions, which are difficult to dissolve and do not decompose completely at 180°C at atmospheric pressure (Table 7.2). Therefore, due to the anomalous deviation from the weighted average age, which likely indicates uranium loss, these samples have been excluded from further discussion of the results. Sample 14–40 was also excluded from the age calculations due to low levels of radiogenic helium and fracture oxidation of pyrite.

Pyrite helium concentrations at the Kariernoe ore occurrence range from 6.26 – 1.48×10^{-5} cm^3/g (249.6 – 52.1 10^{-10} at.), while uranium content ranges from 0.23 to 1.68 μg/g (Th/U = 0.45–2.7). The isochron age obtained from seven measurements is 421±6 Ma (2σ, MSWD= 6) as shown in Figure 7.2.

Table. 7.2 – Results of (U,Th)–He dating of pyrite from volcanogenic rocks of the Kariernoe ore occurrence

Sample	№ sample	U, 10^{10}at.	σ, %	Th, 10^{10}at.	σ, %	Th/U	^{4}He, 10^{10}at.	σ, %	ω ^{4}He$_{low}$ $_t$, %	T, Ma	±, (2σ)
14-32	892	424.0	1.0	189.4	1.0	0.4	249.6	0.4	0.27	402	7
	902	136.9	1.1	65.0	0.9	0.5	85.9	1.0	0.21	425	11
	903	240.0	1.3	113.2	0.9	0.5	149.6	0.7	1.44	423	11
	904	287.2	1.1	133.5	0.8	0.5	180.1	0.7	0.15	425	10
	905	212.6	3.1	93.6	2.7	0.4	127.5	0.7	0.30	409	22
	1095	172.0	1.1	80.8	1.0	0.5	99.9	0.8	2.55	395	9
14-27	1075	58.8	3.4	157.0	2.6	2.7	52.1	0.8	0.63	416	18
*14-7	1078	19.4	1.9	26.5	2.6	1.4	16.7	2.6	0.00	492	27
*14-26	1079	154.7	1.2	59.6	1.3	0.4	122.8	0.8	0.36	541	13
	1083	278.6	1.5	108.3	2.3	0.4	183.0	2.6	1.51	451	7
**14-40	1062	–	–	–	–	–	8.1	4.5	0.00	–	–
Qu blank		1.3	97.0	6.0	74.0	–	1.1	37.0		–	–

***excluded due to anomalous deviation from the weighted average age value*
*** low ^{4}He isotopic contents*

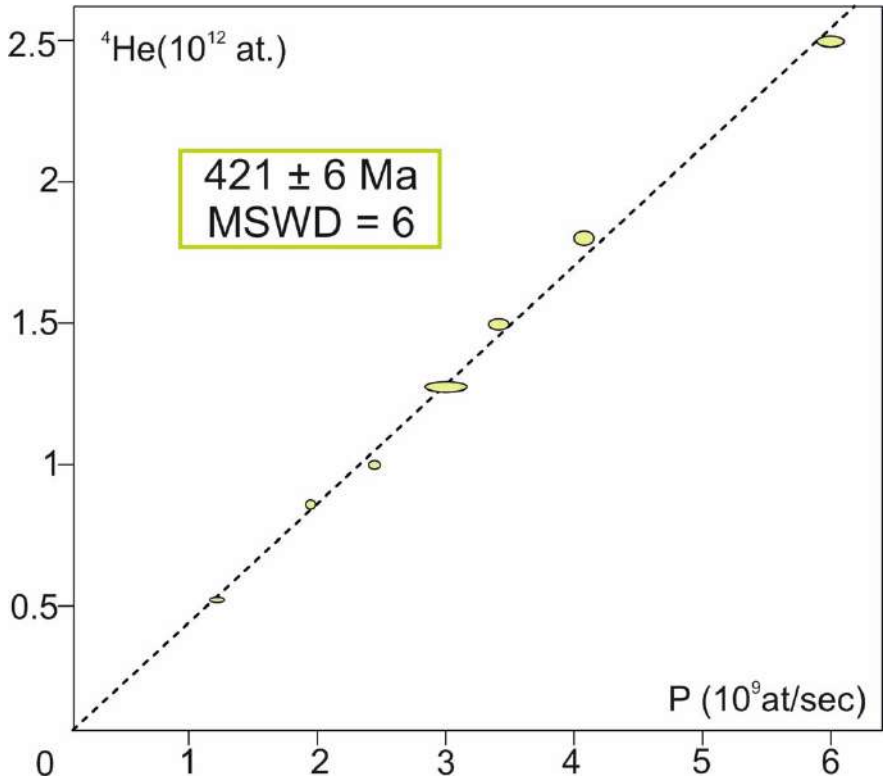

Figure 7.2 – (U,Th)–He isochrone for pyrite from the Kariernoe ore occurrence. P is the present–day rate of 4He formation (Vermeesch, 2018). Age determination error is given at 2 σ.

Interpretation

The isochronous (U,Th)–He age of pyrite from Silurian volcanogenic rocks of the Kariernoe ore occurrence is 421±6 Ma, which is consistent with geological estimates of the age of rock formation and ore mineralization in the region (Pryvnanosov et al., 1994; Dushin et al., 2014; Vikentyev et al., 2017). At the same time, a high MSWD and a wide range of (U,Th)–He ages of pyrite between 402–425 Ma are observed, which may be due to multi–stage formation of pyrite and/or partial recrystallization during superimposed processes (Ivanova et al., 2024).

It is possible that pyrite of several different age generations occurs within the Kariernoe ore occurrence. Scanning microscopy results indicate that some grains have a zonal structure of arsenic distribution (Figure 6.1). Arsenic pyrite is an indicator of the impact of hydrothermal processes (Kesler et al., 2010). It can be hypothesized that the formation of arsenic pyrite rims reflects the later superimposed impact of magmatic fluids on earlier pyrite from volcanogenic rocks, which is supported by the dating results.

The dating results reveal two clusters of ages, suggesting the probability of several generations of pyrite in the sample (Figure 7.3). The age of the Toupugol Formation's sedimentation is 424±6 Ma (2σ, n=4, MSWD = 0.6), which corresponds to the Late Wenlock–Ludlow age according to biostratigraphy data (Pryamonosov et al., 1994; Dushin et al., 2014; Zyleva et al., 2014). Thus, this early generation corresponds to the initial stage of ore formation that occurred during active volcanism, with the accumulation of lavas and tuffs of basaltic, andesibasaltic, and andesite compositions (Silaev, 2003).

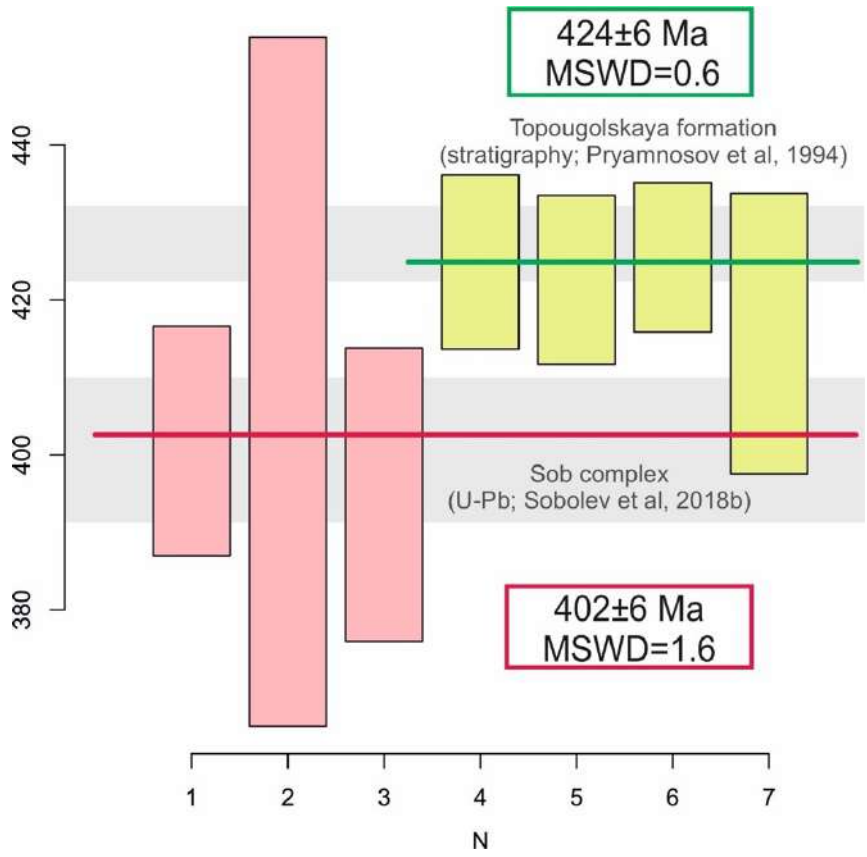

Figure 7.3 – Weighted average age of pyrite from volcanogenic rocks of the Kariernoe deposit obtained from 7 suspensions (from two pyrite samples).

The age of 402±6 Ma (2σ, n=4, MSWD = 1.6) is similar to the Early Devonian ages of zircons from metasomatized diorites of the main phase (410±2 Ma (Vikentyev et al., 2017)) and dyke plagiogranites of the late phase (403±4 Ma; Sobolev et al., 2018b) of the Sobo complex. This similarity may be due to pyrite formation and/or recrystallization. The geological data support the obtained conclusions: the rocks of the Sobo complex are present within the first tens of meters from the sampling site (Figure 4.4). The presence of thin disseminated sericite phenocrysts may indicate superimposed hydrothermal activity associated with their intrusion.

Th/U ratios in pyrite (Wignall and Twitchett, 1996) serve as an indicator of the redox conditions of the geological environment, allowing for reconstruction. 1) reducing (Th/U <2); 2) transitional (2≤Th/U≤7); and 3) oxidizing (Th/U >7) environments. The uranium concentration in the analyzed pyrite grains significantly exceeds the thorium content. Most values of Th/U ratios in pyrite from the Kariernoe ore occurrence range narrowly from 0.4 to 0.5, with a deviation of up to 2.6 in a

single case. This range of values may indicate that the medium of accumulation of metal–bearing volcanogenic–sedimentary rocks had strongly reducing conditions, which is typical of relatively deep–water conditions. These reducing conditions are favorable for the concentration of indifferent elements, such as gold, in solutions. Additionally, the further enrichment of hydrogen sulfide solutions with alkali metals is an important factor in the concentration of chalcophilic metals and gold (Markushev, 1979).

The age of the early pyrite generation, 424±6 Ma, corresponds to the age of formation of tuffs and tuffites of the Toupugol Formation. Therefore, this stage of ore mineralization likely reflects the formation of stratiform sulfide mineralization under deep–water conditions. The preservation of early volcanogenic–sedimentary (cuprous) ores is favored by the geological position of the site, which is sufficiently remote from large intrusive bodies.

The Early–Middle Devonian Soba complex experienced intrusion of island–arc granites, which may have caused hydrothermal alteration of the host rocks near the intrusive contacts. The (U,Th)–He age of the later mineralization (402±6 Ma) aligns with the previously established formation time of granitoids of the Soba Complex. Mineralogical and geochemical observations indicate that newly formed pyrite of late generation is enriched in gold and arsenic, as evidenced by the rims of its arsenic variety.

7.1.2 Novogodnee-Monto deposit

For the Novogodnee-Monto deposit 9 pyrite samples were analyzed: from quartz–sericite near–metasomatites (n=6) and skarns (n=3). The results of U, Th and ^{4}He concentrations are presented in Table 7.3. The specific volume of ^{4}He ranges from 1.30×10^{-5} to 4.83×10^{-6} cm^3/g (51.2 – 17.8 10^{-10} at.) for the beresites and $7.37 – 1.14\times10^{-6}$ (45.2 – 3.2 10^{-10} at.) for the deposit skarns. The mass fraction of U varies from 0.1 to 0.5 μg/g, and the Th/U ratio values for each rock group ranged from 2.1 to 4.9.

Table 7.3 – Results of (U,Th)–He dating of pyrite from metasomatites of Novogodnee-Monto deposit

Sample	№ sample	U, 10^{10}at.	σ, %	Th, 10^{10}at.	σ, %	Th/U	^{4}He, 10^{10}at.	σ, %	ω $^4He_{low\ t}$, %	T, Ma	±, (2σ)
Pyrite–sericite–quartz metasomatites											
HM-17	872	16.6	2.7	81.1	2.5	4.9	17.8	1.9	0.93	384	8
	875	54.0	2.5	136.2	2.3	2.5	42.0	0.9	0.00	374	6
	877	33.2	2.5	126.6	3.2	3.8	34.0	1.1	0.76	414	7
	878	43.5	4.4	170.9	3.8	3.9	41.7	1.5	1.31	383	10
	889	51.4	5.7	208.8	1.3	4.1	51.2	0.6	0.00	391	11
	890	42.7	2.9	181.7	1.8	4.3	46.4	0.9	0.15	417	7
Skarns											
HM-27**	967	9.5	4.0	5.8	2.9	0.6	3.2	3.5	0.72	224	11
HM-31a**	968	6.5	4.1	10.1	2.5	1.6	5.5	3.1	43.07	467	18
	971	111.4	1.8	235.8	1.5	2.1	45.2	1.5	11.78	209	8
Qu blank		1.3	97.0	6.0	74.0	–	1.1	37.0		–	–

*** low isotopic contents of ^4He*

Pyrite from pyroxene–epidote–garnet skarns

Helium contents in pyrite from skarns are rather low. Only one of the samples showed significant amounts of helium. Pyrite from pyroxene–epidote–epidote skarns is closely associated with chalcopyrite, which forms accretions and films on its surface. However, chalcopyrite's complex ^{4}He emission kinetics and low helium migration activation energy make it unsuitable for (U,Th)–He dating (Yakubovich et al., 2019). Sample 971 has been excluded from the calculations due to its potential impact on helium losses and anomalous age rejuvenation.

Pyrite from pyrite–sericite–quartz metasomatites

(U,Th)–He ages of pyrite from berezites are quite reproducible, but show a large scatter in the 370–420 Ma range. The central age calculated for six pyrite samples from pyrite–sericite–quartz metasomatites is 395±6 Ma (2σ; n=6) (Figure 7.4). The age of pyrite from the Novogodnee-Monto deposit is consistent with independent geological estimates for the age of ore formation (380–400 Ma) (Vikentyev et al., 2017; 2019; Udoratina et al., 2005). There is no correlation

between age and the concentration of U, Th, or He in grains (Figure 7.5). This indicates that there is little likelihood of an effect of trapped or implanted 4He on the dispersion of (U,Th)–He ages, since trapped He is dependent on the U and Th concentrations.

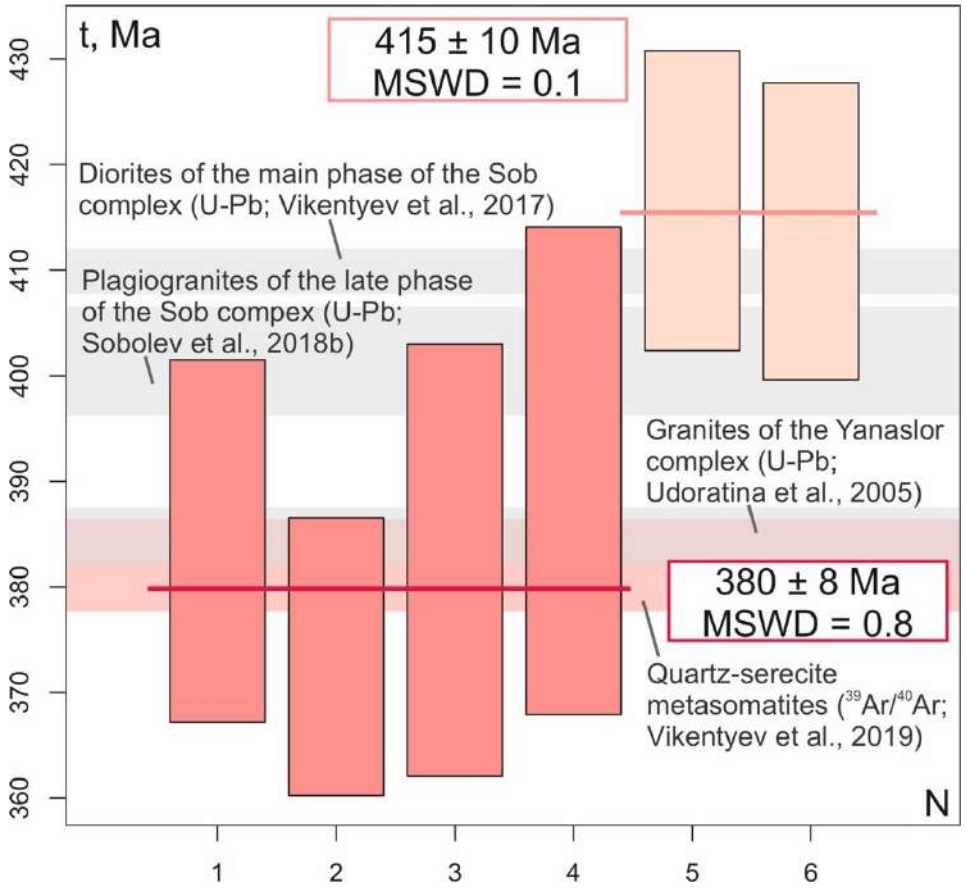

Figure 7.4 – Graph of weighted average values for pyrite of Novogodnee-Monto deposit (outcrop NM–17) for 6 samples, plotted in Isoplot R program (Vermeesch, 2018).

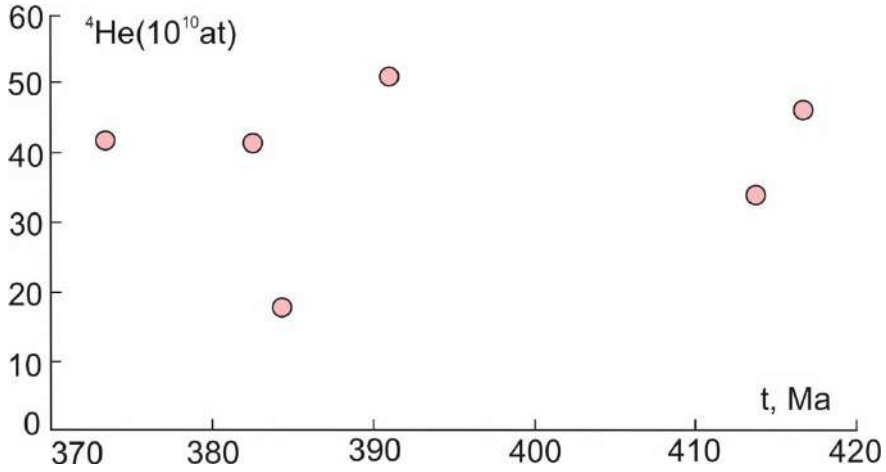

Figure 7.5 – Dependence of (U,Th)–He age on helium concentration in pyrite of Novogodnee-Monto deposit

All (U,Th)–He ages fall within the time frame of magmatic and metasomatic activity associated with the formation of the volcanic–plutonic belt in this region (382–418 Ma) (Sobolev, 2019 and references in this paper). The relatively large scatter of (U,Th)–He ages can be attributed to different phases of oreogenesis and crystallization of pyrite, as evidenced by the zonal structure of some pyrite grains (Figure 6.2). Sample NM–17 may contain two generations of pyrite. The first generation (415±10 Ma (2σ; n=2)) corresponds to the skarn stage of deposit formation. Most researchers attribute the age of skarn–magnetite mineralization within the Novogodnee-Monto deposit to the main intrusion phase of the Soba complex (410±2; U–Pb by zircon Vikentyev et al., 2017) at the boundary of lenses of limestone and volcanics of basic composition. The age obtained corresponds to the main stage of dioritic magmatism in the Polar Urals (Yakubovich et al., 2021).

The second generation of pyrite (380±8 Ma (2σ; n=4)) corresponds to a lower–temperature bresite stage (382–360 Ma) (Vikentyev et al., 2019). The (U,Th)–He age of pyrite from the Novogodnee-Monto deposit is supported by independent geological observations (references). The age derived from the data is correlated with the emplacement time of the Middle–Late Devonian minor granitoid intrusions of the Janaslor complex in the Voykar zone (387–383 Ma) (U–Pb; Udoratina et al., 2005). The Rb–Sr isochron age of the dyke of montsodiorite porphyries of the Musyur complex (some researchers distinguish it as the Kongorian complex) (382±10 Ma Soloviev et al., 2013; Girfanov et al., 2008), which forms the geological section of the deposit, coincides with the obtained values. (U,Th)–He ages are consistent with the results of 40Ar/39Ar dating on sericite from berezitoids of the Petropavlovskoe deposit (382±4 Ma Vikentyev et al., 2019). The 380 Ma boundary is interpreted as the final stage of island–arc magmatism, marking the final extinction of magmatic sources that formed the granitoid bodies of the Sob Batholith, which influenced the processes of gold and Cu–Fe(±Au) mineralization formation (Remizov, 2004; Udoratina et al., 2005; Sobolev et al., 2018).

7.1.3 Petropavlovskoe deposit

At the Petropavlovskoe deposit, 25 pyrite samples were analyzed from various rock types: propylites (n=7), pyrite–sericite–quartz metasomatites (n=12), granodiorites of the Sob complex (n=3), and a carbonate vein (n=1). The results of measuring U, Th and ^{4}He concentrations are presented in Table 7.4.

Table 7.4 – Results of (U,Th)–He dating of pyrite from metasomatites and igneous rocks of Petropavlovskoe deposit

Sample	№ sample	U, 10^{10}at.	σ, %	Th, 10^{10}at.	σ, %	Th/U	^{4}He, 10^{10}at.	σ, %	ω ^{4}He$_{low\ t}$, %	T, Ma	±, (2σ)
Propylites											
308/4	1028	174.9	2.4	264.6	2.4	1.5	105.3	0.3	2.26	339	6
	1035	196.8	1.6	301.1	1.6	1.5	135.3	0.3	1.11	385	5
	1040	221.6	3.4	395.4	3.4	1.8	160.4	0.2	1.07	388	9
309/11**	1021	–	–	–	–	–	3.2	5.5	0.00	–	–
	1027	10.9	2.5	24.7	2.5	2.3	9.4	3.8	12.97	426	17
**	1038	–	–	–	–	–	4.6	2.7	1.78	–	–
**	1088	–	–	–	–	–	6.9	2.4	4.40	–	–
Pyrite–sericite–quartz metasomatites											
309-0-40	922	33.0	2.1	198.7	1.5	6.0	27.6	4.8	0.00	268	13
	926	35.1	7.5	198.6	1.4	5.7	31.5	2.7	2.45	298	12
	1018	26.3	1.4	160.9	1.4	6.1	25.3	1.4	0.00	305	4
*	1066	25.9	6.7	127.2	1.2	4.9	35.4	0.9	0.90	485	15
309/15	925	55.0	1.5	172.4	1.5	3.1	47.9	3.1	9.89	384	5
	927	245.8	1.5	659.5	1.5	2.7	154.1	0.4	0.38	296	3
	928	230.6	2.1	565.6	1.7	2.5	182.0	2.3	0.33	383	12
	929	374.5	1.4	815.0	1.6	2.2	209.0	0.8	1.21	284	13
	977	260.6	1.0	748.5	1.0	2.9	227.1	0.3	0.00	398	3
	983	367.0	1.0	515.1	0.8	1.4	269.2	0.5	2.71	418	4
	1063	264.7	2.6	680.2	1.3	2.6	247.8	0.8	0.67	444	8
**	1065	–	–	–	–	–	6.7	3.2	0.00	–	–
Plagiogranite porphyries											
S 85/15	1082	148.6	7.0	137.0	1.9	0.9	97.5	0.6	1.71	408	23
	1090	290.0	2.2	188.4	1.5	0.6	146.5	0.6	1.06	333	6
	1092	316.3	2.3	218.1	3.4	0.7	146.6	0.6	4.81	304	6

Carbonate vein											
308/34**	1106	–	–	–	–	–	1.8	3.9	0.00	–	–
Qu blank		1.3	97.0	6	74.0	–	1.1	37.0		–	–

***excluded due to anomalous deviation from the weighted average age value*
*** low ^{4}He isotopic content*

Pyrite from propylitized rocks

Four suspensions of pyrite from two samples were analyzed. The specific volume of ^{4}He in pyrite from propylites ranges from 4.15×10^{-5} to 3.64×10^{-6} cm^3/g (160.4 – 9.4 $\times10^{-10}$ at.). The mass fraction of U ranges from 0.1 to 0.9 μg/g, and the Th/U ratio ranges from 1.5–2.3. One measurement from sample 308/4 deviated markedly from the mean age and was excluded from the plot. From a geological perspective, the single rejuvenated age value of 339±6 Ma (2) aligns with the known 40Ar/39Ar plagioclase age estimates of 339±4 Ma (Sobolev et al., 2020) for the late dacites of montsodiorite porphyries of the Musyur complex.

The isochron age obtained for the propylites of the Petropavlovskoe deposit is 394±10 Ma (MSWD=1; (2σ); n=3) (Figure 7.6). The probability of incomplete decomposition of inclusions in pyrite grains is minimized due to their rare and fine dissemination (Figure 6.3). Propylites are closely related to near–neutral and weakly acidic low–temperature solutions by nature of origin (Korzhinsky, 1953). Propylite mineralization zones are limited to the contacts of plagiogranite dikes (403±4 Ma; zircon U–Pb; Sobolev et al., 2018b), confirming the association of hydrothermal alteration with magmatic waters of the Soba complex (Mansurov, 2013).

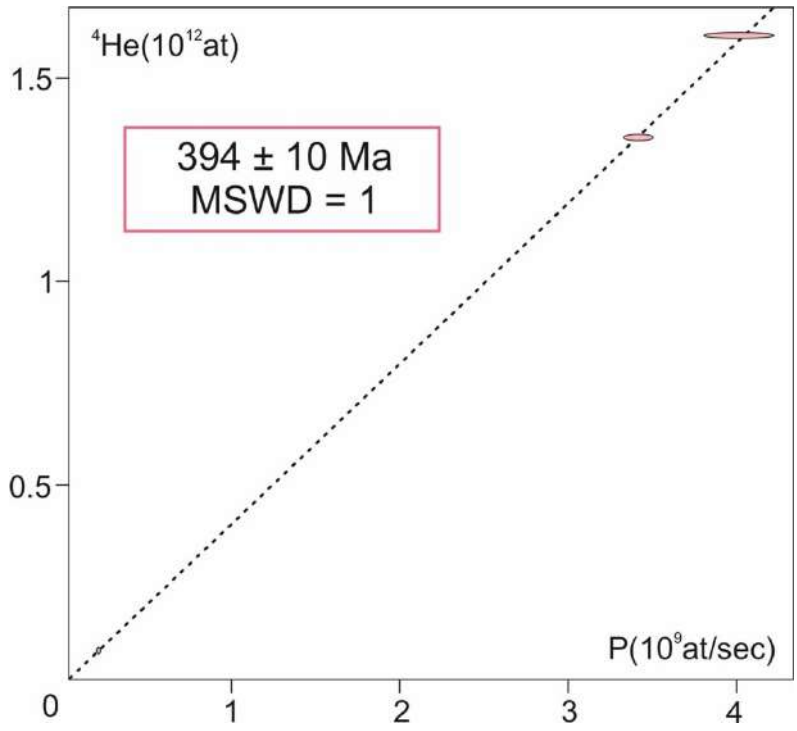

Figure 7.6 – (U,Th)–He isochron for pyrite from propylites of Petropavlovskoe deposit. P is the reduced modern rate of ^{4}He formation.

Pyrite from pyrite–sericite–quartz metasomatites

The volume of ^{4}He in pyrite from berezitoids of the Petropavlovskoe deposit ranges from 6.912×10^{-5} to 5.24×10^{-6} cm^3/g ($227.1 – 25.3 \times10^{-10}$ at.). The mass fraction of U varies widely from 0.1 to 1.5 μg/g, and the Th/U ratio ranges from 1.5 to 6.0. Despite the wide range of U values, there is no observed correlation between its content and age distribution, confirming the lack of contribution of the ejected and implanted component (Figure 7.7).

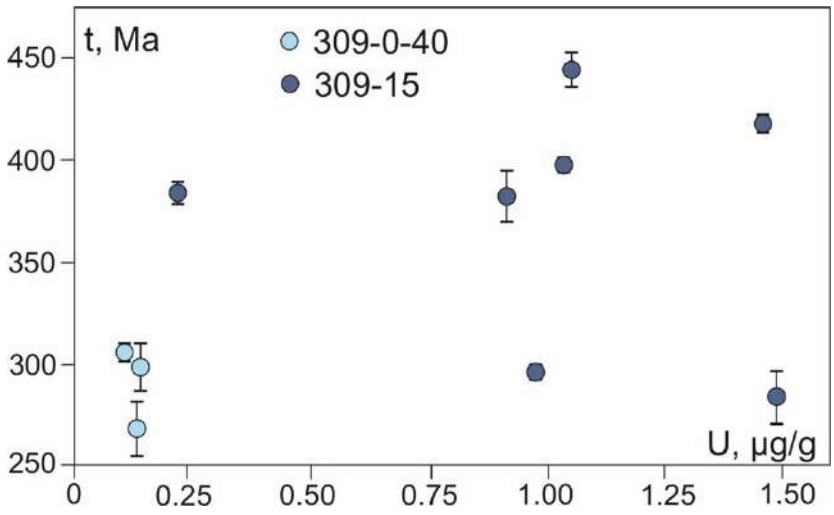

Figure 7.7 – Dependence of (U,Th)–He age on uranium content in pyrite of pyrite–sericite–quartz metasomatites of Petropavlovskoe deposit

The dating results were divided into two age clusters: 293±4 Ma (MSWD=5; 2σ; n=5) and 396±5 Ma (MSWD=1.6; 2σ; n=3) (Figure 7.8). The distribution of values appears random and is not correlated with uranium isotopic contents, ruling out the possibility of age cluster separation due to trapped or implanted 4He (Figure 7.7). The age of sample 309–0–40 was determined to be 382±4 Ma through 40Ar/39Ar dating of a sericite monofraction (Vikentyev et al., 2019). This age is similar to one of the values obtained for pyrite–sericite–quartz rocks. The (U,Th)–He age of pyrite (396±5 Ma) from quartz–sericite metasomatites is closest to the age of zircons (403±4 Ma) from plagiogranite porphyries of the Soba complex (Sobolev et al., 2018a) during the Early–Middle Devonian period. A part of the pyrite may be associated with the formation of the largest dioritoid plutons of the Sob Batholith.

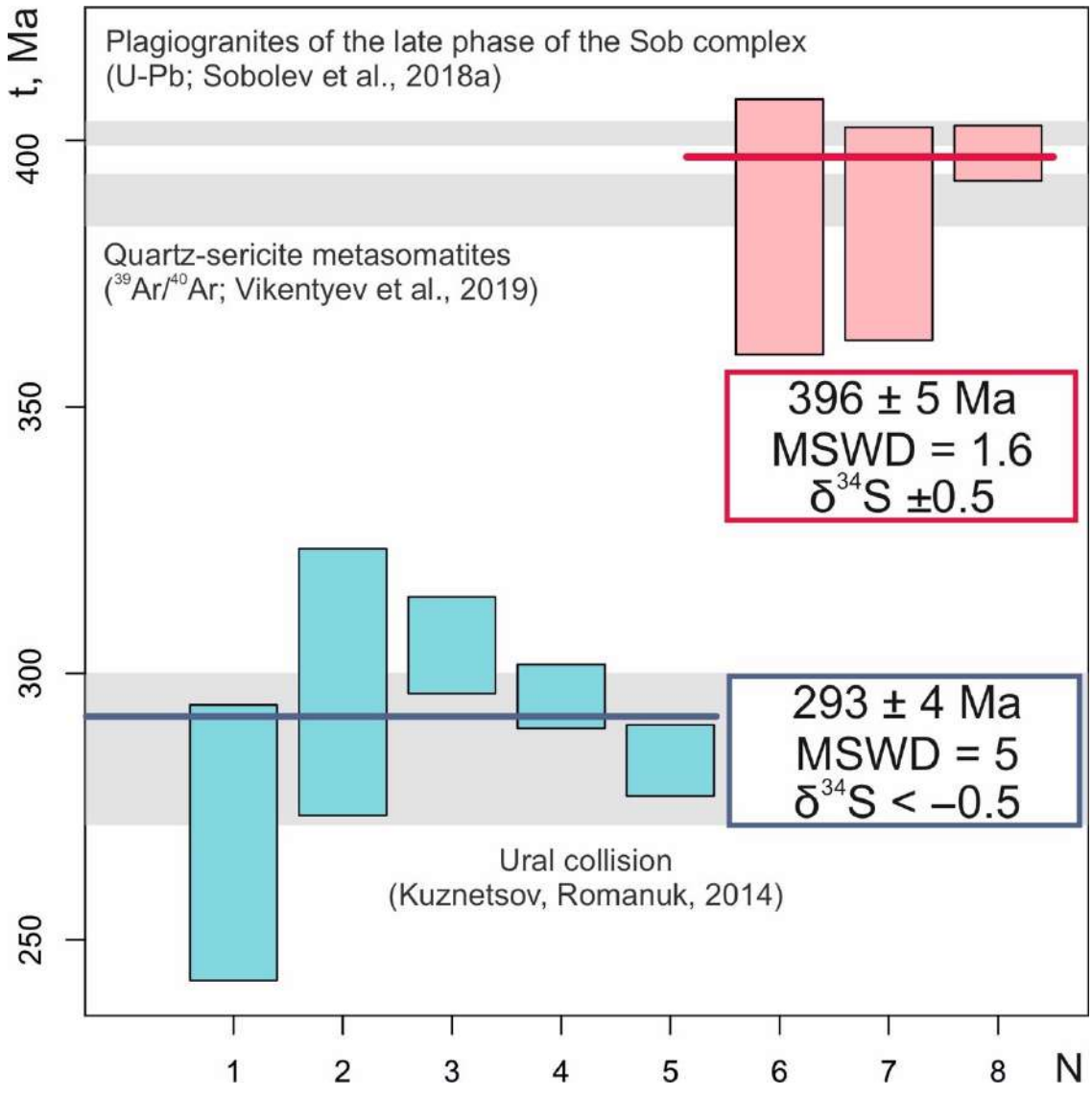

Figure 7.8 – Graph of weighted average values for pyrite of the Petropavlovskoe deposit.

The Early Permian age of the pyrite (293±4 Ma) is consistent with known isotopic data in the region, and the youngest U–Pb ages of zircons from gabbrodolerites (256±7 Ma) and lamprophyres (248±7 Ma) of the Musyur Complex (Vikentyev et al., 2017) are not inconsistent.

The tectonic structure of the deposit facilitates the migration, concentration, and redeposition of chemical elements in paleostratigraphic zones. On a regional scale, northwest strike–slip fault systems control quartz–pyrite–sericite alteration. These tectonic disturbances are perpendicular to the Main Ural Fault and represent the late stage of deformation associated with the action of shear stresses during the collisional process (Sychev and Kulikova, 2010). The (U,Th)–He age of Early Permian berezitoids correlates with the collisional stage of the Arct–Laurussia and Siberia–Kazakhstan–Kyrgyzstan continents (270–300 Ma; Kuznetsov and Romanuk, 2014), which probably caused partial redistribution of ore material or new formation of pyrite. The complex morphology and saturation of pyrite inclusions (Figure 6.3) confirm active tectonic–metasomatic workings of the ore substrate.

The results of (U,Th)–He dating were correlated with the data on the distribution of isotopic composition $\delta^{34}S$ (–12 to +0.5‰) within the deposit (Vikentyev et al., 2017). The central part of the deposit is characterized by a homogeneous sulfur isotopic composition with deviations from –0.5 to +0.5‰ from the meteoric standard 34S. Pyrite with significantly lower $\delta^{34}S$ values (–12 to –5‰) occurs in the northwestern part of the deposit. The sulfur isotopic composition of sulfur in pyrite found in the mantle is indicative of mineralization that occurred during the Devonian period. Pyrite from the northwestern part of the deposit is dominated by younger Early Permian age estimates and is characterized by a light sulfur isotopic composition ($\delta^{34}S$ <–5‰), suggesting the involvement of crustal sources. Therefore, it can be assumed that the most recent generation of pyrite is associated with collisional tectonic events in the Urals.

Pyrite from igneous rocks

We analyzed five samples of pyrite from igneous rocks: plagiogranite porphyries of the Soba complex (n=3) and dolerites of the Musyur complex (n=2).

The (U,Th)–He dating of plagiogranite porphyries resulted in a wide range of ages (304–408 Ma). The dating of two pyrite samples yielded Carboniferous ages of 333±6 and 304±6 Ma, respectively. Only one measurement yielded an Early Devonian age of 408±23 Ma (2 σ), which is close to the age of zircons (410±2 Ma) from main–phase diorites of the Soba complex (Vikentyev et al., 2017) dated at the Petropavlovskoe deposit a few meters from the sampling site of sample S85–15. The interpretation of coal–bearing pyrite dating is ambiguous. The young ages of the sample can be explained by the presence of chalcopyrite films on the surface of pyrite, which are characterized by reduced helium preservation and close aggregation with calcite, possibly containing uranium. Alternatively, the Carboniferous dating may be explained by the restart of the (U,Th)–He isotope system in pyrite or the formation of later generations of pyrite as a consequence of accretionary–collisional events in the Urals (Puchkov, 2010). The Novogodnenskoe ore field was intruded by a significant number of Early Carboniferous basite dykes of the Musyur complex, which can be used to date the Early Carboniferous period (Sobolev et al.,). The formation of the island arc occurred during the accretion to the Arct–Laurussia paleocontinent (360–312 Ma) (Glodny et al., 2000; Kuznetsov and Romanuk, 2014; Sobolev et al., 2020). The youngest Late Carboniferous age (270–300 Ma) is well correlated and probably related to the main stage of the Ural continental collision.

Samples of dolerites from the Musyur complex were collected at a location distant from the Novogodnenskoe ore field, within the Amphibolitovoye ore field. Two ages were determined for the dolerites: 383±10 and 324±13 Ma (2σ) (Table 7.5). The first measurement had high values of U and Th measurement errors, and therefore the sample was excluded from the discussion. The age of dolerites only holds estimated value and does not contradict the known results of 40Ar/39Ar dating of dikes of the third phase of the Musyur complex by plagioclase (313±10 Ma) and amphibole (334±3 Ma) (Sobolev et al., 2020).

Table 7.5 – Results of (U,Th)–He dating of pyrite from dolerites of the Amphibolite ore occurrence

Dolerites											
Sample	№ sample	U, 10^{10}at.	σ, %	Th, 10^{10}at.	σ, %	Th/U	^{4}He, 10^{10}at.	σ, %	ω $^4He_{low\ t}$, %	T, Ma	±, (2σ)
S 205b/21	1085	111.8	13.6	410.2	9.1	3.7	104.0	0.7	0.91	383	10
	1086	127.2	7.0	358.0	3.3	2.8	89.1	0.7	1.45	324	13
Qu blank		1.3	97.0	6	74.0	–	1.1	37.0		–	–

Pyrite from a carbonate vein

The pyrite vein has a low helium content and was excluded from the calculations. The kinetics of helium release are complicated by the tight intergrowth of grains with chalcopyrite and calcite.

7.2 Results of the Re–Os dating

To verify the results of (U,Th)–He dating of pyrite, Re–Os dating of 5 pyrite samples from the Petropavlovskoe deposit was perfomed on a thermal Ionization mass spectrometer in the laboratory Jamsrec (Japan) and presented (Table 7.6).

Table 7.6 – Description of samples for Re–Os dating based on geological data

Sample number	Description
308/31	Quartz diorites with lenses and pyrite clusters
308/34	Carbonate vein with rare disseminated pyrite mineralization
309/44	Mafic volcanics with sulfide veins
309/48	Late quartz vein with sulfide mineralization (pyrite, rarely chalcopyrite)
310/43	Metasomatic rocks with abundant pyrite phenocrysts and thin sulfide veins, in contact with late unaltered dyke

The absence of isochron dependence and the wide range of values may be due to isotopic heterogeneity of trapped Os or disruption of the isotopic system by

superimposed processes. The Petropavlovskoe deposit is characterized by a complex, multistage formation, making it difficult to obtain a single Re–Os isochrone corresponding to the time of ore formation (Figure 7.9).

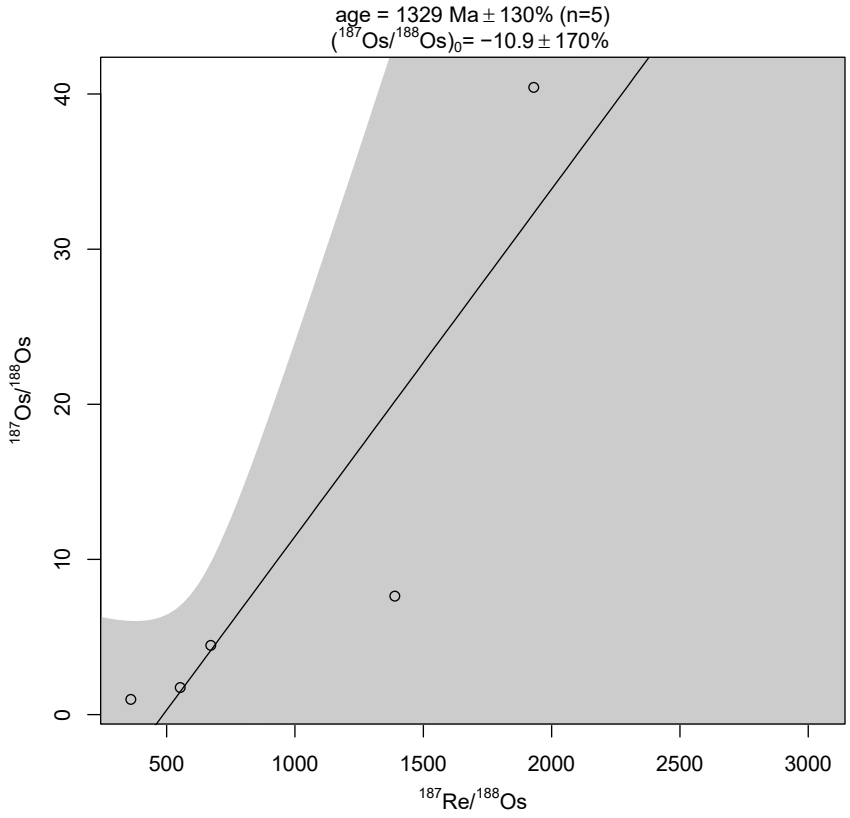

Figure 7.9 – Re–Os isochron for pyrite from the Petropavlovskoe deposit.

The non–reproducibility of ages indirectly indicates the transformation of pyrite and its intermediate enrichment during oreogenesis. Many of the results obtained are not geologically significant. Elevated $^{187}Os/^{186}Os$ ratios for sample 309/48 (late quartz vein) reflect the strong influence of a crustal source. This may indirectly indicate the formation of mineralization in a collisional geotectonic setting.

Table 7.7 – Results of Re–Os dating of pyrite from Petropavlovskoe deposit

Sample	Re, mg/t	Os, mg/t	$^{187}Re/^{188}Os$	2σ, %	$^{187}Os/^{188}Os$	2σ, %	Re/Os	T_{mod}, Ma
308/31	1.82	0.03	360.15	1.86	0.98	0.01	67.84	1496

308/34	3.99	0.03	1388.89	23.90	7.64	0.08	162.01	428
309/44	3.26	0.04	552.92	5.32	1.74	0.02	96.88	449
309/48	1.03	0.01	1930.16	38.19	40.43	0.60	255.63	1490
310/43	0.90	0.01	671.66	8.72	4.46	0.05	101.71	759

Discussion of results

Isotopic and mineralogical evidence suggest a long and multistage formation of ore–magmatic systems within the formation cycle of the Toupugol–Khanmeishor area. The stages of ore formation in the studied region are associated with the evolution of the Polar–Ural Paleozoic Island arc (Vikentyev et al., 2017; Ivanova et al., 2020). The results of (U,Th)–He dating of pyrite can be divided into three groups of ages that correlate with the main geodynamic events of the Paleozoic history of the Polar Urals (Figure 7.10).

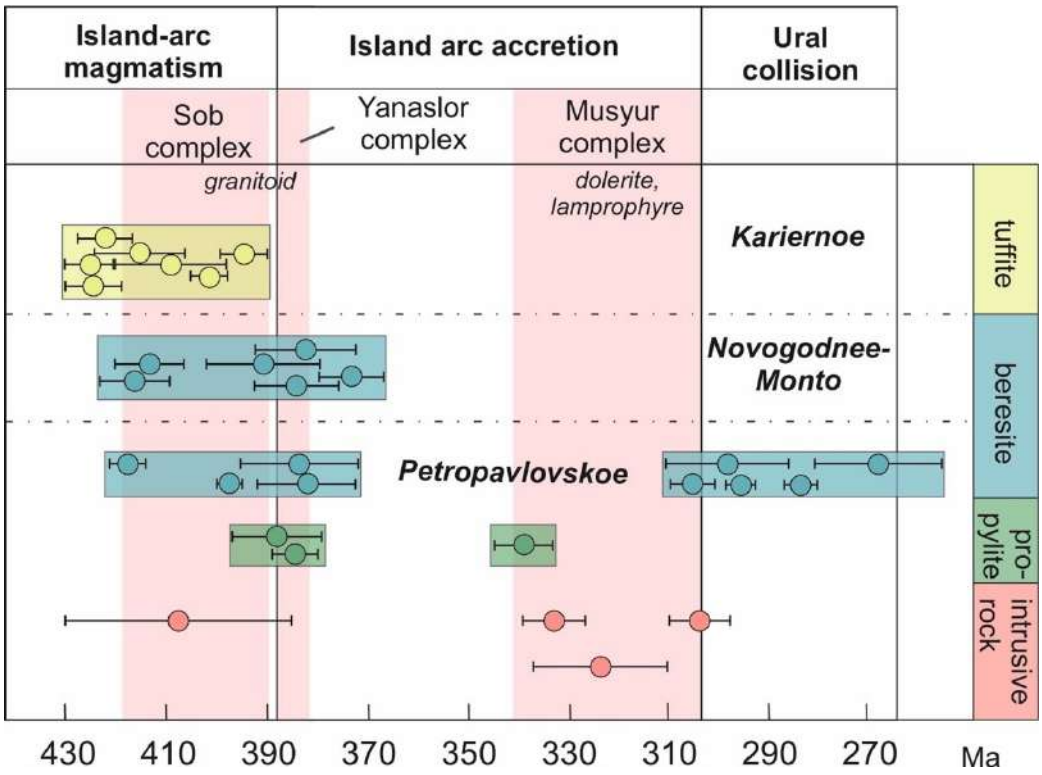

Figure 7.10. – Scheme of age distribution of (U,Th)–He dating of pyrite of the Toupugol–Khanmeishor ore district

The early sulfide stage (400–430 Ma) is characterized by the active eruption of tholeiitic and calcareous–alkaline lavas of basalt–andesibasalt composition in

deep sea conditions. Additionally, tuff accumulates and spatially associated carbonate biohermal structures of the Tupuogol formation form. The Kariernoe ore occurrence's structure preserved the original appearance of volcanogenic rocks and the earliest colcaustic ore mineralization due to the limited participation of intrusive formations. The stratiform pyrite mineralization is near–synchronous with the Wenlock–Ludlow island–arc volcanism and likely served as one of the sources of sulfur and ore material involved in forming the Petropavlovskoe and Novogodnee-Monto deposits (Figure 7.11).

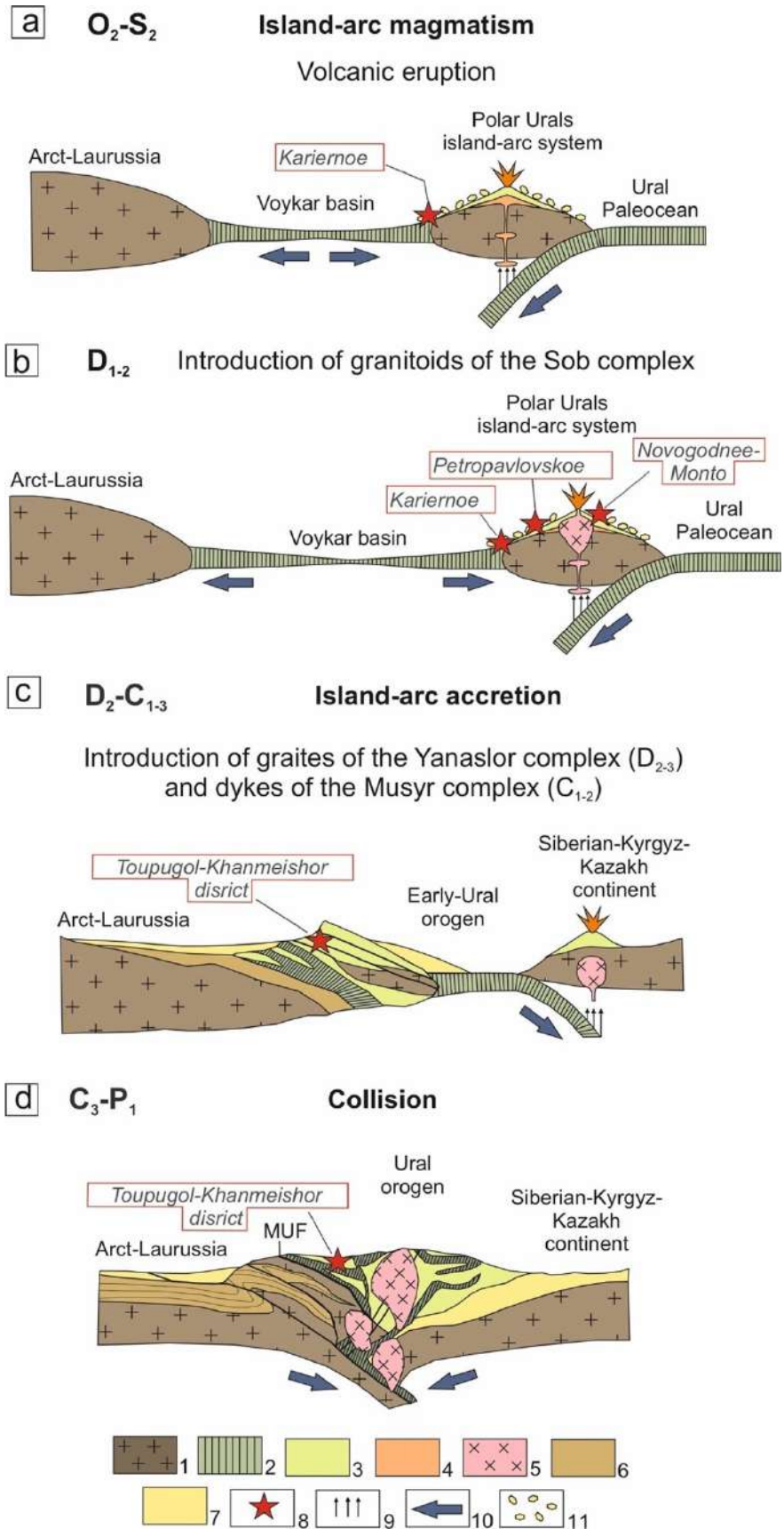

Figure 7.11. – Paleotectonic reconstructions of the Polar Urals island–arc system (according to (Kuznetsov and Romanuk, 2014; Sobolev, 2019) with modifications). Paleoprofiles across the Polar Urals segment of the Ural orogen: a – Middle Ordovician–Silurian, b – Early–Middle Devonian; c – Middle Devonian–

Carboniferous; d – Late Carboniferous–Permian. 1 – predominantly Precambrian crust; 2 – oceanic crust; 3 – Ordovician–Middle Devonian volcanogenic and volcanogenic–sedimentary island–arc formations; 4 - Middle-Upper Ordovician volcanogenic and volcanogenic-sedimentary formations of the Ustkongorskaya Formation; 5 – Early–Middle Devonian gabbroids and plagiogranitoids of the Soba batholith; 6 – Late Cambrian–Early Ordovician riftogenic magmatic formations; 7 – flysch deposits; 8 – studied deposits and ore occurrences of the Polar Urals; 9 – slab dehydration; 10 – directions relative to plate motion; 11 – clastic rocks.

During the final stage of island–arc magmatism (390–410 Ma), the Sob batholith served as the primary endogenous source of metals, sulfur, and heat in the Polar Urals, supporting the activity of the ore–magmatic system (Vikentyev et al., 2017; Sobolev et al., 2018b). The formation of dioritoids in the main phase of the Soba complex indicates new physical and chemical conditions in the ore–forming environment. This is reflected in the diverse composition of the host rocks, as well as in the chemical composition and morphology of pyrite. The recrystallization of sinter mineralization was initiated by the formation of island–arc diorites during the skarn–porphyry stage of deposit formation. The cooling of the main phase of the Soba complex, along with the subordinate influence of dykes of diorite–porphyrites and plagiogranite–porphyries from the late phase of the Soba complex, led to the development of propylitic alteration that hosts sulfide mineralization. This also contributed to the formation of gold–porphyry stockworks at the beginning of the Eifel (Vikentyev et al., 2017).

During the accretion of the island arc (313–360 Ma (Kuznetsov, Romanuk, 2014; Sobolev et al., 2020) to the Ural margin of Arct–Laurussia, the final stage of granitoid magmatism occurred in the Polar Urals. The Yanaslor complex (383–387 Ma; Udoratina et al., 2005) was introduced in small massifs in the southern part of the region, which was synchronous with manifestations of berezite alteration within the gold deposits of the Toupugol–Khanmeishor area (≈380 Ma). During the final stage, dykes and lamprophyres of the Musyur complex were introduced, but they do not contribute to gold concentration.

The collision of Arct–Laurussia with the Siberian–Kazakhstan–Kyrgyz continent (250–270 Ma) formed a divergent orogen, as reported by Kuznetsov and

Romanuk (2014) and Sobolev (2019). The Ural collision was a global geodynamic event that caused a complex of tectonic deformations, increasing rock permeability and potentially favoring the movement of upward fluid solutions. The northwestern section of the Petropavlovskoe deposit, where the Permian (U,Th)–He age of pyrite was obtained, has a complex tectonic structure. In contrast to the central part of the deposit, this area contains newly formed non–productive sulfide mineralization. The sulfur isotopic composition of sulfur in pyrite in this zone is also characterized by a lighter isotopic composition (δ ^{34}S от -12 до -5‰).

A complex polystage history of ore formation in the Toupugol–Khanmeishor area can be traced as a result of active tectonic–metasomatic workings of volcanogenic ore material during the development of the Polar Urals island–arc system and its further accretion to the East European paleocontinent. The cycle of the island–arc ore–forming system involves primary sinter mineralization. During subsequent tectonic processes accompanied by hydrothermal activity, additional magmatic matter inflow is responsible for redistributing and enriching the ore substrate. The transition from magmatic to hydrothermal ore formation during the development of an ore–magmatic system is supported by the chemical composition, pyrite crystal morphology, and metasomatic transformations of volcanogenic rocks in several locations, including Kariernoe, Novogodnee-Monto, and Petropavlovskoe. The collision of the Arct–Laurussia and Siberian–Kyrgyz–Kazakh continents resulted in the formation of a complex of stretches and dislocations at the Petropavlovskoe deposit. However, this event did not contribute to the formation of gold mineralization. The data obtained from this study can be used as an additional criterion for forecasting gold mineralization in adjacent territories.

CONCLUSION

On the example of gold deposits of the Topougol-Haimeshor ore district:

1. The possibility of (U,Th)-He dating of pyrite from volcanogenic and metasomatic rocks has been demonstrated. It is shown that (U,Th)-He ages of pyrite agree with ages determined by independent methods (biostratigraphy, 39Ar-40Ar) and with geological ideas about the history of development of the region,

2. The technique of sampling and preparation of samples for (U,Th)-He dating has been improved. It is shown that autoclave decomposition of pyrite samples in Teflon bouquets in a mixture of hydrofluoric, nitric and chloric acids (in the ratio 10:2:1) at 220 °C, 48 hours, provides complete dissolution of micron inclusions of uranium (thorium)-bearing minerals, which are one of the sources of radiogenic helium.

3. New data on the age of pyrite from volcanogenic-sedimentary, skarn-porphyritic and berezite stages were obtained. These data allowed us to confirm the 424 Ma (±6) sinter stage and to identify a new post-arc Permian stage of 293 Ma (±4).

REFERENCES

1. Aciego S., Kennedy B., DePaolo D., Christensen J., Hutcheon I. (U–Th)/He age of phenocrystic garnet from the 79 AD eruption of Mt.Vesuvius // Earth and Planetary Science Letters. 2003 V. 219. P. 209–219.

2. Andreev A.V. Geological structure, localization conditions and regularities of formation of gold ores of Novogodnee-Monto deposit (Polar Urals) // Geology, Mineral Resources and Geoecology of North–West Russia: Mater. XIV Young Scientist Conference Petrozavodsk: KarRC RAS. 2006. P. 7–9. (In Russian).

3. Andreichev V.L. Isotope geochronology of ultramafic–mafic and granitoid associations of the eastern slope of the Polar Urals. Syktyvkar: Geoprint. 2004. 44 p. (In Russian).

4. Badash L. Rutherford and Boltwood: Letters on Radioactivity. New Haven: Yale University Press. 1969. P. 378.

5. Baranov E.N., Vertepov G.I. Uranium content in sulfides as an indicator of uranium mineralization // Atomic Energy. 1966. V. 20. № 2. P. 170–172. (In Russian).

6. Barrie C.D., Pearce M.A., Boyle A.P. Reconstructing the Pyrite Deformation Mechanism Map // Ore Geol. Rev. 2011. V. 39. P. 265–276.

7. Benedek R. Pseudopotential calculation of the screening of a helium atom in aluminium // Journal of Physics F. 1978. V. 8. P. 807.

8. Betekhtin A.G. Mineralogy course: textbook. Moscow: KDU. 2007. 720 p. (In Russian).

9. Bortnikov N. S., Ikorskii S. V., Kamenskii I. L., Vikentyev I. V., Bogdanov Y. A., Stavrova O. O., Avedisyan A. A. A. Helium isotopic composition and hydrocarbons in fluid inclusions from serpentinites and sulfides of the Logachev and Rainbow hydrothermal fields (Mid–Atlantic Ridge) // Reports of the Academy of Sciences. 2000. V. 375. №3. P. 375–379. (In Russian).

10. Boschman W., Lippolt H.J., Wernicke R.S. ^{4}He diffusion in specular hematite // Physics and Chemistry of Minerals. 1993. V. 20. №6. P. 415–418.

11. Burnard P.G., Polya D.A. Importance of Mantle Derived Fluids during Granite Associated Hydrothermal Circulation: He and Ar Isotopes of Ore Minerals from Panasqueira // Geochim. Cosmochim. Acta. 2004. V. 68. P. 1607–1615.

12. Christensen J.N., Halliday A.N., Leigh K.E., Randell R.N., Kesler S.E. Direct Dating of Sulfides by Rb–Sr: A Critical Test Using the Polaris Mississippi Valley–Type Zn–Pb Deposit // Geochim. Cosmochim. Acta. 1995. V. 59. P. 5191–5197.

13. Craig J.R., Vokes F.M. The Metamorphism of Pyrite and Pyritic Ores: An Overview // Mineral. Mag. 1993. V. 57. P. 3–18.

14. Danisik M., Mcinnes B.I.A., Kirklard C.L., McDonald B.J., Evans N.J., Becker T. Seeing is believing: Visualization of He distribution in zircon and implications for thermal history reconstruction on single crystals // Sci. Adv. 2017. V. 3. e1601121.

15. Deditius A.P., Kesler S.T., Ewing R.C. Behavior of trace elements in arsenian pyrite in ore deposits // 10th Biennial SGA Meeting of the Society for Geology Applied to Mineral Deposits. 2009.

16. Dedeev V.A. Facies and geologic history of the Middle Paleozoic of the eastern slope of the Polar Urals (Shchuchyinsky synclinorium) // Geological Collection. 1959. № 131. P. 111–139. (In Russian).

17. Didenko A.N., Kurenkov S.A., Ruzhentsev S.V., Simonov V.A., Lubnina N.V. Tectonic history of the Polar Urals. Moscow: Nauka. 2001. 191 p. (In Russian).

18. Dobretsov N.L., Moldavantsev Yu.E., Kazak A.P. et al. Petrology and metamorphism of ancient ophiolites (on the example of the Polar Urals and Western Sayans). Novosibirsk: Nauka, 1977. 219 p. (In Russian).

19. Dodson M.H. Closure temperature in cooling geochronological and petrological systems // Contributions to Mineralogy and Petrology. 1973. V. 40. P. 259–274.

20. Dunai T.J. Forward Modeling and interpretation of (U–Th)/He ages // Rev. Mineralogy and Geochemistry. 2005. V. 58. P. 259–274.

21. Dushin V.A., Malyugin A.A., Kozmin V.S. Metallogeny of gold of the Polar Urals // Bulletin of St. Petersburg State University. Ser. "Geology and Geography. 2002. V. 2. № 7. P. 72–81. (In Russian).

22. Dushin V.A., Malyugin A.A., Kozmin V.S., Serdyukova O.P., Prokopchuk D.I., Kurchavov V.V., Demina L.A., Afanasyev E.A. Some features of the location of noble–metal mineralization within the Ural North // Izvestiya Vuzov. Mining Journal. 2013. № 8. P. 34–41. (In Russian).

23. Dushin V.A., Serdyukova O.P., Malyugin A.A. et al. State geologic map of the Russian Federation. Scale 1: 200000. Second edition. Polar–Ural Series. Sheet Q–42–VII, VIII (Obskaya). Explanatory note. SPb.: VSEGEI, 2014. 384 p. (In Russian).

24. Evans N.J., Byrne J.P., Keegan J.T., Dotter L.E. Determination of Uranium and Thorium in Zircon, Apatite, and Fluorite: Application to Laser (U–Th)/He Thermochronology // J. Anal. Chem. 2005. V. 60. P. 1300–1307.

25. Farley K.A. Helium diffusion from apatite: General behavior as illustrated by Durango fluorapatite // Journal of Geophysical Research. 2000. V. 105. №2. P. 2903–2914.

26. Farley K.A. Helium diffusion parameters of hematite from a single–diffusion–domain crystal // Geochimica at Cosmochimica Acta. 2018. V. 231. P. 117–129.

27. Farley K.A., Stockli D. (U–Th)/He dating of phosphates: apatite, monazite, and xenotime // Rev. Mineralogy and Geochemistry. 2002. P. 559–577.

28. Farley K.A., Wolf R.A. and Silver L.T. The effects of long a–stopping distances on (U–Th)/He ages // Geochim. Cosmochim. Acta. 1996. V. 60. P. 4223–4229.

29. Farley K.A. (U–Th)/He dating: techniques, calibrations, and applications // Reviews in Mineralogy and Geochemistry. 2002. V. 47. P. 819–843.

30. Flowers R.M., Zeitler P.K., Danišík M., Reiners P.W., Gautheron C., Ketcham R.A., Metcalf J.R., Stockli D.F., Enkelmann E., Brown R.W. (U–Th)/He

Chronology: Part 1. Data, Uncertainty, and Reporting // GSA Bulletin. 2022. April. P. 1–33.

31. Gautheron C., Hueck M., Ternois S., Heller B., Schwartz S., Sarda P., Tassan-Got L. Investigating the Shallow to Mid-Depth (>100–300°C) Continental Crust Evolution with (U-Th)/He Thermochronology: A Review // Minerals. 2022. V. 12. №563.

32. Gerling E.K. Modern state of argon method of absolute age determination and its application in geology. M., L.: Izd. of the USSR Academy of Sciences. 1961. 130 p. (In Russian).

33. Gerling E.K. Forms of helium in minerals and helium migration in them: autoref. dokt. diss. 1939. (In Russian).

34. Girfanov M., Volchkov A., Kryazhev S.G., Novikov V. Gold–Iron Oxide Bearing Ore–Magmatic System of the Auerbakh–Novogodnee Volcano–Plutonic Belt, the Polar Urals // In Proceedings of the 33rd International Geological Congress. Oslo, Norway. 6–14 August 2008. P. 1.

35. Glodny J., Montero P., Austrheim H. et al. The Marun–Keu metamorphic complex, Polar Urals: protolith evolution and its geodynamics significance // Intas Europrobe Timpebar–Uralides Workshop, St. Petersburg, 2000. Abst. P. 13–14.

36. Grabezhev A.I. Problems of copper porphyry mineralization formation in the Urals // Actual problems of magmatic geology, petrology and ore formation. Ekaterinburg: Institute of Geology and Geochemistry, Ural Branch of the Russian Academy of Sciences. 1995. P. 192–198. (In Russian).

37. Harley P. Helium Method of Age Determination, Prevalence and Migration of Helium in Rocks // In the book: Starik I.E., ed. Nuclear Geology. Moscow: Publishers of Foreign Literature. 1956. P. 391–434. (Translation from English: H.Faul, Edit. Nuclear Geology. A Simposium on Nuclear Phenomena in the Earth Sciences. J.Wilei & Sons, Inc.N.Y. 1954.) (In Russian).

38. Hey M.H. A new review of the chlorites // Mineral. Mag. 1954. V. 30. P. 277–292.

39. Hnatyshin D., Creaser R.A., Meffre S., Stern R.A., Wilkinson J.J., Turner E.C. Understanding the Microscale Spatial Distribution and Mineralogical Residency of Re in Pyrite: Examples from Carbonate–Hosted Zn–Pb Ores and Implications for Pyrite Re–Os Geochronology // Chem. Geol. 2020. V. 533. P. 419–427.

40. Ivanov A.V., Vanin V.A., Demonterova E.I., Gladkochub D.P., Donskaya T.V., Gorovoy V.A. Application of the ‘no fool’s clock’ to dating the Mukodek gold field, Siberia, Russia // Ore Geology Reviews. 2015. V. 69. P. 352–359.

41. Ivanova E.S., Ivanova Y.N. Mineralogical and petrographic characterization of host rocks of iron–skarne ore occurrence Pervaya Rudnaya Gorka, Polar Urals // Bulletin of Peoples' Friendship University of Russia. Series: Engineering Research. 2021. V. 22. № 3. P. 305–316. (In Russian).

42. Ivanova E.S., Sobolev I.D., Vikentyev I.V., Anosova M.O., Podolskaya M.M., Tyukova E.E., Yakubovich O.V. U–Th–He dating of pyrite from island–arc volcanogenic rocks on the example of the Kariernoe ore occurrence, Polar Urals // Bulletin of St. Petersburg State University. Earth Sciences. 2024. 69 (1). (In Russian).

43. Ivanova Yu.N., Vykhristenko R.I., Vikentyev I.V. Structural control of gold mineralization in the central part of the Malouralsky volcanic–plutonic belt (Polar Urals) based on the results of analysis of multispectral images from the Landsat 8 spacecraft // Earth Exploration from Space. 2020. №4. P. 56–62. (In Russian).

44. Ivanova Y.N. Localization conditions and mineralogical and geochemical features of the Petropavlovsk gold porphyry deposit (Polar Urals): Cand. geol.–min. sciences: 25.00.11. Moscow: IGEM RAS. 2016. 151 p. (In Russian).

45. Kelly N.M., Flowers R.M., Metcalf J.R., Mojzsis S.J. Late accretion to the Moon recorded in zircon (U–Th)/He thermochronometry: Earth and Planetary // Science Letters. 2018. V. 482, P. 222–235.

46. Kendrick M.A., Burgess R., Pattrick R.A.D., Turner G. Fluid Inclusion Noble Gas and Halogen Evidence on the Origin of Cu–Porphyry Mineralising Fluids // Geochim. Cosmochim. Acta. 2001. V. 65. P. 2651–2668.

47. Kenig V.V., Butakov K.V. Ore gold deposits Novogodnee-Monto and Petropavlovskoe – a new gold ore district in the Polar Urals // Exploration and protection of subsoil. 2013. № 11. P. 22–24. (In Russian).

48. Kesler S.E., Deditius A., Reich M., Utsunomiya S., Ewing R. Role of Arsenian Pyrite in Hydrothermal Ore Deposits: A History and Update // 6th Geological Society of Nevada on Great Basin Evolution and Metallogeny. 2010.

49. Kontar E.S. Geological and industrial types of copper, zinc, lead deposits in the Urals (geological conditions of location, history of formation, prospects): scientific monograph. Ekaterinburg: UGGU. 2013. 199 p. (In Russian).

50. Korzhinsky D.S. Outline of metasomatic processes // Basic problems in the doctrine of magmatic ore deposits. Moscow: Izd. of the USSR Academy of Sciences. 1953. P. 332–352. (In Russian).

51. Krasnobaev A.A. Zircon as an indicator of geologic processes. Moscow: Nauka. 1986. 202 p. (In Russian).

52. Kuznetsov N.B., Romanuk T.V. Paleozoic evolution of the Polar Urals: Voykar basin with the oceanic type crust existed for at least 65 Ma // Bulletin of MOIP. MOIP. Geological Department. 2014. №5. P. 56–70. (In Russian).

53. Liu G.–Q., Zhao K.–D., Jiang S.–Y., Chen W. In–situ sulfur isotope and trace element analysis of pyrite from the Xiwang uranium ore deposit in South China: Implication for ore genesis // Journal of Geochemical Exploration. 2018. V. 195. P. 49–65.

54. Luders V., Niedermann S. Helium isotope composition of fluid inclusions hosted in massive sulfides from modern submarine hydrothermal systems // Sci. Commun. 2010. V. 105. P. 443–449.

55. Jean–Baptiste, P., Fouquet, Y. Abundance and Isotopic Composition of Helium in Hydrothermal Sulfides from the East Pacific Rise at 13° N // Geochim. Cosmochim. Acta. 1996. V. 60. P. 87–93.

56. Malkin, P. Desorption of helium from irradiated materials: monograph / P. Malkin. – Saratov. 2018. 74 p. (In Russian).

57. Mansurov R.H., Andreev A.V., Dvurechenskaya S.S., Vikentyev I.V. Geological and structural features of large–volume vein–embedded gold–sulfide mineralization of the Petropavlovsk deposit (Polar Urals) // Bulletin of the Institute of Geology Komi NTs Ural RAS. 2017. №3. P. 3–13. (In Russian).

58. Mansurov R.Kh. The structure of mineralized zones of the Petropavlovsk gold porphyry deposit (Polar Urals) // Vestnik Permskogo Usta. 2016. V. 4. №3. P. 49–69. (In Russian).

59. Mansurov R.Kh. Geological structure of the Petropavlovsk gold ore deposit (Polar Urals) // Ores and Metals. 2009. № 5. P. 70–74. (In Russian).

60. Marakushev A.A. Petrogenesis and ore formation (geochemical aspects). Moscow: Nauka. 1979. 260 p. (In Russian).

61. Marin Yu.B. Petrography: Textbook. St. Petersburg: National Mineral Resources of Mining University. 2015. 408 p. (In Russian).

62. Marsden R.C., Danišík M., Ahn U.S., Friedrichs B., Schmitt A.K., Kirkland C.L., McDonald B.J., and Evans N.J. Zircon double–dating of Quaternary eruptions on Jeju Island, South Korea // Journal of Volcanology and Geothermal Research. 2021. V. 410.

63. McDowell F.W., McIntosh W.C., Farley K.A. A precise ^{40}Ar–^{39}Ar reference age for the Durango apatite (U–Th)/He and fission–track dating standard // Chem. Geol. 2005. V. 214. № 3–4. P. 249–263.

64. Meesters A. G. C. A. and Dunai T. J. A moniterative solution of the (U-Th)/He age equation // Geochem. Geophys. Geosyst. 2005. V 6. Q04002.

65. Moses C. O., Nordstrom D. K., Herman J. S. and Mills A. L. Aqueous pyrite oxidation by dissolved oxygen and by ferric iron // Geochim. Cosmochim. Acta 1987. V. 51. P. 1561–1571.

66. Melekestseva I.Y., Tret'yakov G.A., Nimis P. et al. Barite–rich massive sulfides from the Semenov–1 hydrothermal field (Mid–Atlantic Ridge, 13°30.87′

N): evidence for phase separation and magmatic input // Marine Geology. 2014. V. 349. P. 37–54.

67. Min K., Farley K.A., Renne P.R., Marti K. Single grain (U–Th)/He ages from phosphates in Acapulco meteorite and implications for thermal history // Earth and Planetary Science Letters. 2013. V. 209. P. 323–336.

68. Nalivkin D.A. Geological history of the Urals. Sverdlovsk: OGIS. 1943. 96 p. (In Russian).

69. Perevozchikov B.V. Genetic types of gabbroids of the southern frame of the Rai–Iz massif // Geology and Mineral Resources of the Subpolar and Polar Urals. Proc. ZapSibNIGNI. 1974. Issue. 74. Tyumen: ZapSibNIGNI. P. 49–58. (In Russian).

70. Peyve A.V. Deep faults in geosynclinal areas // Izv. of the USSR Academy of Sciences. Geological Series. 1945. №5. P.23–46. (In Russian).

71. Plotitsyn A.N., Sobolev I.D., Matveeva N.A., Ivanova R.M., Vikentyev I.V. Stratigraphic volume of the Toupugoljegarta Formation (Lower–Middle Devonian, Polar Urals) // Geosciences Bulletin. 2022. 12(336). P. 29–37. (In Russian).

72. Podolskaya M.M., Yakubovich O.V. Development of (U,Th)–He dating of pyrite: measurements of uranium and thorium content on ICP MS Element XR // New in the knowledge of ore formation processes: a collection of scientific and practical school. Moscow: IGEM RAS. 2019. P. 301–303. (In Russian).

73. Practical petrology: methodological recommendations for the study of magmatic formations in relation to the tasks of the state geological maps / ed. by L.N. Sharpenok, co–editor: M.V. Naumov et al. St. Petersburg: VSEGEI. 2017. 166 p. (In Russian).

74. Pryamonosov, A.P.; Nayuk, S.A.; Pryamonosova, M.A. (1994) Group geologic survey and geologic till study at a scale of 1:50,000 in the Sob–Khanmeyskaya area (GGS–sheets Q–41–48–V,d,G–V,d; Q–42–38–A–V,B–a; GDP–sheets Q–41–48–B,B–a,b,G–a,b; Q–42–37–A,B,B–a,b,G–a,b; b; Q–42–38–

A–a,b,B–a,b). Informational report. Settlement. Polyarny: AOOT PU GGP. (In Russian).

75. Pryvnanosov A.P., Stepanov A.E. et al. Geological study and evaluation of mineral resources of the subsoil of the Russian Federation and its continental shelf (prospecting and exploration for gold in the Kharbeyskaya area): report on the PPR. Ekaterinburg: OKHNIR PARGI UGGA. 2004. (In Russian).

76. Pryamonosov A. P., Borozdina G. N., Pryamonosova M. A. Toupugoljegarta Formation and Varchatinskaya Formation of the Voykarskaya SFZ in the Polar Urals // Ural Geological Journal. 2009. V. 69. № 3. P. 52–55. (In Russian).

77. Pshenichkin A.Ya., Korobeinikov A.F., Matsyushevsky A.V. Features of crystallomorphology and thermoelectric properties of pyrite gold deposits of different types // Izv–ia Tomsk. polytechnic institute. 1976. №260. P. 39–48. (In Russian).

78. Pshenichny G.N. Gayskoye copper–coal deposit of the Southern Urals. Mineralogy, geochemistry, structure and conditions of ore formation. Moscow: Nauka. 1975. (In Russian).

79. Puchkov V.N. Geology of the Urals and the Urals (topical issues of stratigraphy, tectonics, geodynamics and metallogeny). Ufa: DesignPolygraphService. 2010. 280 p. (In Russian).

80. Puchkov V.N. Tectonics of the Urals. Modern representations // Geotectonics. 1997. № 4. P. 42–61. (In Russian).

81. Puska M.J., Nieminen R.M. Theory of hydrogen and helium impurities in metals // Physical Review. 1984. V. 29. P. 5382.

82. Reich M., Ewing R., Ehlers T., Becker U. Low–temperature anisotropic diffusion of helium in zircon: Implications for zircon (U–Th)/He thermochronometry // Geochimica Cosmochimica Acta. 2007. V.71. P. 3119–3130.

83. Reich M, Deditius A., Chryssoulis S., Li J.–W., Ma C.–Q., Parada M., Barra F., Mittermayr F. Pyrite as a record of hydrothermal fluid evolution in a

porphyry copper system: A SIMS/EMPA trace element study // Geochimica et Cosmochimica Acta. 2013. V. 104. P. 42–62.

84. Reiners P.W. Zircon (U–Th)/He Thermochronometry // Rev. in Mineralogy and Geochemistry. 2005. V. 58. P. 151–179.

85. Reiners P.W., Carlson R.W., Renne P., Cooper K.M., Granger D.E., McLean N.M., Schoene B. The (U–Th)/He System. In Geochronology and Thermochronology. NJ, USA: John Wiley & Sons. 2017. P. 291–363.

86. Remizov D.N. Island–arc system of the Polar Urals (petrology and evolution of deep zones). Yekaterinburg: Ural Branch of the Russian Academy of Sciences. 2004. 221 p. (In Russian).

87. Rindziunskaya N.M., Andreev A.V., Zubova T.P., Girfanov M.M., Shchegolkov Y.V., Nikolaeva L.A. Lithologic and mineralogical composition of weathering crust of the Novogodnee-Monto gold deposit (Polar Urals) // Ores and Metals. 2005. № 6. P. 34. (In Russian).

88. Rosso. Low Temperature Thermochronometry // Rev. Mineralogy and Geochemistry. 2005. V. 58. P. 623.

89. Rutherford E. Radioactive Transformations. N.Y.: Charles Scriber's Sons. 1906. P. 180.

90. Savelyev A.A. Geology and chromite–bearing capacity of the Voykaro–Synyinsky massif (Polar Urals). Abstract of the dissertation for the degree of Candidate of Geol.–Min. of Sciences. Sverdlovsk, 1974. 25 p. (In Russian).

91. Savelyev A.A., Savelyeva G.N. Ophiolites of the Voykaro–Synyinsky Massif (Polar Urals) // Geotectonics. 1977. № 6. P. 46–60. (In Russian).

92. Savelyeva G.N. Gabbro–ultrabasite complexes of the Ural ophiolites and their analogs in the modern oceanic crust. Moscow: Nauka, 1987. 230 p. (In Russian).

93. Shadrin A.N., Sobolev I.D. Results of geochronologic studies of igneous rocks of the Sibileyskaya area (Eastern slope of the Polar Urals) // Gornye vedomosti. 2017. № 2 (150). P. 54–69. (In Russian).

94. Shukolyukov Yu.A. Fission of uranium nuclei in nature. Moscow, Atomizdat. 1970. 249 p. (In Russian).

95. Shukolyukov Yu.A., Fugzan M.M., Paderin I.P. et al. Geothermochronology on noble gases: a study of the stability of the uranium–xenon isotope system in non–metamict zircons // Petrology. 2009. V. 17. № 1.P. 3–27. (In Russian).

96. Shukolyukov Yu.A., Yakubovich O.V., Rytzk E.Yu. On the possibility of isotopic dating of nugget gold (U,Th)–He – method // Reports of the Academy of Sciences. 2010. V.430. №2. P. 243–247. (In Russian).

97. Shukolyukov Yu.A., Yakubovich O.V., Yakovleva S.Z., Salnikova E.B., Kotov A.B., Rytzk E.Yu. Geothermochronology on noble gases: III. Migration of radiogenic helium in the crystal structure of nugget metals and possibilities of their isotopic dating // Petrology. 2012a. V.20. №1. P. 3–24. (In Russian).

98. Shukolyukov Yu.A., Yakubovich O.V., Mochalov A.G., Kotov A.B., Salnikova E.B., Yakovleva S.Z., Korneev S.I., Gorokhovsky B.M. New isotopic geochronometer for direct dating of platinum nugget minerals (190Pt–4He method) // Petrology. 2012b. V. 20. №6. C. 545–559.

99. Silaev, V.I., Khazov, A.F., Sokerin, M.Yu. Novogodnee-Monto gold deposit in the Polar Urals. Petrology and Mineralogy of the Northern Urals and Timan // Proceedings of the IG KomiNTs Ural RAS. 2003. №113, P. 159–172. (In Russian).

100. Sirin N.A. Magmatism of the Subpolar and Polar Urals. Moscow: Gosgeoltekhizdat, 1962. 288 p. (In Russian).

101. Smith P.E., Evensen N.M., York D., Szatmari P., Oliveira, D.C. Single–Crystal ^{39}Ar– ^{40}Ar Dating of Pyrite: No Fool’ s Clock // Geology. 2001. V. 29. P. 403–406.

102. Sobolev I.D., Vikentyev I.V., Travin A.V., Bortnikov N.S. Coal–bearing magmatism of the Polar Urals // Reports of the Academy of Sciences. Earth Sciences. 2020. V. 494. №2. P. 22–28. (In Russian).

103. Sobolev I.D. Main time boundaries and evolution of magmatism of the Polar Urals island–arc system: Cand. geol.–min. sciences: 25.00.01. Moscow: Moscow State University. 2019. 211 p. (In Russian).

104. Sobolev I.D., Vikentyev I.V., Soboleva A.A., Travin A.V. Results of U/Pb SIMS dating of zircons and 39Ar/40Ar age of plagioclase from rocks of the Soba complex (Petropavlovskoe gold deposit, Polar Urals) // Proceedings of VII con–tion on isotope geochemistry. Moscow: IGEM RAS. 2018a. P. 398–401. (In Russian).

105. Sobolev I.D., Soboleva A.A., Udoratina O.V., Varlamov D.A., Hourigan J.K., Khubanov V.B., Buyantuev M.D., Soboleva D.A. Devonian island–arc magmatism of the Voykarskaya zone of the Polar Urals // Geotectonics. 2018b. №5. P. 39–74. (In Russian).

106. Sobolev I.D., Soboleva A.A., Udoratina O.V., Kaneva T.A., Kulikova K.V., Vikentyev I.V., Khubanov V.B., Buyantuev M.D., Hourigan J.K. First results of U–Pb (LA–ICP–MS) dating of detrital zircons from Paleozoic island–arc clastic rocks of the Polar Urals // Bulletin of the Moscow Society of Nature Researchers. Department of Geology. 2017. V. 92. №4. P. 3–26. (In Russian).

107. Sobolev I.D., Shadrin A.N., Rastorguev V.A., Kozyreva D.A. Early–ostrovodugunge granitoids of the Shchuchyinskaya zone of the Polar Urals (results of U–Pb (SIMS) dating of zircons) // MSU Bulletin. Series 4. Geology. 2017. № 1. P. 22–32. (In Russian).

108. Starkov V.D. Intrusive magmatism of eugeosynclinal zones of the Polar Urals. Sverdlovsk: UNTS AS USSR, 1985. 148 p. (In Russian).

109. Svetukhin V.V.; Suslov D.N.; Risovanny V.D. Mechanisms of Helium Thermodesorption from Irradiated Boron Carbide // Atomic Energy. 2005. V. 98. №3. P. 187–191. (In Russian).

110. Sychev S. N., Kulikova K. V. Plastic deformations in the area of the Main Ural Rift (Sredny Kechpel River) // Structure, substance, and history of the lithosphere of the Timan–Severo–Ural segment: Proceedings of the 19th scientific conference. Syktyvkar: Geoprint. 2010b. P. 171–174. (In Russian).

111. Soloviev S.G., Kryazhev S.G., Dvurechenskaya S.S. Geology, mineralization, stable isotope geochemistry, and fluid inclusion characteristics of the Novogodnee-Monto oxidized Au–(Cu) skarn and porphyry deposit, Polar Ural, Russia // Mineralium Deposita. 2012. V. 47. P. 1–25.

112. State Geologic Map of the Russian Federation. Scale 1:1,000,000 (third generation) // Zapadno–Sibirskaya Series. Sheet Q–42 (Salekhard) / Ed. A.V. Zhdanov. Explanatory note. SPb.: VSEGEI. 2014. 396 p. (In Russian).

113. State Geological Map of the Russian Federation. Scale 1:1 000 000 (third generation) // Ural Series. Sheet Q–41 (Vorkuta) / Ed. V.P. Vodolazskaya. Explanatory note. SPb.: VSEGEI. 2007. 541 p. (In Russian).

114. Stein H.J., Morgan J.W., Scherstén A. Re–Os Dating of Low–Level Highly Radiogenic (LLHR) Sulfides: The Harnäs Gold Deposit, Southwest Sweden, Records Continental–Scale Tectonic Events // Econ. Geol. 2000. V. 95. P. 1657–1672.

115. Stuart F.M., Burnard P.G., Taylor R.P., Turner G. Resolving Mantle and Crustal Contributions to Ancient Hydrothermal Fluids: HeAr Isotopes in Fluid Inclusions from Dae Hwa WMo Mineralisation, South Korea // Geochim. Cosmochim. Acta. 1995. V. 59. P. 4663–4673.

116. Tremblay M.M., Cooperdock E.H.G., Zeitler P.K. Noble Gas Thermochronology: // Elements. 2020. V. 16. №5. P. 331–336.

117. Trofimov A.P., Lyuchkin V.A., Pivovarov A.P., Funtikov B.V. Geological and geochemical model of gold–iron–skarne deposit Novogodnee-Monto in the Polar Urals // Skarns, their genesis and ore–bearing (Fe, Cu, Au, W, Sn): Mater. scientific conf. (XI Readings of A.N. Zavaritsky). Ekaterinburg: Institute of Geology and Geochemistry, Ural Branch of the Russian Academy of Sciences. 2005. P. 102–107. (In Russian).

118. Tugarinov A.I., Bibikova E.V. Geochronology of the Baltic Shield. Moscow: Nauka. 1980. 132 p. (In Russian).

119. Udoratina O.V., Kuznetsov N.B. Sob plagiogranite complex of the Polar Urals // Bulletin. MOIP. Geological Department. V. 82. № 3. 2007. P. 49–59. (In Russian).

120. Udoratina O.V., Kuznetsov N.B., Matukov D.I. Age of granitoids of the Yanaslor massif: U–Pb data // Petrology of magmatic and metamorphic complexes. Proceedings of the V All–Ros. Conf. / Ed. by A.I. Chernyshov. Tomsk: CNTI. 2005. V. 1. №5. P. 135–142. (In Russian).

121. Vermeesch P., Seward D., Latkoczy C., Wipf M., Guenther D., Baur H. Alpha–emitting mineral inclusions in apatite, their effect on (U–Th)/He ages, and how to reduce it // Geochimica et Cosmochimica Acta. 2007. V.71. P. 1737–1746.

122. Vermeesch, P. Three New Ways to Calculate Average (U–Th)/He Ages. Chem. Geol. 2008, 249, 339–347.

123. Vikentyev I.V., Belogub E.V., Novoselov K.A., Moloshag V.P. Metamorphism of Volcanogenic Massive Sulphide Deposits in the Urals // Ore Geology. 2017. V. 85. P. 30–63.

124. Vikentyev I.V., Sobolev I.D., Travin A.V. First results of 40Ar/39Ar dating of sericite from metasomatites of the Petropavlovsk gold deposit in the context of the Paleozoic island–arc system of the Polar Urals // Metallogeny of ancient and modern oceans. Miass: IMin Ural Branch of the Russian Academy of Sciences. 2019. P. 185–189. (In Russian).

125. Vikentyev I.V., Mansurov R.H., Ivanova Y.N. et al. Gold porphyry Petropavlovskoe gold deposit (Polar Urals): geological position, mineralogy and formation conditions // Geology of ore deposits. 2017. V. 59. №6. P. 501–541. (In Russian).

126. Vikentyev I.V., Abramova V.D., Ivanov Y.N., Tyukova, E.E., Kovalchuk E.V., Bortnikov N.S. Micro–impurities in pyrite of the gold porphyry deposit Petropavlovskoe (Polar Urals) according to LA–ICP–MS // Reports of the Academy of Sciences. 2016. V. 470. №3. P. 326–330. (In Russian).

127. Vikentyev I.V., Tyukova E.E., Murzin V.V., Vikentyeva O.V., Pavlov L.G. Vorontsovskoye gold deposit. V., Vikentyeva O.V., Pavlov L.G.

Vorontsovskoye gold ore deposit. Geology, gold forms, genesis. Ekaterinburg: Fort Dialog–Iset. 2016. 204 p. (In Russian).

128. Vikentyev I., Vikent'eva O., Tyukova E., Nikolsky M., Ivanova J., Sidorova N., Tonkacheev D., Abramova V., Blokov V., Spirina A. Noble Metal Speciations in Hydrothermal Sulphides // Minerals. 2021. V. 11. P. 488.

129. Volchkov A.G., Girfanov M.M., Kryazhev S.G., Andreev A.V., Cheremsin A.A., Mansurov R.H., Dvurechenskaya S.V., Zelikson B.S., Sapozhnikov V.G. Position of gold mineralization manifestations of the Toupugol–Khanmeyshor ore knot in ore–bearing complexes, their mineralogical and geochemical characteristics and comparison with reference objects of the Novogodnensky ore field: report under contract No. 94d. M.: FGUP TSNIGRI. 2008. (In Russian).

130. Wignall P.B., Twitchett R.J. Oceanic anoxia and the end permian mass extinction // Science. 1996. V. 5265. №272. P. 1155–1158.

131. Whitmore M.D. Helium heat of solution in Al and Mg using non–linear self–consistent screening of the nucleus // Journal of Physics. 1976. V. 6. P. 1259.

132. Wilson W.D., Bisson C.L., Baskes M.I. Self–trapping of helium in metals // Physical Review. 1981. V. 24. P. 5616.

133. Wolf R.W., Farley K.A., Silver L.T. Helium diffusion and low temperature thermochronometry of apatite // Geochimica et Cosmochimica Acta. 1996. V. 60. P. 4231–4240.

134. Wolf R.A., Farley K.A., Kass D.M. Modelling of the temperature sensitivity of the apatite (U–Th)/He thermochronometer // Chemical Geology. 1998. V. 148. P. 105–114.

135. Yakubovich O.V. New 190Pt–4He method of isotope geochronology for dating of platinum minerals: Cand. Sci. (in Russian): 25.00.09. St. Petersburg: SPbSU. 2013. 123 p. (In Russian).

136. Yakubovich O.V., Gedz A.M., Vikentyev I.V., Kotov A.B., Gorokhovsky B.M. Migration of radiogenic helium in the crystal lattice of sulfides

and the possibility of their isotopic dating // Petrology. 2019. V. 27. №1. P. 1–22. (In Russian).

137. Yakubovich O.V., Mochalov A.G., Sluzenikin S.F.: Sperrylite (PtAs2) as 190Pt–4He geochronometer // Reports of the Academy of Sciences. 2015. T 462. №1. P. 1–4. (In Russian).

138. Yakubovich O., Podolskaya M., Vikentyev I., Fokina E., Kotov A. (U,Th)–He Geochronology of Pyrite from the Uzelga VMS Deposit (South Urals) – New Perspectives for Direct Dating of the Ore–Forming Processes // Minerals. 2020. V. 10. №629.

139. Yakubovich O.V., Shukolyukov Yu.A., Kotov A.B., Yakovleva S.Z., Salnikova E.B. Geothermochronology on noble gases: II. Study of stability of the uranium–uranium–helium isotope system in zircons // Petrology. 2010. V. 18 №6. P. 3–18. (In Russian).

140. Yakubovich O., Stuart F., Ivanova E., Gervilla F. Constant ^{4}He concentration and ^{190}Pt–^{4}He age of detrital Pt–alloy grains from Santiago River, Ecuador: Potential as a ^{4}He mineral reference material // Geostandars and Geoanalytical Research, 2023.

141. Yakubovich O., Vikentyev I., Ivanova E., Podolskaya M., Sobolev I., Tyukova E., Kotov A. (U,Th)–He Geochronology of Pyrite from Alteration of the Au–Fe–Skarn Novogodnee-Monto Deposit (Polar Urals, Russia) – The Next Step in the Development of a New Approach for Direct Dating of Ore–Forming Processes // Geosciences. 2021. V. 11. №408.

142. Yakutseni V.P. Geology of helium. L: Nedra. 1968. 232 p. (In Russian).

143. Yang J.H., Zhou X.H. Rb–Sr, Sm–Nd, and Pb Isotopes Systematics of Pyrite: Implications for the Age and Genesis of Lode Gold Deposits // Geology. 2002. V. 29. P. 711–714.

144. Yazeva R.G., Bochkarev V.V. Voykar volcanic–plutonic belt (Polar Urals). Sverdlovsk: UNC AS USSR. 1984. 156 p. (In Russian).

145. Ziegler J.F., Ziegler M.D., Biersack J.P. SRIM – The Stopping and Range of Ions // Matter. Nucl. Inst. Methods Phys. Res. B. 2010. V. 268. P. 1818–1823.

146. Zeitler P.K., Herczig A.L., McDougall I., Honda M. (U,Th)–He dating of apatite: A potential thermochronometer // Geochimica et Cosmochimica Acta. 1987. V. 51. P. 2865–2868.

147. Zharikov V.A., Rusinov V.L. Metasomatism and metasomatic rocks. Moscow: Nauchny Mir. 1998. 492 p. (In Russian).

148. Zylyova, L.I., Konovalov, A.L., Kazak, A.P., Zhdanov, A.V., Korkunov, K.V., Denisov, V.A., Novikova, L.P., Rumyantseva, N.A., Cherepanov, Yu. Scale 1 : 1000000 (third generation). West Siberian series. Sheet Q–42 – Salekhard: Explanatory note. SPb.: VSEGEI. 2014. 396 p. (In Russian).